

JUACEP Medium/Short Program 2013 at University of Michigan & UCLA



Copyright © JUACEP 2013 All Rights Reserved.

Published in November, 2013

Leaders of JUACEP

Professor Noritsugu Umehara

Professor Yang Ju

Japan-US Advanced Collaborative Education Program (JUACEP)

Graduate School of Engineering

Nagoya University 
NAGOYA UNIVERSITY

Furo-cho, Chikusa-ku, Nagoya, 464-8603, JAPAN

JUACEP@engg.nagoya-u.ac.jp

<http://www.juacep.engg.nagoya-u.ac.jp>

Table of Contents

<1> About the Program	
a) Overview	...5
b) Participants	...6
<2> Research Reports	
Research Themes	...10
Research Reports	...12
<3> The 7 th Workshop on October 9, 2013	
Workshop Time Table	...86
Presentations	...88
Pictures	...119
<4> Reports on JUACEP Program	...121

<1> About the program

a) Overview

b) Participants

1-a. Overview

JUACEP's medium term and short term courses are organized for graduate students of Nagoya University to earn international experience. Both courses provide an opportunity to them to study with the students from all over the world being supervised by the top universities' faculty in the US.

Each student stays at a laboratory of University of Michigan or UCLA and basically works on his/her own master course's thesis. They may participate in experimental activity, lab seminar, group discussion and be given chance to audit the regular course lectures. At the same time they are obliged to report their research achievement to the faculty respectively at the end of the duration, then conclude the courses giving presentations at a plenary workshop after coming back.

For the medium course 2013, one graduate student for University of Michigan and two for UCLA left Japan at the end of March and returned at the end of September. For the summer short course, eight students worked on at University of Michigan from August 3 to September 27, and six at UCLA from August 4 to September 13. The 7th JUACEP Workshop took place for them at Venture Hall of Nagoya University on October 9, 2013. Here is the compilation.

2013 JUACEP Medium/Short Term Course Flowchart

	Medium Term Course (6 months)	Short Term Course (2 months)
November 2012	Public announcement, accepting application and screening candidates.	
December		
January 2013	Approach to UM/UCLA faculty by the selected students. English qualification checkup by the faculty for the UM course and application for VGR* for the UCLA course. (on DS-2019 procedure)	Public announcement and accepting application.
February		Closing application and screening candidates.
March	Applying for J-1 Visa.	Approach to faculty of UM/UCLA by the selected students.
April		English qualification checkup by the faculty for the UM course and application for VGR* for the UCLA course. (on DS-2019 procedure)
May	Medium term course study at UM or UCLA.	Applying for J-1 Visa
June		
July		
August		Short term course study at UM or UCLA
September		
October		
	The 7 th JUACEP Workshop (Oct.9)	

*VGR: Visiting Graduate Researcher

1-b. Participants

• *Medium term course studying at UCLA, from March 26 to September 24, 2013*

Name	Year	Advisor at Nagoya University	Advisor at UCLA
Takafumi Hattori hattori@ume.mech.nagoya-u.ac.jp	M1	Prof. Noritsugu Umehara Mechanical Science and Engineering ume@mech.nagoya-u.ac.jp	Prof. Chang-Jin Kim Mechanical and Aerospace Engineering cjkim@seas.umich.edu
Yoko Okuda y-okuda@na.cse.nagoya-u.ac.jp	M1	Prof. Shao-Liang Zhang Computational Science and Engineering zhang@na.cse.nagoya-u.ac.jp	Prof. Stanley Osher Mathematics sjo@math.ucla.edu

• *Medium term course studying at University of Michigan, from March 27 to September 29, 2013*

Name	Year	Advisor at Nagoya University	Advisor at University of Michigan
Fumitake Nonoyama nonoyama@ume.mech.nagoya-u.ac.jp	M1	Prof. Noritsugu Umehara Mechanical Science and Engineering ume@mech.nagoya-u.ac.jp	Prof. Albert J. Shih Mechanical Engineering shiha@umich.edu

• *Short term course studying at University of Michigan, from August 3 to September 27, 2013*

Name	Year	Advisor at Nagoya University	Advisor at University of Michigan
Yasunori Iijima ijijima.yasunori@f.mbox.nagoya-u.ac.jp	M1	Prof. Masashi Hasegawa Crystalline Materials Science hasegawa@numse.nagoya-u.ac.jp	Prof. Richard M. Laine Materials Science and Engineering talsdad@umich.edu
Akitomo Matsumoto matsumoto.akitomo@d.mbox.nagoya-u.ac.jp	M1	Prof. Eiichi Tanaka Mechanical Science and Engineering tanaka@mech.nagoya-u.ac.jp	Prof. Gregory M. Hulbert Mechanical Engineering hulbert@umich.edu
Tomoya Nishiyama nishiyama.tomoya@a.mbox.nagoya-u.ac.jp	M1	Prof. Yoji Yamada Mechanical Science and Engineering yamada-yoji@mech.nagoya-u.ac.jp	Prof. Gregory M. Hulbert Mechanical Engineering hulbert@umich.edu
Tomoko Ozawa ozawa.tomoko@f.mbox.nagoya-u.ac.jp	M1	Prof. Naoyuki Kanetake Materials, Physics and Energy Engineering kanetake@numse.nagoya-u.ac.jp	Prof. Katsuyo Thornton Materials Science and Engineering kthorn@umich.edu
Hiroki Shigematsu h_shigematsu@nuem.nagoya-u.ac.jp	M1	Prof. Tsuyoshi Inoue Mechanical Science and Engineering inoue@nuem.nagoya-u.ac.jp	Prof. Bogdan Epureanu Mechanical Engineering epureanu@umich.edu
Shunji Shibata shibata.shunji@h.mbox.nagoya-u.ac.jp	M1	Assoc. Prof. Mitsuhiro Shikida Micro-Nano Systems Engineering shikida@mech.nagoya-u.ac.jp	Prof. Euisik Yoon Electrical Engineering and Computer Science esyoon@umich.edu
Shun Tamamura tamamura.shun@h.mbox.nagoya-u.ac.jp	M1	Prof. Eiichi Tanaka Mechanical Science and Engineering tanaka@mech.nagoya-u.ac.jp	Prof. Scott Hollister Biomedical Engineering scottho@umich.edu
Takayuki Yamada yamada.takayuki@g.mbox.nagoya-u.ac.jp	M1	Assoc. Prof. Mitsuhiro Shikida Micro-Nano Systems Engineering shikida@mech.nagoya-u.ac.jp	Prof. Yogesh B. Gianchandani Electrical Engineering and Computer Science yogesh@eecs.umich.edu

• Short term course studying at UCLA, from August 4 to September 13, 2013

Name	Year	Advisor at NU	Advisor at UCLA
Hiroshi Fuji h_fuji@nuem.nagoya-u.ac.jp	M1	Prof. Tatsuya Suzuki Mechanical Science and Engineering t_suzuki@nuem.nagoya-u.ac.jp	Prof. Tsu-Chin Tsao Mechanical and Aerospace Engineering ttsao@seas.ucla.edu
Shinichi Hayashi s_hayashi@nuem.nagoya-u.ac.jp	M2	Prof. Toshiro Matsumoto Mechanical Science and Engineering t.matsumoto@nuem.nagoya-u.ac.jp	Prof. Ertugrul Taciroglu Civil and Environmental Engineering etacir@ucla.edu
Sakina Kondo kondou.sakina@b.mbox.nagoya-u.ac.jp	M1	Prof. Chikara Ohtsuki Crystalline Materials Science chikaraohsuki@gmail.com	Prof. Benjamin M. Wu Bioengineering benwu@ucla.edu
Kazuki Miyazaki miyazaki@ume.mech.nagoya-u.ac.jp	M1	Prof. Noritsugu Umehara Mechanical Science and Engineering ume@mech.nagoya-u.ac.jp	Prof. Jenn-Ming Yang Materials Science and Engineering jyang@seas.ucla.edu
Shoya Ono ohno@prop2.nuae.nagoya-u.ac.jp	M2	Assoc. Prof. Hosei Nagano Aerospace Engineering nagano@nuae.nagoya-u.ac.jp	Prof. Ivan Catton Mechanical and Aerospace Engineering catton@ucla.edu
Toshihiro Sato satou.toshihiro@b.mbox.nagoya-u.ac.jp	M1	Prof. Yang Ju Mechanical Science and Engineering ju@mech.nagoya-u.ac.jp	Prof. Benjamin M. Wu Bioengineering benwu@ucla.edu

Coordinators at Partner Universities

Prof. Katsuo Kurabayashi	Mechanical Engineering, University of Michigan	katsuo@umich.edu
Prof. Jenn-Ming Yang	Materials Science and Engineering, UCLA	jyang@seas.ucla.edu

JUACEP Members

Prof. Noritsugu Umehara	Mechanical Science and Engineering	ume@mech.nagoya-u.ac.jp
Prof. Yang Ju	Mechanical Science and Engineering	ju@mech.nagoya-u.ac.jp
Assoc. Prof. Hirofumi Aoki	Mechanical Science and Engineering	aoki@mech.nagoya-u.ac.jp
Assoc. Prof. Yasumasa Ito	Mechanical Science and Engineering	yito@nagoya-u.jp
Tomoko Kato	Administrative Officer	tomoko@mech.nagoya-u.ac.jp
Chiharu Yada	Administrative Officer	yada@mech.nagoya-u.ac.jp

<2> Research Reports

Research themes at University of Michigan

- [M] Fumitake Nonoyama supervised by Prof. Albert J. Shih:
3D-Printed Bone-Mimicking Material for Orthopedic Surgical Simulation (p.11)
- [S] Yasunori Iijima supervised by Prof. Richard M. Laine:
Research of Organic Functionalized Silsesquioxanes (p.12)
- [S] Akitomo Matsumoto supervised by Prof. Gregory M. Hulbert:
Effects of Soft Tissue Stiffness on Stress Values of Femur Neck (p.17)
- [S] Tomoya Nishiyama supervised by Prof. Gregory M. Hulbert:
Kinematics and Compliance Testing Simulation of an Automobile Using a Rigid Body Suspension Model (p.22)
- [S] Tomoko Ozawa supervised by Prof. Katsuyo Thornton:
Analysis of Fluid Flow of Molten Magnesium into Micro-Particles (p.29)
- [S] Hiroki Shigematsu supervised by Prof. Bogdan Epureanu:
Development of a Vibration Excitation System Forced on Piezoelectric Elements (p.34)
- [S] Shunji Shibata supervised by Prof. Euisik Yoon:
Tapered Etch Profile (p.40)
- [S] Shun Tamamura supervised by Prof. Scott Hollister:
Evaluation of Auricular Biomechanical Property by FEM (p.41)
- [S] Takayuki Yamada supervised by Prof. Yogesh B. Gianchandani:
Calibration of a Strain Gauge for Force Measurement in a Palatal Expander (p.42)

Research themes at UCLA

- [M] Takafumi Hattori supervised by Prof. Chang-Jin Kim:
Characterization of Molded Superhydrophobic Surfaces (p.43)
- [M] Yoko Okuda supervised by Prof. Stanley Osher:
How Split Bregman Can Apply for Non-Negative Matrix Factorization (p.44)
- [S] Hiroshi Fuji supervised by Prof. Tsu-Chin Tsao:
Modeling for a Nano-Precision System (p.50)
- [S] Shinichi Hayashi supervised by Prof. Ertugrul Taciroglu:
Numerical Simulation of Wave Propagation in Composite Structures (p.56)
- [S] Sakina Kondo supervised by Prof. Benjamin M. Wu:
Effect of Protein Charge on Adsorption to Apatite and Cell Viability (p.62)
- [S] Kazuki Miyazaki supervised by Prof. Jenn-Ming Yang:
Impact Tolerance of Metal, Composites, and FMLs (p.63)
- [S] Shoya Ono supervised by Prof. Ivan Catton:
Study on an Aluminum Two-Phase Heat Transfer Device Using IAS Fluid (p.71)
- [S] Toshihiro Sato supervised by Prof. Benjamin M. Wu:
Mechanical Stimulation on Rat Intestinal Smooth Muscle Cells to Improve Maturity (p.77)

[M]: Medium term course, [S]: Short term course

3D-PRINTED BONE-MIMICKING MATERIAL FOR ORTHOPEDIC SURGICAL SIMULATION

Fumitake Nonoyama

Department of Mechanical Science and Engineering, Graduate School of Engineering, Nagoya University
nonoyama@ume.mech.nagoya-u.ac.jp

Supervisor: Albert Shih

Graduate School of Engineering, University of Michigan
shih@umich.edu

ABSTRACT

3D-printing technology has advanced to the point where complex models can be made at low cost. The 3D-printed material is sometimes infiltrated with liquid material to improve those mechanical properties. In this study, 3D-printed material soaked with liquid material was used as a novel material to simulate the human cortical bone for orthopedic drilling. This composite was evaluated by drilling tests with three orthopedic tools, drill bit, kirschner wire (K-wire), and diamond bur, and compared to a bovine cortical bone in terms of thrust force, torque and temperature response. As for K-wire, the bone-mimicking material showed similar results to those of the bovine bone, but behaved softer for drill bit and diamond bur. However, discrepancy in temperature response of the bone-mimicking material was less than 20% to that of a bovine cortical bone for all three tools. The composite will potentially be an alternative training material for orthopedic bone drilling.

Undisclosed

RESEARCH OF ORGANIC FUNCTIONALIZED SILSESQUIOXANES

Yasunori Iijima

Crystalline Materials Science and Engineering, Graduate School of Nagoya University, Furo-cho, Chikusa-ku, 464-8603 Nagoya (Japan)
ijijima.yasunori@f.mbox.nagoya-u.ac.jp

Supervisor: Joseph Furgal

PhD. Materials Chemistry, University of Michigan, Ann Arbor, MI 48109-2136, USA
furgaljc@umich.edu

ABSTRACT

Silsesquioxanes are a collective term of composites of silica, which have formulas of $\text{RSiO}_{1.5}$. In these composites, the atom of silica, which has four atomic bondings, combines with one organic group or hydrogen atom (R) and three oxygen atoms. The structures of silsesquioxanes have been reported as random structure, ladder structure, cage structure, and partial cage structure as illustrated in Figure 1. Silsesquioxanes have a high potential for not only industrial applications but also academic standings because they can be functionalized by various organic groups.^{1,2}

In this research, we worked with the T type full cage silsesquioxanes and tried to establish novel reaction processes of silsesquioxanes. Moreover, we tried to synthesize novel cysteine functionalized silsesquioxanes. We evaluated the samples by Fourier Transform Infrared Spectroscopy (FT-IR), Gel Permeation Chromatography (GPC) and MALDI-ToF mass spectrometry.

INTRODUCTION

T cage silsesquioxanes

Phenyl and vinyl groups are well known as substituents of silsesquioxanes. Most of the syntheses of T cage silsesquioxanes are derived from hydrolysis and condensation of trichlorosilane, trialkoxysilane or triethoxysilane. The hydrolysis products are usually polymerized at random. This is because variety of polyhedron silsesquioxanes (mainly T_8 , T_{10} , T_{12}) and partial cages silsesquioxanes are synthesized simultaneously. Since they exist as a mixture, it is necessary to be isolated. In this research, we had adjusted the solvents, and tried to establish new reactions from the viewpoint of separation.

Cysteine functionalized silsesquioxane

The molecules, which do not match their image on a mirror are called 'chiral molecule'. Though chiral molecules are present in various drugs, it can be dangerous if we use chiral molecules in a drug composite because even if one enantiomer has beneficial effect, another enantiomer can be devastating. Therefore, chiral separation materials are very important for making drugs cheaper and safer. In this research, we tried to synthesize the organic-inorganic hybrid material (n-acetyl-L-cysteine, octa vinyl silsesquioxane) as a novel chiral separation material.³

EXPERIMENTAL

*T cage silsesquioxanes*⁴

Hydrolyses and condensations of phenyl triethoxysilane or vinyl triethoxysilane were conducted in various solvents as summarized in Table 1, 2 with tetra-n-butylammonium fluoride (TBAF) as a catalyst and H_2O as a hydrolyzate. The product mixtures were separated by using vacuum filtration and/or rotary evaporation.

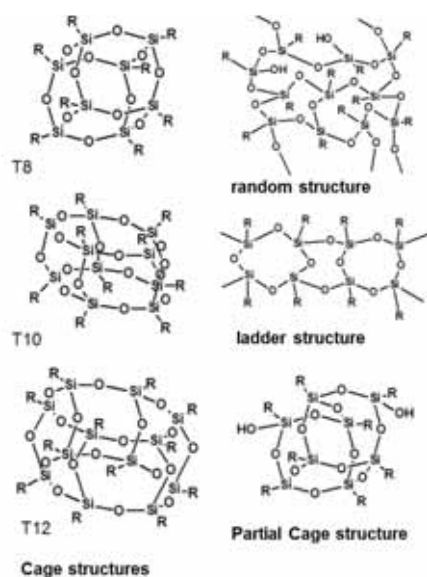


Figure 1. Structures of silsesquioxanes

Table 1. The new phenyl silsesquioxanes reactions

The differences among 1–3 are the quantity. The difference between 5 and 6 is the ratio.

Number	Solvent
1	CH ₂ Cl ₂
2	CH ₂ Cl ₂
3	CH ₂ Cl ₂
4	Acetonitrile-THF
5	Acetonitrile- CH ₂ Cl ₂
6	Acetonitrile- CH ₂ Cl ₂

Table 2. The new vinyl silsesquioxanes reactions

Number	Solvent
7	Acetonitrile
8	Acetonitrile- CH ₂ Cl ₂

Cysteine functionalized silsesquioxane

The cysteine functionalized silsesquioxane was synthesized by using octa-vinyl silsesquioxane (OVS), L-acetyl-n-cysteine, azobisisobutyronitrile (AIBN) as a catalyst and tetrahydrofuran (THF) as the solvent (Fig. 2). We also tried to convert the hydroxy group of the OVS-cysteine product to a chloro group using thionyl chloride (Fig. 3). Moreover we evaluated the cysteine functionalized silsesquioxane by chiral chromatography.

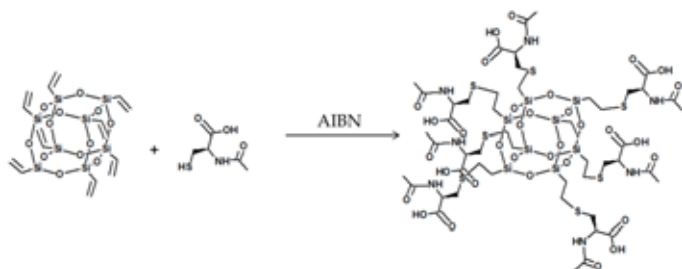


Figure 2. L-acetyl-n-cysteine functionalized OVS

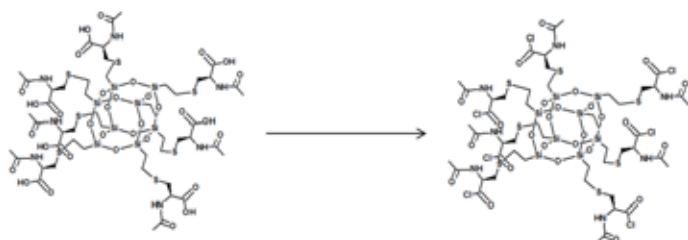


Figure 3. conversion of -OH to -Cl

RESULTS AND DISCUSSION

T cage silsesquioxanes

New phenyl silsesquioxanes reactions

1-3

CH₂Cl₂ was used as solvents of these reactions. The samples of powder could be recovered using a difference in solubility. The samples that could not be precipitated and remained in solution were attributed to partial cage structure type silsesquioxanes. The FT-IR spectra (Figure 4) show that all of the samples contain phenyl groups and Si-O bonds. These results showed that these samples are phenyl silsesquioxanes.

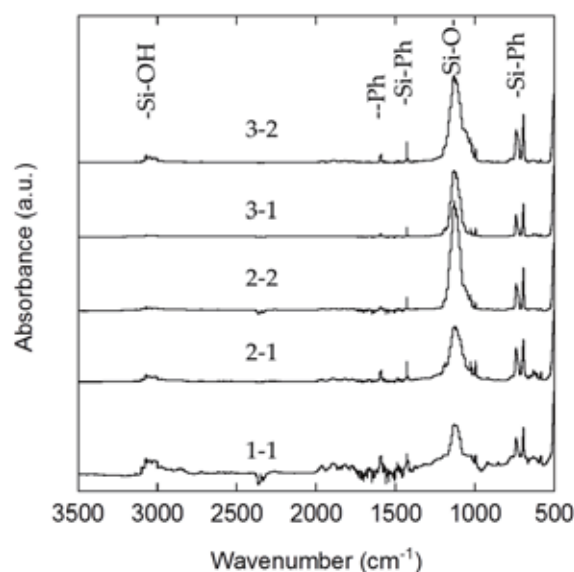


Figure 4. FT-IR spectra of the powder samples of reaction number 1-3

4

A mixture of acetonitrile and THF was used as a solvent. In this reaction, two powders and one solution were recovered. The solution was likely to be partial cage structure type silsesquioxanes because of the solubility. According to the FT-IR spectra (Figure 5), the products were likely to be phenyl silsesquioxanes. The second product had moisture absorbency. This is why O-H bond appeared in the spectra or partial cage structure.

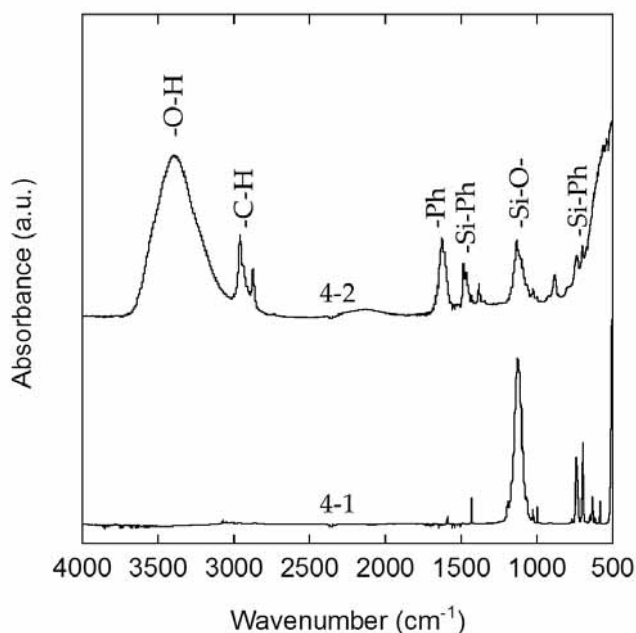


Figure 5. FT-IR spectra of the powder samples of reaction number 4

5.6

The mixture of acetonitrile and CH_2Cl_2 was used as solvents in these reactions. Two powders and one solution were recovered for each reaction. Considering the solubility of the solution, they were likely to be partial cage structure type silsesquioxanes. The powders are likely to be phenyl silsesquioxanes from the FT-IR spectra (Figure 6). It is highly possible that the second powder of reaction number 5 is pure T10 cage phenyl silsesquioxane from the GPC spectra (Figure 7).

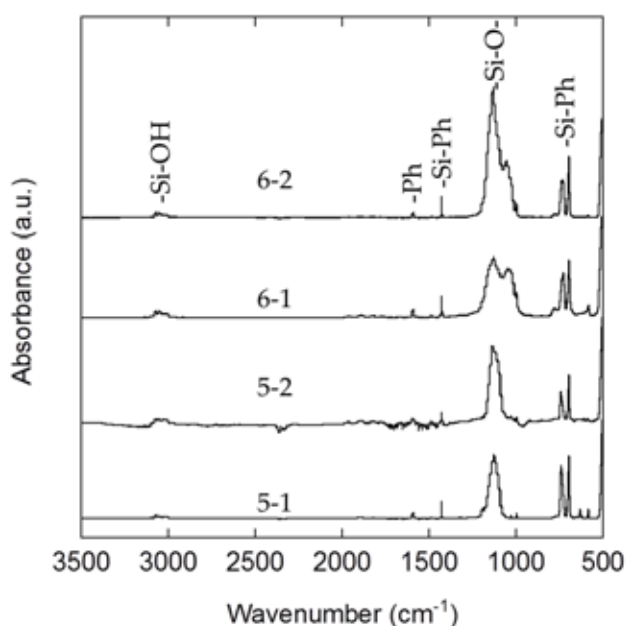


Figure 6. FT-IR spectra of the powder samples of reaction number 5, 6

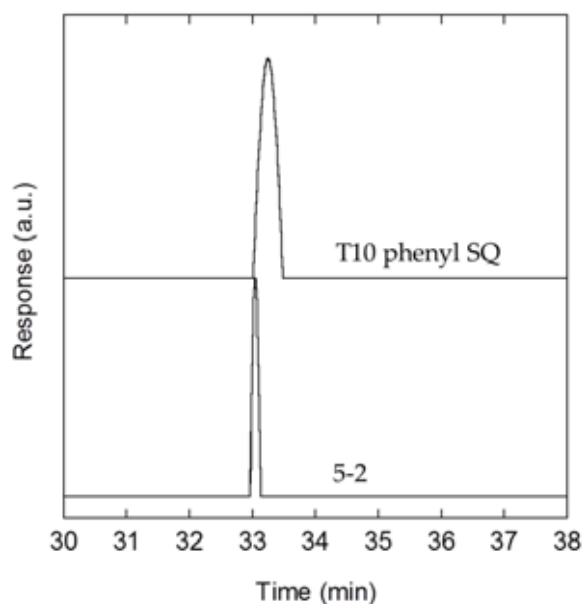


Figure 7. GPC spectra of the second powder of reaction 5 and T10 phenyl silsesquioxane

The T10 phenyl silsesquioxane was synthesized by previously. The half width on GPC spectrum means the dispersion of the molecule weight.

New vinyl silsesquioxanes reactions

7.8

Acetonitrile and acetonitrile- CH_2Cl_2 mixture were used as solvents. One powder and one solution were recovered for each reaction. According to FT-TR spectra (Figure 8), Si-O bond and Si-vinyl group bond were detected. This showed that vinyl silsesquioxanes were synthesized.

The GPC spectra of each solution are shown in Figure 9. This figure shows that each sample contains two materials. The detection times of two peaks are faster than that of OVS. So, T10 or T12 vinyl silsesquioxanes can be synthesized under this condition.

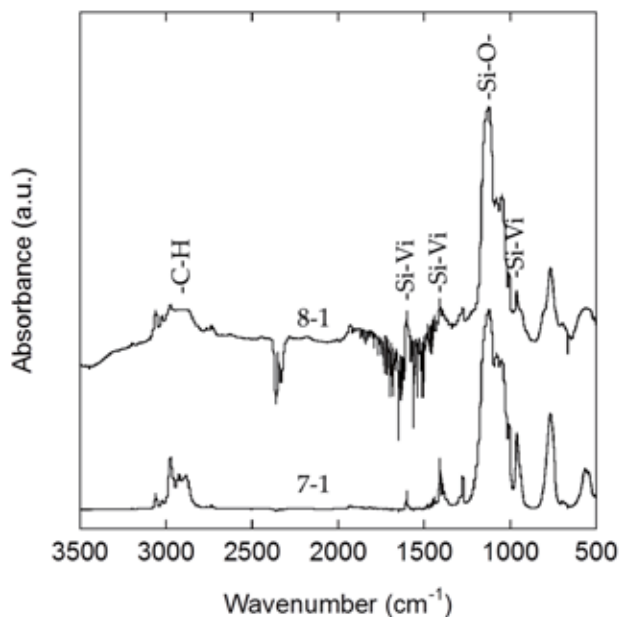


Figure 8. FT-IR spectra of the powder samples of reaction number 7, 8

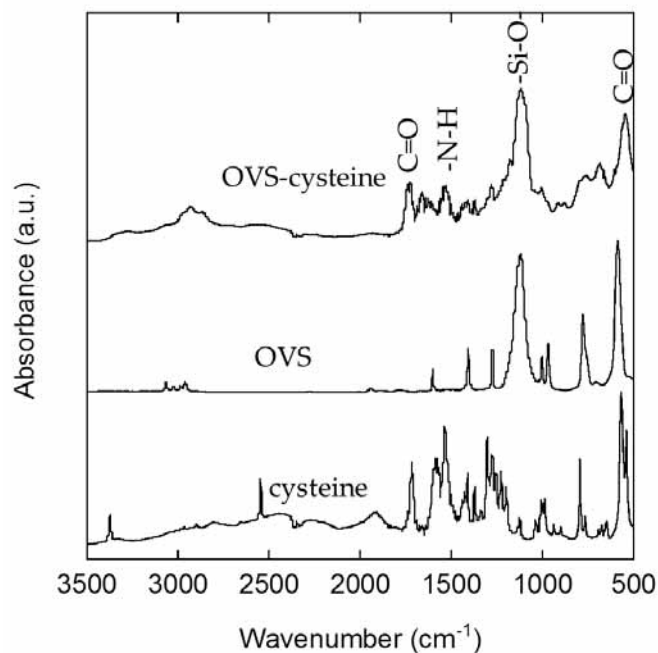


Figure 10. FT-IR spectra of the samples of OVS-cysteine reaction

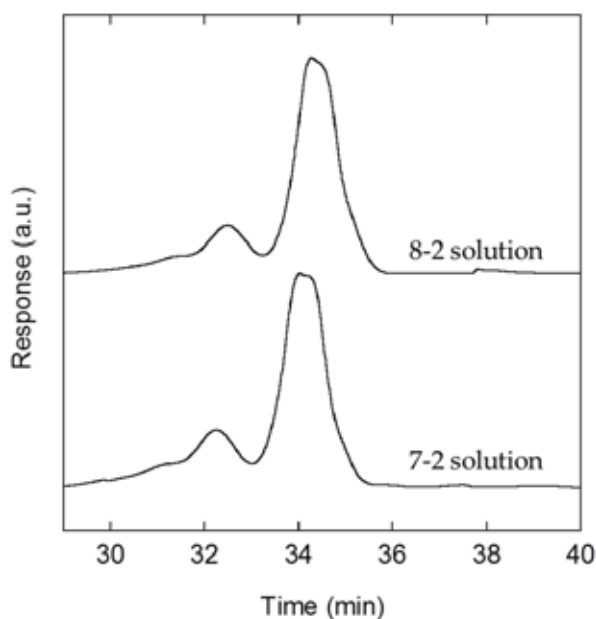


Figure 9. GPC spectra of the solution samples of reaction number 7, 8

Cysteine functionalized silsesquioxane

Synthesis of *n*-acetyl-L-cysteine functionalized OVS

According to IR spectra of OVS-cysteine compound, the Si-O absorption (around 1100 cm^{-1}) from the silsesquioxane and C=O absorption (around 1650 cm^{-1}) from carboxylic acid and N-H absorption (around 1550 cm^{-1}) from amide can be seen (Fig.10). This means OVS was successfully functionalized by *n*-acetyl-L-cysteine under this condition.

Synthesis of chloro group converted cysteine-OVS

According to IR spectrum of thionyl reaction (Figure 11), there were many new peaks which starting material of OVS-cysteine compound did not have. This could be caused by contamination of *N*-methyldicyclohexylamine which was used in neutralization. Moreover, the C-Cl stretch absorption ($600\text{--}800\text{ cm}^{-1}$) was not clear. So it is unlikely that the chloro group converted cysteine silsesquioxane was synthesized.

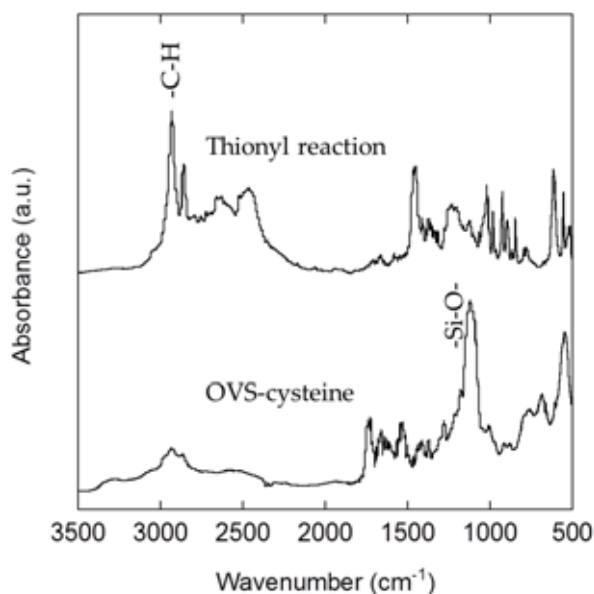


Figure 11. FT-IR spectra of recovered sample of thionyl reaction

Chiral chromatography of limonene using OVS-cysteine compound

We evaluated whether the OVS was functionalized by n-acetyl-L-cysteine or not by chiral chromatography. We chose L and D-limonene as isomers. After we conducted chiral chromatography using OVS-cysteine compound which we synthesized, keep the samples and put each sample a little bit on Thin-Layer Chromatography (TLC) plate and dyed them by potassium permanganate. It showed that the mixture of isomers was separated as shown in Figure 12. We will evaluate these samples by circular dichroism (CD) measurement.



Figure 12. A picture of Thin-Layer Chromatography (TLC) plate dyed by potassium permanganate after chiral chromatography

The left black spot shows one limonene, and the right spot shows the other limonene. The middle one is a mixture of the isomers.

CONCLUSIONS

In this research of new T cage structure silsesquioxanes reactions, it was found that we can get phenyl silsesquioxanes in nearly every solvent. We can get pure T10 phenyl silsesquioxane as a powder by using the solvent of Acetonitrile- CH_2Cl_2 mixture (reaction number 5). In vinyl reaction, we could get vinyl silsesquioxanes which molecule weight is heavier than that of OVS. In order to do further research, we should identify all the samples by using Matrix Assisted Laser Desorption / Ionization (MALDI) to decide the molecule weight and kind of polyhedron. In the future, we should also make sure the repeatability, purity and yield ratio of these reactions and to find the best solvent systems to make T cage structure silsesquioxanes.

Regarding novel functionalized silsesquioxanes, the FT-IR spectra and chiral chromatography showed that we could synthesize n-acetyl-L-cysteine functionalized OVS as a novel chiral separation material. To research further

functionalization of OVS-cysteine compound, the chloro group conversion is expected.

ACKNOWLEDGEMENTS

I would like to thank Professor Richard M Laine for accepting me and giving me such a chance to learn about silsesquioxanes. Ms. Georgia Knope is also acknowledged for her help of my procedure to get a J1 visa. I would especially like to thank Mr. Joseph Furgal for continued support and advice and day-to-day direction. Mr. Phi Doan and Mr. David Pan are also greatly acknowledged for their continued help of basic handling of chemical experiments. Mr. Eongyu Yi, Mr. Jae Hwan Jung, Mr. Andrew Pottebaum, Mr. Nathan Taylor, Ms. Sandra Stangeland-Molo, Ms. Mozghan Bahrami, Ms. Daphne Chou and Ms. Mitra Maghadam, those who spent time together in Laine's laboratory, are also acknowledged. The financial support was from Japan Student Services Organization via Japan-US Advanced Collaborative Education Program.

REFERENCES

- [1] Ronald H. Baney, Maki Itoh, Akihito Sakakibara, Toshio Suzuki, *Chemical Review*, 1995, 95, 1409-1430
- [2] Maki Itoh, 'Chemistry of Silsesquioxane Materials and Their Applications', cmcbooks, 2013
- [3] <http://www.jstshingi.jp/abst/p/07/09/cicA06.pdf>
- [4] J. H. Jung, J. C. Furgal, T. Goodson, III, T. Mizumo, M. Schwartz, K. Chou, J.F. Vonnet, R. M. Laine, "3-D Molecular Mixtures of Catalytically Functionalized $[\text{vinySiO}_{1.5}]_{10}$ / $[\text{vinySiO}_{1.5}]_{12}$. Photophysical Characterization of Second Generation Derivatives," *Chem. Mater.* 2012, 24 (10), 1883-1895, DOI: 10.1021/cm300587s.
- [5] Furgal, J.C.; Jung, J.H.; Goodson, T.; Laine, R.M. "Analyzing Structure-Photophysical Property Relationships of Isolated T_8 , T_{10} , and T_{12} Stilbenevinyl Silsesquioxanes," 2013, 135, 12259-12269, DOI: 10.1021/ja4043092.
- [6] Furgal, J. C.; Goodson, III, T.; Laine, R. M.; "Synthesis of Decaphenyl Silsesquioxane ($D5_h-T_{10}$) and larger cages by Fluoride Catalyzed Rearrangement of $[\text{PhSiO}_{1.5}]$ and Phenyltriethoxysilane with Steady State Spectroscopy Compared to Simple SQs (Q and T type) and Proposed Mechanism. (Manuscript in Preparation)

EFFECTS OF SOFT TISSUE STIFFNESS ON STRESS VALUES OF FEMUR NECK

Akitomo Matsumoto

Department of Electrical Engineering & Computer Science, Graduate School of Engineering
amatsumo@umich.edu

Supervisor: Professor Gregory M. Hulbert

Graduate School of Engineering, Nagoya University
matsumoto.akitomo@d.mbox.nagoya-u.ac.jp

ABSTRACT

Hip fracture due to falls are a serious problem especially for elderly women. To research the effects of body type on hip fracture, a series of simulation was carried out with different elastic modulus of soft tissue using Multi-body model which combined with finite element model of hip joint. As a results, well-muscled people have a higher risk of femur fracture than fat people. It is worthwhile to know that response of the stress is different depending on the elastic modulus.

1. INTRODUCTION

Hip fractures due to sideways falls are a serious problem especially for elderly women. They invariably require an emergency department visit, hospitalization, surgery, and rehabilitation. As a result of the aging society, it has been estimated that the total number of hip fracture in the world will increase from 1.3 million in 1990 to 2.6 million by the year 2025 and to 4.5 million by the year 2050 [1]. Therefore, prevention of a hip fracture is not only for improving quality of life but also reducing cost of the treatment.

A lot of research has been carried out to simulate a falling leading hip fracture using finite element model of the pelvis-femur complex. For example, Majumder et al. (2007, 2008) developed a computed tomography scan based three-dimensional finite element model of the pelvis-femur complex [2], [3]. Using this model, they evaluated the effects of trochanteric soft tissue thickness and impact velocity which causes hip fractures during sideways fallings. However, body types have not been considered. Risk of fracture is considered to be affected by fat and muscle. As a first step of clarifying the effects of body type on hip fracture, subject of this research is to evaluate the effects of soft tissue stiffness.

2. METHOD

To represent whole body configuration and to assess the fracture risks of the femur neck based on the distributions of stress, I used the Multi-body model which combined with finite element model of hip joint (Figure. 1). In this model, the left femur, pelvis, skin, ligament, and soft tissue around femur were modeled with finite elements using hexahedron solid and square shell elements. Other parts of the whole human body were modeled as multi-body model, a system where 11 rigid bodies with mass and inertia moment are connected by three-dimensional kinematic joints such as a spherical joint and free joint. The model represented a Japanese female whose average age was 149.3 cm and weight was 55.3 kg, which are the average values of 50 Japanese female whose average age was 66.9 years old [4].

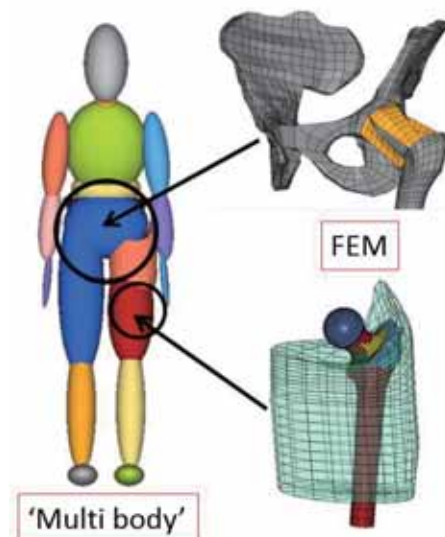


Figure. 1. Multi-body model combined with finite element model of hip joint.

The mechanical properties of the finite element model of femur, pelvis, skin, and ligament are shown by Tsuchida (2012) [5]. The soft tissue around femur is modeled as a visco-elastic material approximated by Maxwell model.

Material property of soft tissue (Table. 1) is decided from Yamada (1970) [6]. Using these models, the kinematic behavior of a fall and the resulting stress values of femur were analyzed by MADYMO (TNO Automotive).

As a reference of elastic modulus values of visco-elastic material, I chose a literature of Bandak et al. (2001) [7]. They developed finite element model of the planter to understand the mechanical behavior of the ankle joint under injurious situations. The model of planter is consists of three layers and each of these represent fat, muscle and ligament. From material properties of these layers (Table. 2), muscle is defined much softer than fat.

To close material property to muscle layer of the literature, elastic modulus is changed to one-tenth and one-hundredth of original value. Furthermore, changing elastic modulus from 5 [MPa] to 25 [MPa] taking interval 5 [MPa], to evaluate the effects of soft tissue hardness on stress values of femur neck. At this time, bulk modulus and Dynamic shear modulus were calculated from two equations (1) and (2). Those values are shown in Table 3.

$$K = \frac{E}{3(1-2\nu)} \quad (1) \quad G = \frac{E}{2(1+\nu)} \quad (2)$$

Table 1. Material properties of original soft tissue.

Modulus of longitudinal elasticity [Mpa]	Poisson ratio	Density [kg/m3]	Bulk modulus [Mpa]	Dynamic shear modulus [Mpa]
15.0	0.49	1.0E+03	2.5E+02	5.03

Table 2. Material properties of the planter (Bandak et al.).

	Elastic modulus [Mpa]	Poisson ratio	Density [kg/m3]	Bulk modulus [Mpa]
Plantar ligament	6.01	0.49	0.75E+03	1.00E+02
Muscle layer	0.152	0.49	0.75E+03	2.53E+00
Fat layer	20.0	0.49	0.75E+03	3.33E+02

Short term shear modulus [Mpa]	Long term shear modulus [Mpa]
2.02	1.51
0.0509	0.0382
6.71	5.03

Table 3. Material properties of soft tissue in each simulation.

Elastic modulus [Mpa]	Bulk modulus [Mpa]	Dynamic shear modulus [Mpa]
0.15	2.500	0.05034
1.5	25.00	0.5034
5	83.33	1.677
10	166.7	3.355
15	250.0	5.034
20	333.3	6.711
25	416.7	8.389

To reproduce the initial conditions of backward fall, buttocks of the model were arranged at height 500 [mm] from the ground. The positions of legs were asymmetrically allocated. The angle to the side of the trunk axis were set to 0° and 20° (Fig. 2). Then, the model was exposed to gravity, and fell on the ground in the condition of hitting trochanter.

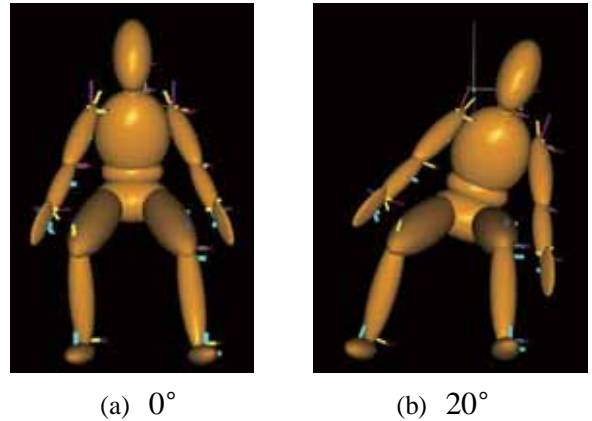
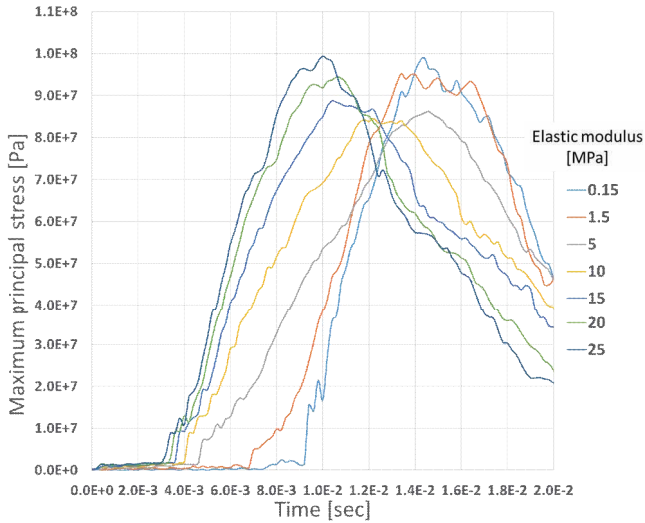


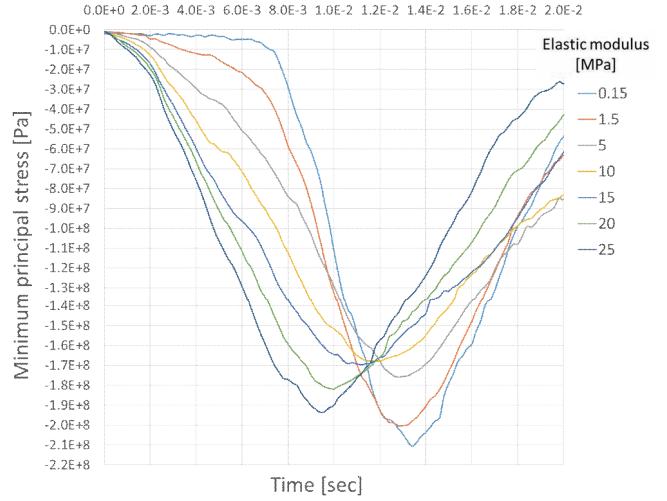
Figure. 2. Angle to the side of trunk axis

3. RESULTS

To research the effects of elastic modulus on stress values of femur neck, maximum principal stress, minimum principal stress and maximum shear stress were compared. These stresses were observed in one of the femur neck element which showed the highest value. Fig. 3, 4, 5 show the time history of each stresses. Starting points of the horizontal axis are the time soft tissue contact to the ground. Under the conditions of elastic modulus arranged between 25 [MPa] to 10 [MPa], maximum principal stress and shear stress decrease as elastic modulus decrease except the case of maximum principal stress setting trunk axis 20°. On the other hand, under the condition of elastic modulus arranged between 10 [MPa] to 0.15 [MPa], these stress values increase as elastic modulus decrease. Same tendency was also observed in the absolute values of Minimum principal stress. In other words, stress values became bigger when elastic modulus leaves from original of 15 [MPa]. In addition, stress values of setting trunk axis 20° become bigger than the case setting trunk axis 0°. There are differences in the time when stress began to increase. As elastic modulus become smaller, stress starts to increase lately. Therefore, the time that stress takes maximum value also become later.

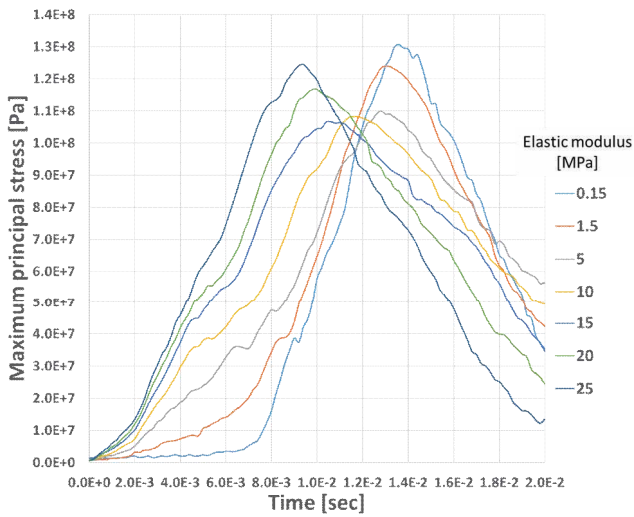


(a) Angle to the side of trunk axis 0°



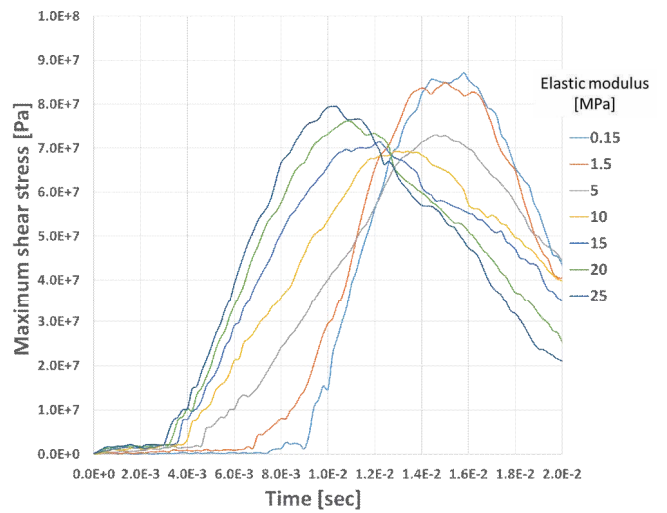
(b) Angle to the side of trunk axis 20°

Fig. 4, (a)(b). History of minimum principal stress.

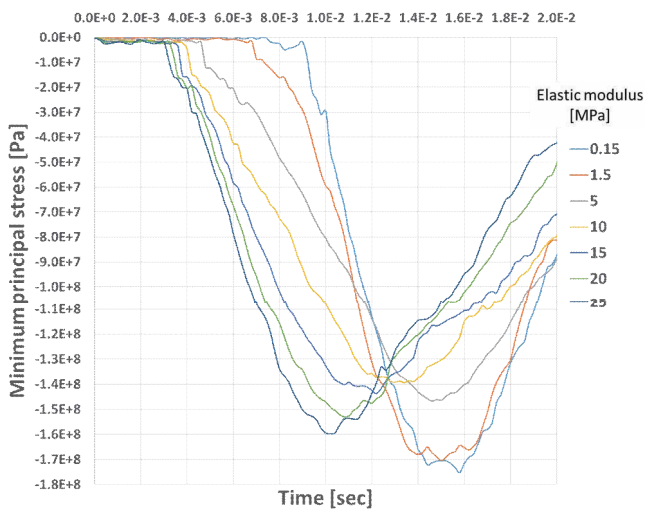


(b) Angle to the side of trunk axis 20°

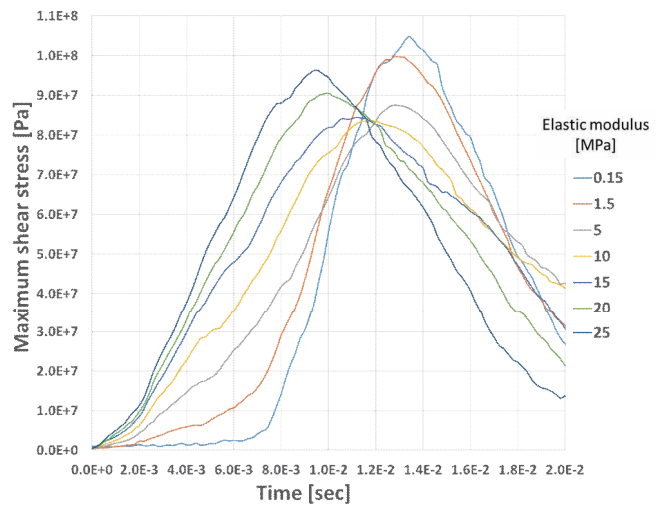
Fig. 3, (a)(b). History of maximum principal stress.



(a) Angle to the side of trunk axis 0°



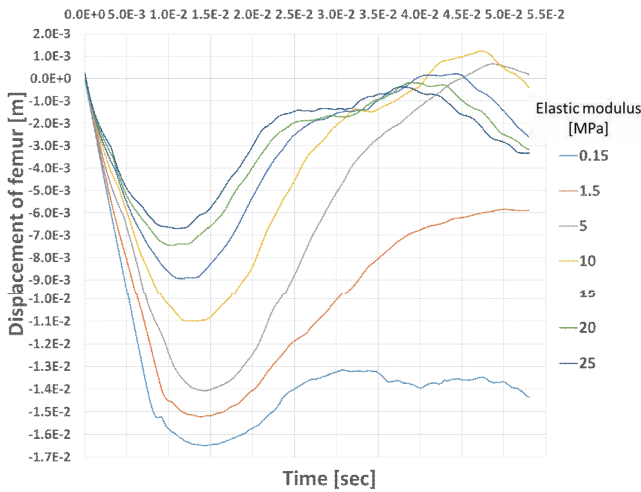
(a) Angle to the side of trunk axis 0°



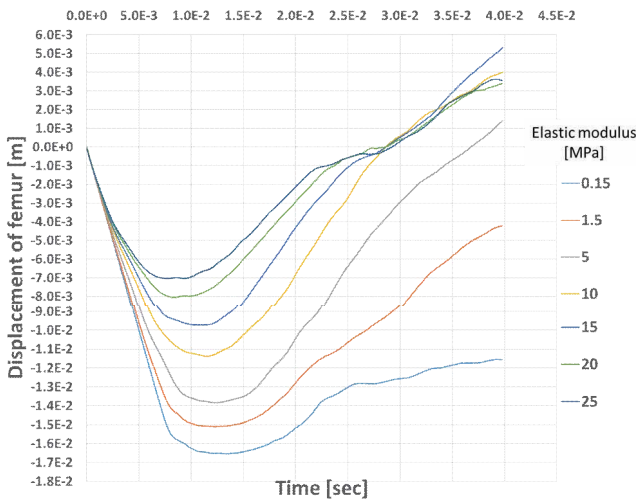
(b) Angle to the side of trunk axis 20°

Fig. 5, (a)(b). History of maximum shear stress.

Fig. 6 shows the time history of displacement of vertical direction. These displacements are measured from same element of femur neck compared stress values. Starting points of the horizontal axis are the time soft tissue contact to the ground. At that time height of femur neck element was defined as zero. These graphs show that the element fall in proportion to time after soft tissue contacts to the ground. Then, displacements no longer change and elements rebounded. As elastic modulus became smaller, the element sank deeply because of the softness of the soft tissue.



(a) Angle to the side of trunk axis 0°



(b) Angle to the side of trunk axis 20°

Fig. 6, (a)(b). Displacement of vertical direction.

In addition, impact speed of vertical direction were compared. These are impact speed of femur neck element and calculated from its displacement. There were not so much differences in minimum value of impact speed. However impact speeds of setting trunk axis 20° are a little faster than the case of setting trunk axis 0° . Main cause of this is considered that the difference of initial body configuration of the model. As elastic modulus become smaller, impact speed close to 0 lately.

4. DISCUSSION

To clarify the reason why the time each stress taking the maximum values become later as elastic modulus decrease, compared the history of stress and displacement. Fig. 7 shows the history of maximum principal stress and displacement in reverse order in the case of elastic modulus 1.5 [MPa] with setting trunk axis 0° . We can understand that the time stress takes the maximum value and the time displacement becomes minimum are coincide. In other words, there is a relationship that stress becomes the biggest when femur closest to the ground. The same tendency was observed in other conditions.

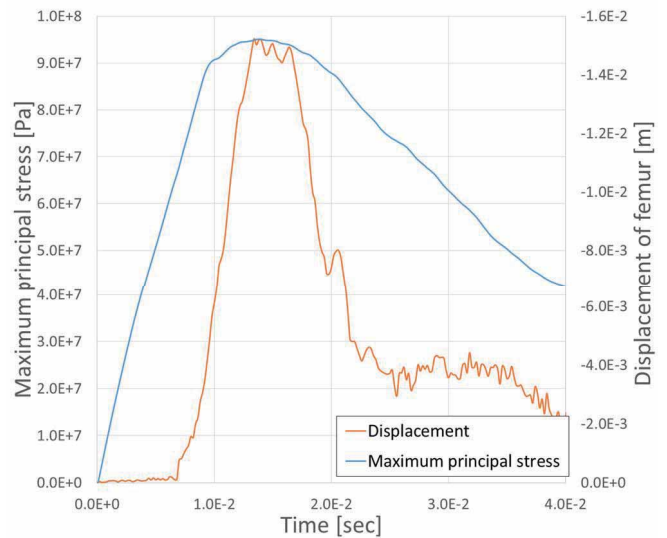


Fig. 7. Relationship between maximum principal stress and displacement.

The maximum values of stress decreased when elastic modulus became smaller between 25 [MPa] and 10 [MPa]. Main cause of this is considered that soft tissue could absorb more shock because of the reduced stiffness. On the other hand, maximum values of stress increased between 10 [MPa] and 0.15 [MPa]. Effects of potential energy became bigger because of displacement of vertical direction and it is considered to be main cause of increasing stress. In addition, stress relaxation function which define instantaneous shear modulus might have some effects on it.

5. CONCLUSIONS

As a consequence, well-muscled people have a higher risk of femur fracture than fat people in my research. This result is contrary to we expected. However, it is worthwhile to know that response of the stress is different depending on the elastic modulus.

The model of soft tissue consists of only one part in this study. Therefore, it is necessary to separate muscle part and fat part in future study. In addition, shape of soft tissue should be made to match body type. Thickness of soft tissue is considered to have some effects on fracture risk.

REFERENCES

- [1] Gullberg, B., Johnell, O., Kanis, J.A., 1997. World-wide Projections for Hip Fracture. *Osteoporosis International* 7, 407-413.
- [2] Santanu Majumder, Amit Roychowdhury, Subrata Pal, 2007. Simulation of hip fracture in sideways fall using a 3D finite element model of pelvis-femur-soft tissue complex with simplified representation of whole body. *Medical Engineering & Physics* 29, 1167-1178.
- [3] Santanu Majumder, Amit Roychowdhury, Subrata Pal, 2008. Effects of trochanteric soft tissue thickness and hip impact velocity on hip fracture in sideways fall through 3D finite element simulations. *Journal of Biomechanics* 41, 2834-2842.
- [4] Kouchi, M. Mochimaru, M. Iwasawa, H. Mitani, S., 2000. Anthropometric database for Japanese Population 1997-98. Japanese Industrial Standards Center (AIST, MITI).
- [5] Tomonari Tsuchida, Satoko Hirabayashi Eiichi Tanaka, Koji Mizuno, 2012. Simulation of mechanisms of hip fractures in backward falls. Department of Mechanical Science & Engineering Graduate School of Engineering, Nagoya University.
- [6] Yamada, H., 1970. In: Evans, F.G. (Ed.), *Strength of biological materials*. The Williams & Wilkins, Baltimore MD.
- [7] F.A. Bandak, R.E. Tannous, T. Toridis, 2001. On the development of an osseo-ligamentous finite element model of the human ankle joint. *International Journal of Solids and Structures* 38, 1681-1697.

Kinematics and Compliance Testing Simulation of an Automobile Using a Rigid Body Suspension Model

Tomoya Nishiyama

Department of Mechanical Science and Engineering, Graduate School of Nagoya University
nishiyama.tomoya@a.mbox.nagoya-u.ac.jp

Supervisor: Prof. Gregory Hulbert

Department of Mechanical Engineering, Graduate School of University of Michigan
hulbert@umich.edu

ABSTRACT

Kinematics and Compliance (K&C) testing is effective and often used to evaluate the ride and handling performance of an automobile. While a typical K&C test is being conducted, the vehicle body is fixed while controlled forces or displacements are applied to the wheels. The results of the test include indexes such as toe and camber, K&C values. Numerical simulations of K&C testing are usually performed using multibody dynamics software. In this paper, using a rigid body suspension model, the investigation of K&C values such as toe and camber is conducted with change of the configuration of the suspension body and the characteristics of the spring.

1. INTRODUCTION

In order to evaluate the performance of an automobile, it is essential to measure the vehicle suspension K&C (Kinematics and Compliance) values. In general, kinematics has been defined the study of motion without reference to mass or force and compliance is deflection resulting from the application of force [1]. In a typical K&C test, vehicle suspension K&C values are measured by the application of the controlled displacements and forces respectively to the wheels.

Multibody dynamics software is widely used for the simulations of a K&C test and the prediction of the vehicle suspension K&C values. Hahn focused that the results of the K&C simulations with rigid components of the vehicle different from actual test results, and proposed a new methodology for K&C testing simulations using a nonlinear finite element model [2].

In this paper, K&C testing simulations are performed using Adams/Car, one of the multibody dynamics software which is widely used for K&C testing simulations. The configuration of the suspension body and the characteristics of the spring are changed, and the simulation results are compared. This contributes to the optimized design of vehicle suspensions.

2. K&C VALUES

K&C values are indexes in order to evaluate the ride

and

handling performance of an automobile. In this paper, toe and camber are considered as K&C values.

2.1 Toe

As shown in Fig. 1, toe is defined as the angle of the wheel as seen from the top of the automobile. More properly, toe is the angle between the vertical plane through the front and rear center of the vehicle and the vertical plane along with the wheel. Toe is related to the attrition and the grip of

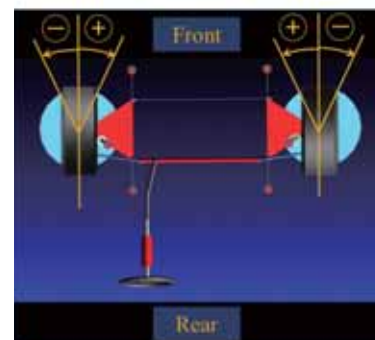


Fig. 1. Toe

the tire.

2.2 Camber

As shown in Fig. 2, camber is defined as the angle of the wheel as seen from the front of the automobile. More properly, camber is the angle between the longitudinal center line and vertical line of the wheel. Camber is related to the driving stability and grip of the tire.

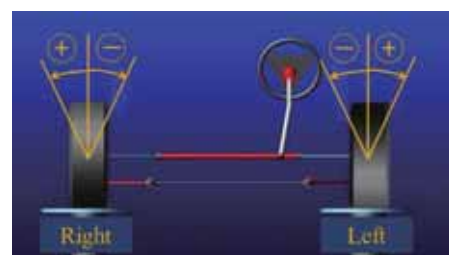


Fig. 2. Camber

3. K&C TESTING SIMULATIONS

As shown in Fig. 3, the K&C testing simulations are performed with a suspension model of MacPherson Strut, which is most widely used for passenger automobiles in the world. The suspension model consists of rigid body, damper and spring.

For both the kinematic and compliance simulations, the front and rear test are performed separately. In this paper, only the front test is considered.

In the simulations, the unloaded radius of the tire, the tire stiffness and wheel mass are respectively 300mm, 200N/mm and 10kg. Gravity is ignored.

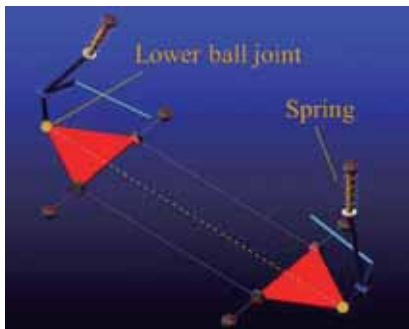


Fig. 3. MacPherson Strut

3.1 Kinematic test simulations

The kinematic test simulations are performed by controlling the displacement of contact patches, which are plates contacting the bottom of the wheels. As shown in Fig. 4, the contact patches are moved 60mm upward (bump) and 60mm downward (rebound) from the set up position. Two types of kinematic test simulations are performed. In the “double bump” tests, the right and left contact patches are moved in the same direction at the same time. On the other hand, in the “roll” tests, the right and left contact patches are simultaneously moved in opposite directions. For example, while the right contact patch goes up, the left contact patch goes down and vice versa.

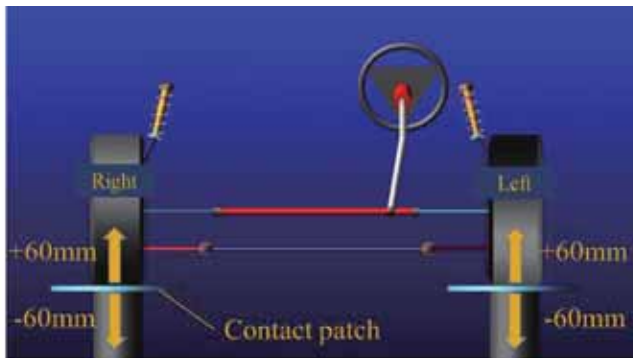


Fig. 4. Kinematic test simulations

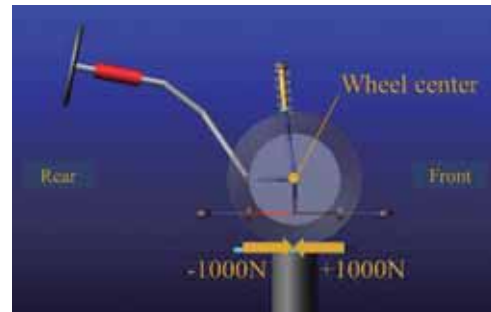
3.2 Compliance test simulations

The compliance test simulations are performed by controlling the forces applied to the contact patches in

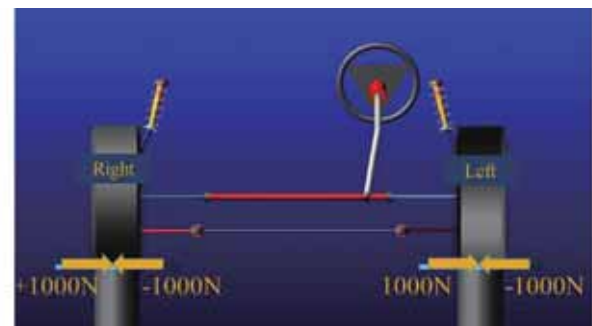
longitudinal and lateral directions. The former is referred to as the longitudinal compliance and the latter is lateral compliance. As shown in Fig. 5, Forces of 1000N are applied to the right and left contact patches in the same direction. In the longitudinal compliance test, the positive value indicates the backward force. In the lateral compliance test, the positive value indicates the leftward force.

3.3 Simulation conditions

K&C testing simulations are conducted by changing four parameters respectively. First, the distance between the right and left lower ball joints is set to 1450mm, 1500mm and 1550mm. Second, the spring stiffness is set to 40N/mm, 50N/mm and 60N/mm. Third, the installed length of spring with zero preload is set to 180mm, 190mm and 200mm. Last, the preload of the spring is set to 0N, 500N and



(a) Longitudinal



(b) Lateral

Fig. 5. Compliance test simulations

1000N.

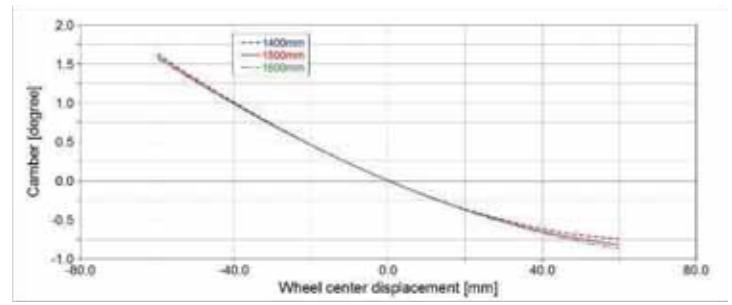
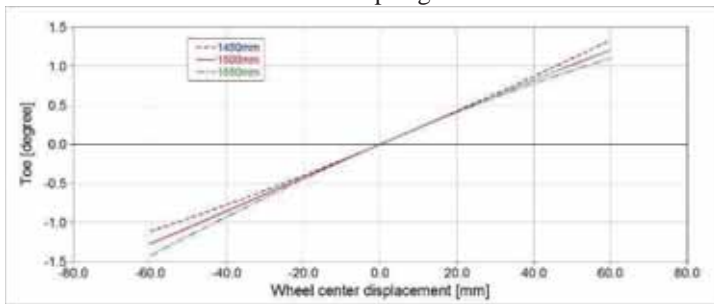
4. Results

The simulation results of the double bump tests, the roll tests, the longitudinal compliance tests and the lateral compliance tests are shown in turn. And the influence of changing four parameters is discussed.

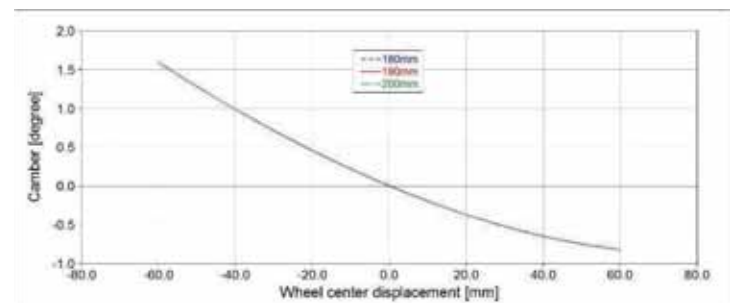
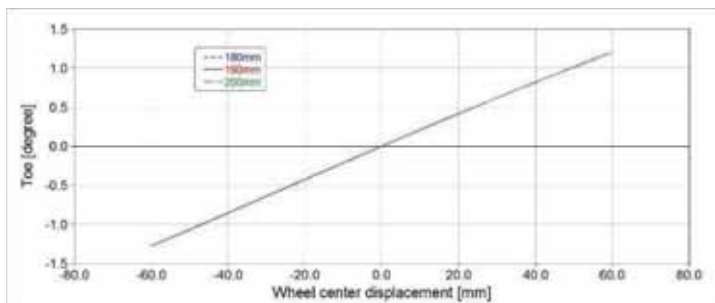
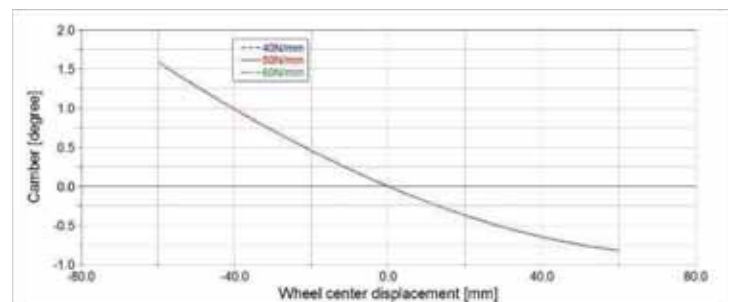
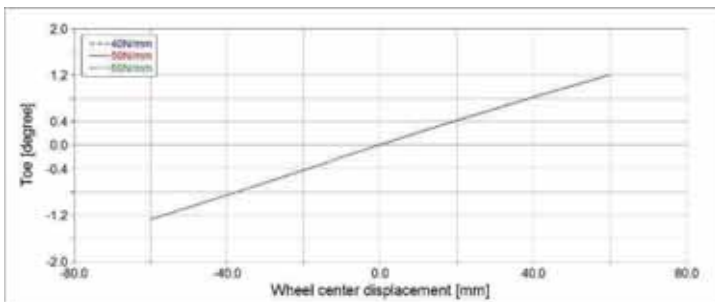
From Fig. 6 to 9, it is found that the K&C values changes depending on the configuration of a suspension body. The results of 1450mm and 1550mm are almost symmetric about those of 1500mm. The distance between the right and left lower ball joints is the most important parameter of the four.

On the other hand, the characteristic of the spring does

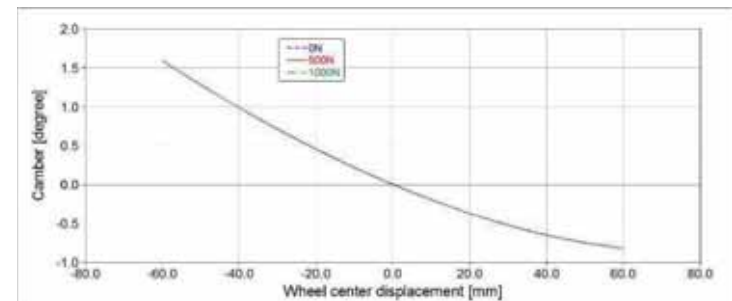
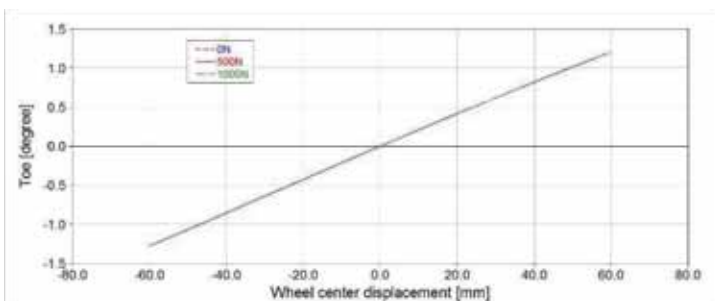
very little influence on the K&C value such as toe and camber. With related to the spring stiffness and the installed



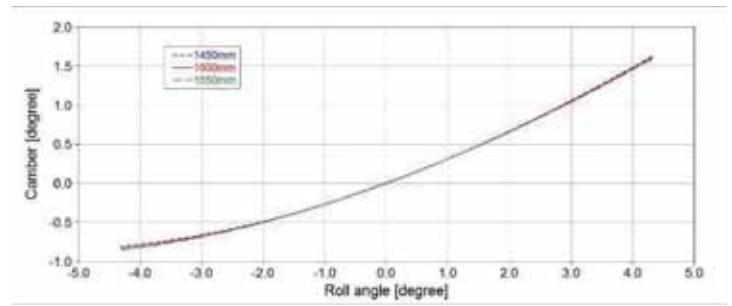
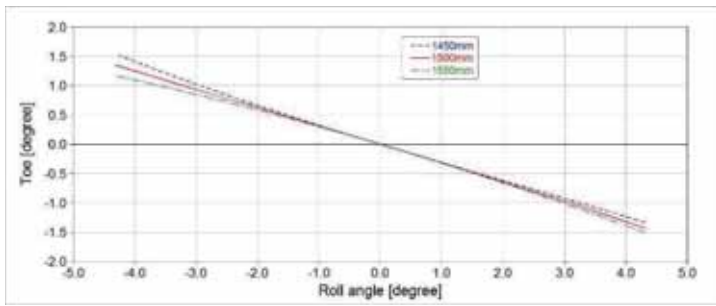
length of the spring, it is possible to say they have no influence on the K&C values.



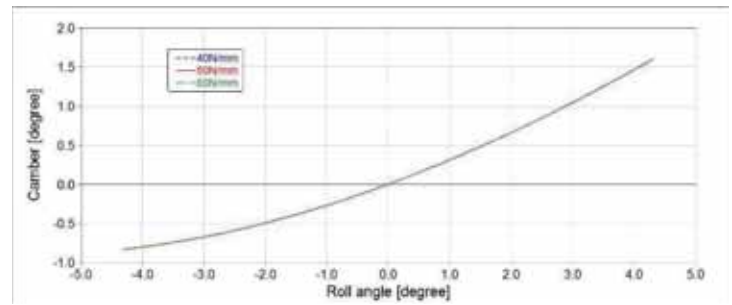
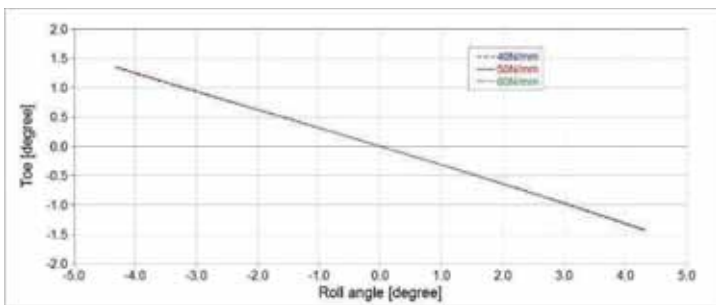
(a) Distance between the right and left lower ball joints



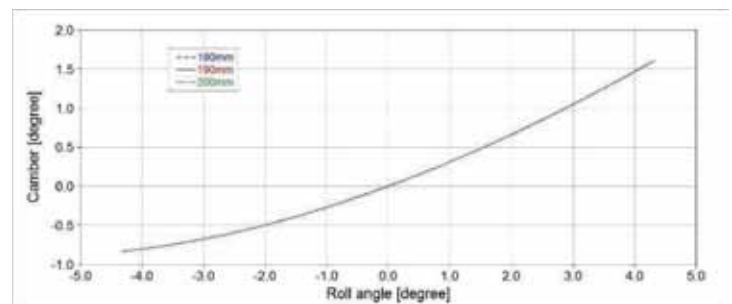
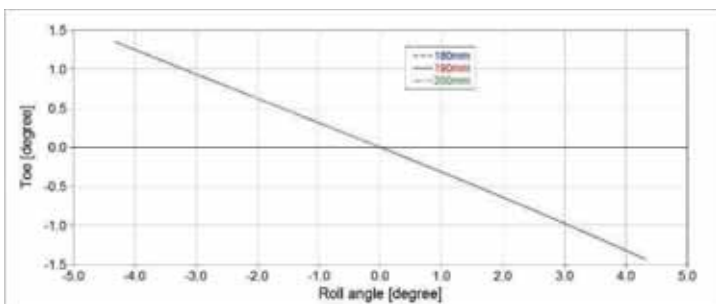
(b) Spring stiffness



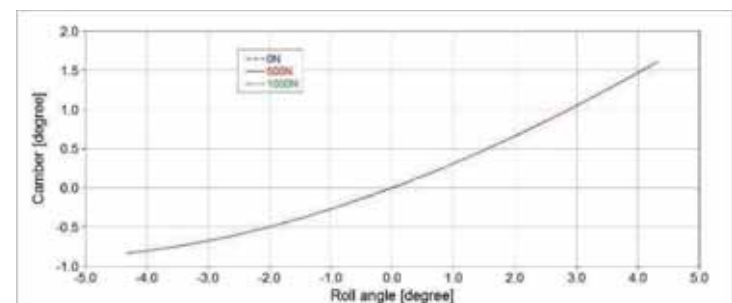
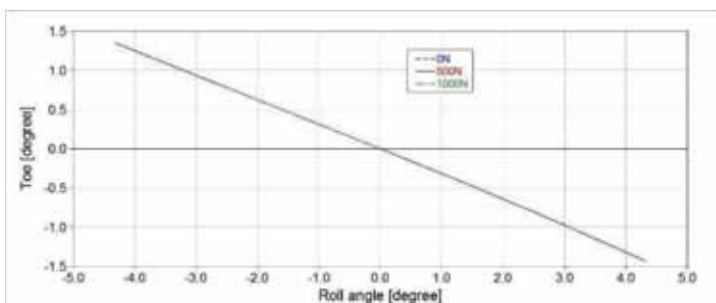
(a) Distance between the right and left lower ball joints



(b) Spring stiffness

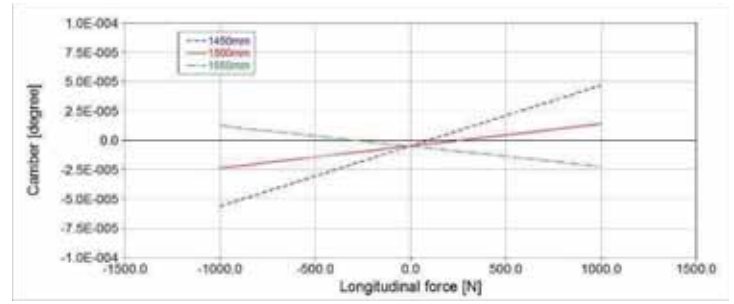
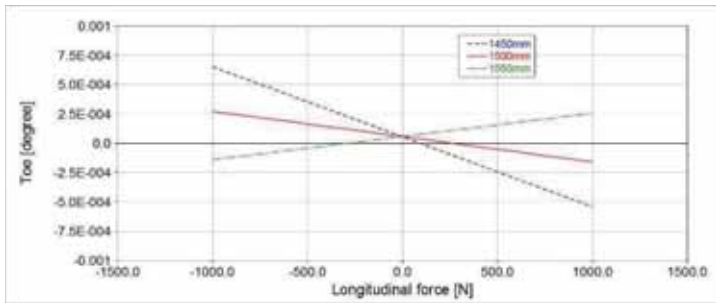


(c) Spring Installed length

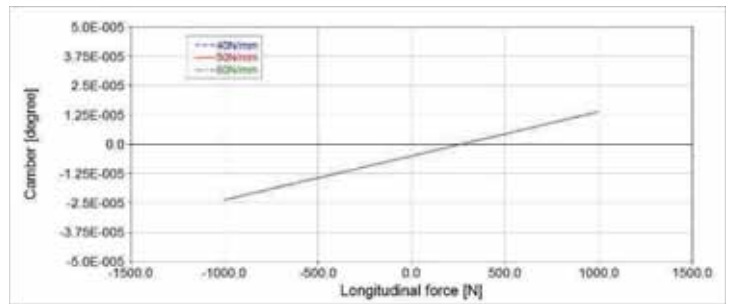
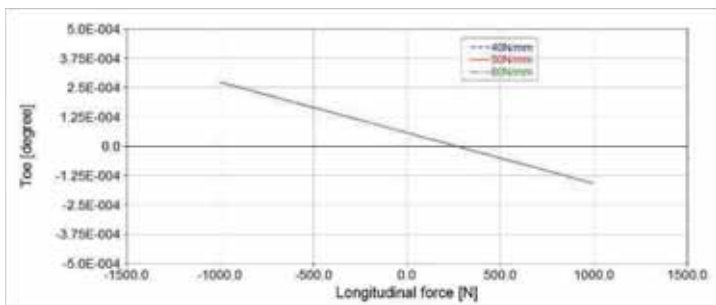


(d) Spring preload

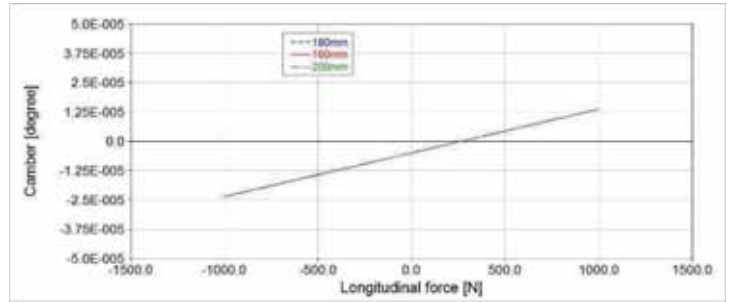
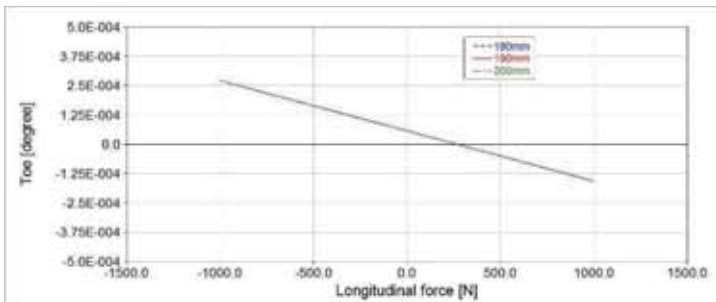
Fig. 7. Roll tests



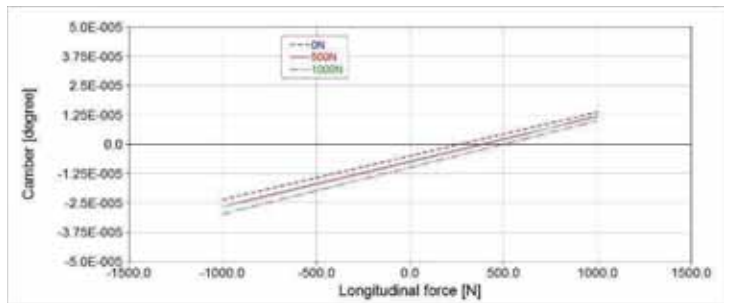
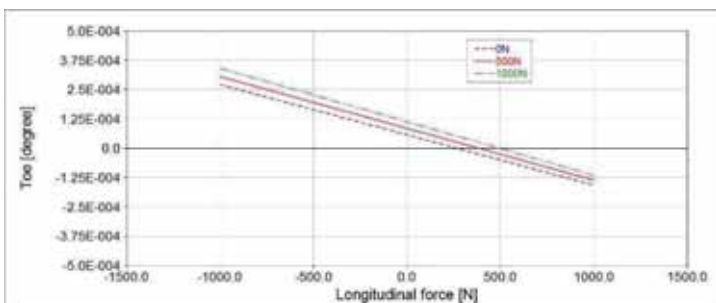
(a) Distance between the right and left lower ball joints



(b) Spring stiffness

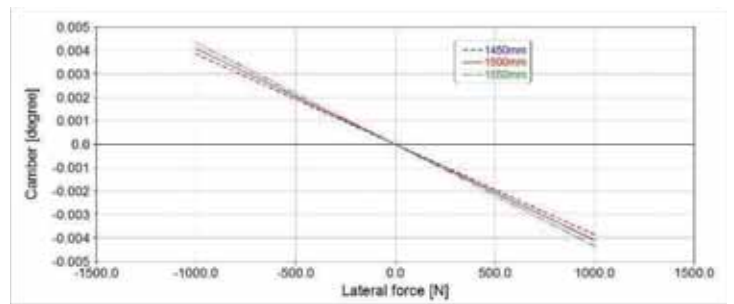
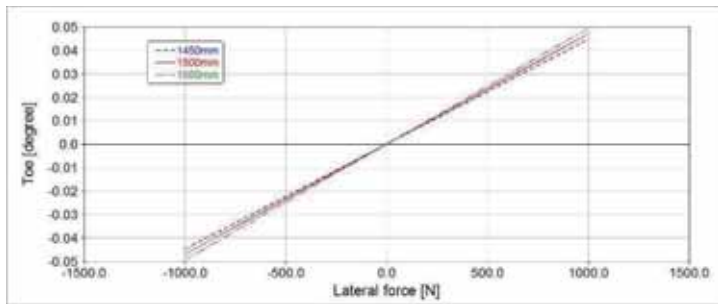


(c) Spring Installed length

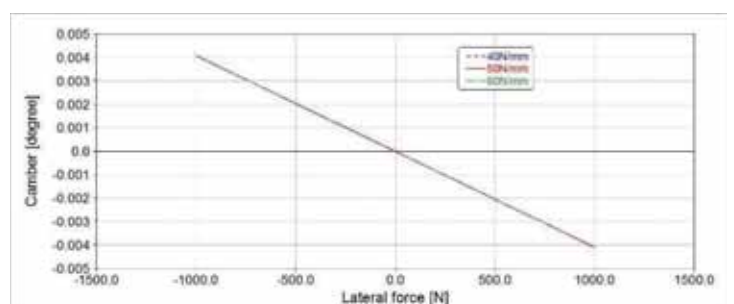
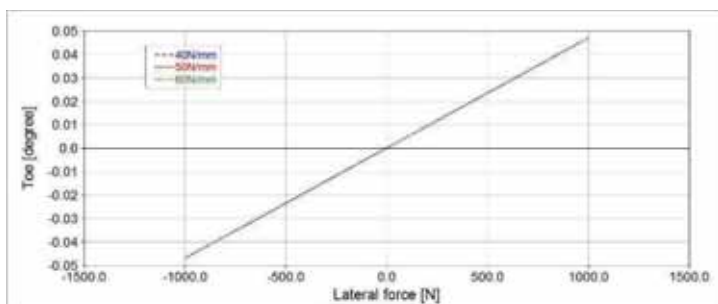


(d) Spring preload

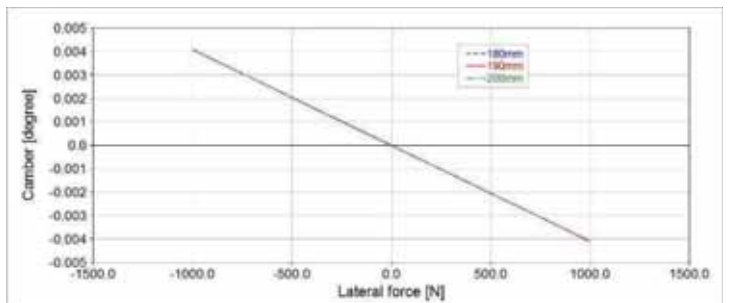
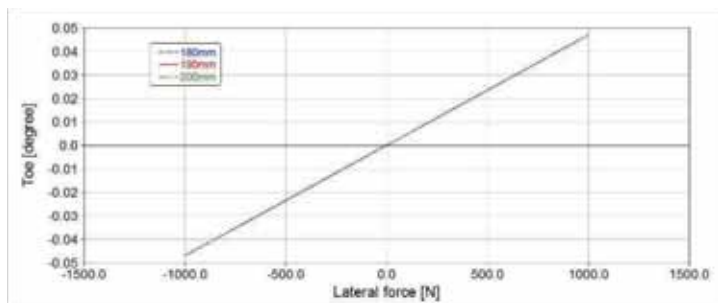
Fig. 8. Longitudinal compliance tests



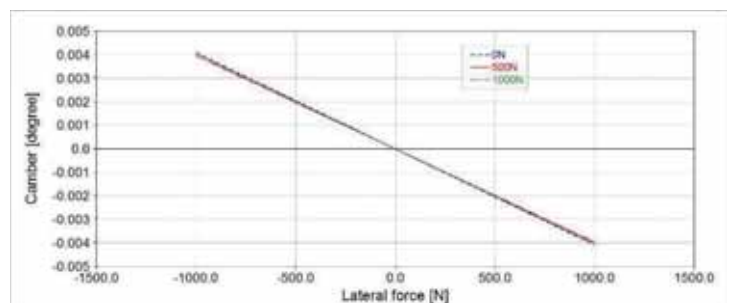
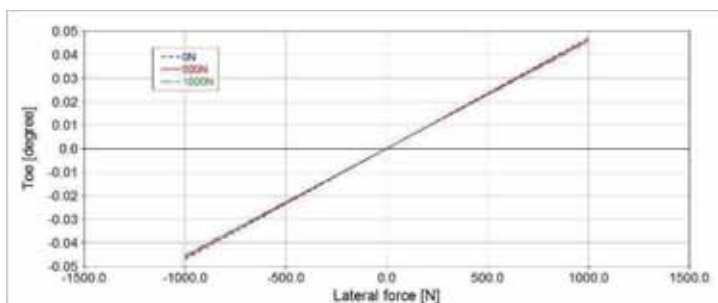
(a) Distance between the right and left lower ball joints



(b) Spring stiffness



(c) Spring Installed length



(d) Spring preload

Fig. 9. Lateral Compliance tests

.CONCLUSION

The comparison of the K&C values such as toe and camber with changing the configuration of the suspension body and the characteristics of the spring shows that the characteristics of the spring is not so important to design suspensions. The configuration of the suspension body is more important and further investigations are needed in addition to the position of the lower ball joint.

REFERENCES

- [1] Mitchell, W.C., Simons, R., Sutherland, T., and Keena-Levin, M., "Suspension Geometry: Theory vs. K&C Measurement," SAE Technical Paper 2008-01-2948, 2008
- [2] Youngwon Hahn, "Kinematics and Compliance (K&C) Simulation Using a Nonlinear Finite Element Model," SAE International 2010-01-0951, 2010

Analysis of fluid flow of molten Magnesium into micro-particles

Tomoko Ozawa

Department of Materials Science and Engineering, Nagoya University,
Tomoko.ozawa@f.mbox.nagoya-u.ac.jp

Supervisor: Katsuyo Thornton

Graduate School of Materials Science and Engineering, University of Michigan
kthorn@umich.edu

ABSTRACT

Due to investigate fluid flow molten metal through different kinds of solid particles exhibited different wettability, capillary action as driving force is defined and applied to Darcy's law. When a ratio of each particle is changed, infiltration distance is calculated. A new approach for analysis of fluid flow in different kinds of micro-particles was developed to apply Darcy's law with original assumption. According to increasing the volume fraction of alumina, the volume fraction of titanium which improves the wettability between molten magnesium and alumina particle decreases at once. Therefore, the infiltration distance also decreases, which corresponds to the experimental result qualitatively.

1. INTRODUCTION

1.1 Previous research

The pressureless infiltration method is one of the fabrication processes of composite materials. Figure. 1 shows this method model. At high temperatures, a metal melts and penetrates into the solid particle interval, and after cooling, a particle reinforced composite is fabricated. For example, Kobashi [1] examined the method to fabricate magnesium matrix composites that is reinforced with alumina particles. In this method, molten magnesium spontaneously penetrates into the solid particle interval when titanium powder is added to alumina powder because titanium powder improves the wettability between solid alumina particles to molten magnesium. It was demonstrated that a preform compound (give size) with 10vol% of titanium and 90vol% alumina was fully infiltrated by molten metal. The phenomenon of infiltration was attributed to capillary action.

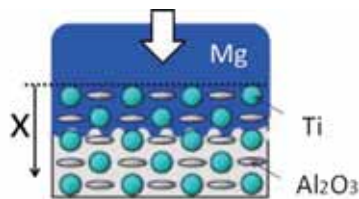


Fig.1. Image structure of and penetration.

For analysis, Darcy's law is used to model the simultaneous flow of two different fluids through a porous medium. The momentum equation, also called Darcy's law,

for the flow of a single liquid in an isotropic porous medium under isothermal conditions is

$$\frac{dx}{dt} = -\frac{K \Delta P}{\mu x} \quad (1)$$

where dx/dt is the liquid velocity and ΔP is the difference of pressure. Here, μ is the liquid viscosity, ϵ is the porosity, and K is the permeability of the porous medium according to the Kozeny-Carmen and Blake-Kozeny descriptions [2].

$$k_{KC} = c \frac{\epsilon^3}{5S_0^2(1-\epsilon)^2} \quad (2)$$

$$k_{BK} = c \frac{Dp^2 \epsilon^3}{150(1-\epsilon)^2} \quad (3)$$

Reza [3] stated that the suction pressure created at the liquid front due to capillary action is responsible for "pulling up" the liquid column along the porous medium. However, there is no analysis of fluid flow of molten metal through different kinds of solid particles exhibiting different wettability.

1.2 Objective

The purpose of this study is to determine how far molten metal penetrates into porous medium. To do this I define capillary action as a driving force by myself and then to analyze the flow of molten metal through the solid particles using Darcy's law. In this study I calculate the number ratio

of titanium to alumina particles from the volume fractions of the samples, which are measured experimentally.

2. METHODS

My analysis is based on the experimental samples of Ref.[1]. The preform is organized into Al_2O_3 and Ti particles, which have diameters of 10~20 μm and <45 μm , respectively. A typical diameter, height, relative density and weight of a preform are 16mm, 14mm, 0.4, and 4g, respectively.

For the 1D flow described in Figure.1, the capillary pressure, p_c , is created at the liquid front due to the capillary action. The relevant boundary conditions in terms of the pore averaged hydrodynamic pressure, p , are

$$\begin{aligned} P_0 &= Patm - \frac{Wg}{Ap} + \rho gx \text{ at } x = 0 \\ P_x &= Patm - P_c - \frac{Wg}{Ap} \text{ at } x = x \end{aligned} \quad (4)$$

Using Eq.4 in Eq.1 leads to

$$\begin{aligned} \frac{dx}{dt} &= \frac{K P_c}{\epsilon \mu x} \\ \frac{dx}{dt} &= \frac{K P_c + \rho gx}{\epsilon \mu x} \end{aligned} \quad (5) \quad (6)$$

where the gravity part is ignored in Eq.5,.

After the separation of variables and subsequent integration, the final implicit equation for the liquid-front height, x , in the preform as a function of time is

$$x = \sqrt{\frac{2k}{\mu} \Delta P \sqrt{t}} \quad (7)$$

$$P_c \ln \left| \frac{P_c}{P_c + \rho gx} \right| + \rho gx = \frac{\rho^2 g^2 k}{\epsilon \mu} t \quad (8)$$

Capillary action is the ability of a liquid to flow in narrow spaces without the assistance and in opposition to, external forces like gravity.

$$P_c = \frac{2\gamma_{l,v} \cos \theta}{r_p} \quad (9)$$

Where h is infiltration distance, $\gamma_{l,v}$ is surface tension of the liquid, ρ is liquid density, r_p is hydraulic radius and θ is contact angle($^\circ$). The contact angle between alumina to magnesium and titanium and magnesium are 70 and 31 degrees under 927K [4] [5].

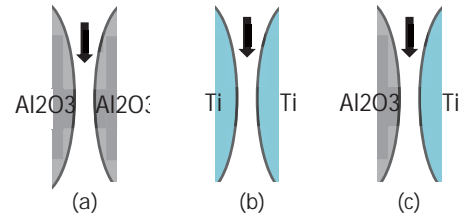


Fig.2. Type of particle combination. Type (a), (b) is the flow between the same particle and type (c) is between another particles.

When molten metal flows between particles, three scenarios are encountered. Figure.2 shows the three different scenarios and the pressure of each scenario is expressed as

$$P_{ca} = \frac{2\gamma_{l,v} \cos \theta_{Al_2O_3}}{r_p} \quad (10)$$

$$P_{cb} = \frac{2\gamma_{l,v} \cos \theta_{Ti}}{r_p} \quad (11)$$

$$P_{cc} = \frac{P_{ca} + P_{cb}}{2} \quad (12)$$

The probability of each type was defined as

$$P_c = \frac{N_{Al_2O_3}}{N_{total}} \times P_{c1} + \frac{N_{Ti}}{N_{total}} \times P_{c2} + N_{mix} \times P_{c3} \quad (13)$$

Where N is the calculated number of particles, N_{total} is the total number of particles and N_{mix} is the probability that two different particles are next to each other (e.g., titanium particle next to alumina particle). All flow analysis was performed using MathWorks by MATLAB.

3. RESULTS

3.1 Decision of N_{mix}

It is important to decide N_{mix} when calculating the capillary pressure, permeability and infiltration distance. Figure.3. shows the infiltration distance per N_{mix} . The infiltration distance extremely depends on N_{mix} . If N_{mix} is defined greater than 0.45, penetration does not happen. Conversely, if N_{mix} is less than 0.45, the infiltration distance increases. N_{mix} is visually approximately from experimental images to be 0.5. Since we need a finite infiltration distance, a value of 0.4 was chosen for N_{mix} in Eq.13.

3.2 Infiltration distance

The evolution of the liquid front distance as a function of volume fraction of alumina with and without gravity is plotted in Figures.4 and 5, respectively. Note that the slope of these plots is the velocity of penetration.

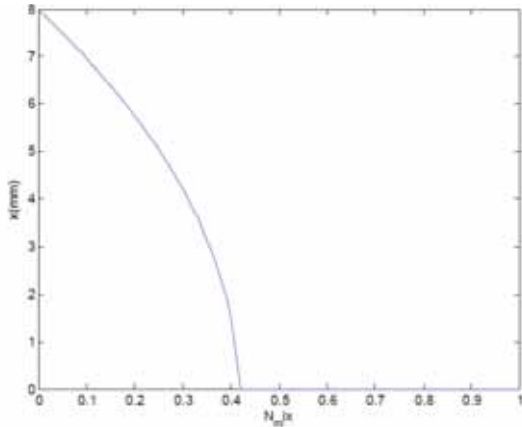


Fig.3. Infiltration distance per N_{mix} , the existence probability of combination with different particles. The volume fraction (Al₂O₃/Ti) is 0.7, and Kozeny-Carmen permeability is used.

The velocity is larger initially, however, gradually decreasing and converges to zero finally.

The Kozeny-Carmen permeability (Eq.2) and Blake-Kozeny permeability (Eq.3) were calculated to be approximately $3.78e-5$ and $6.55e-7$ [mm²]. The plot in Figure.4 (a) is similar with Figure.5 (a), by comparison, the plot in Figure.4 (b) is much different from Figure.5 (b).

It is also found that as the volume fraction of aluminum decreases, the initial velocity becomes faster and infiltration distance after 600 second becomes is larger.

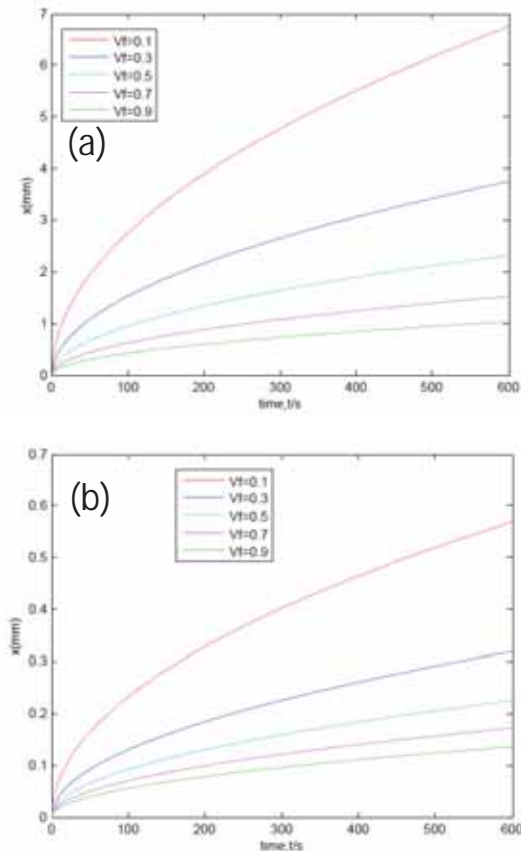


Fig.4. Infiltration distance without gravity. (a) is calculated in Kozeny-Carmen permeability, and (b) is calculated in Blake-Kozeny permeability.

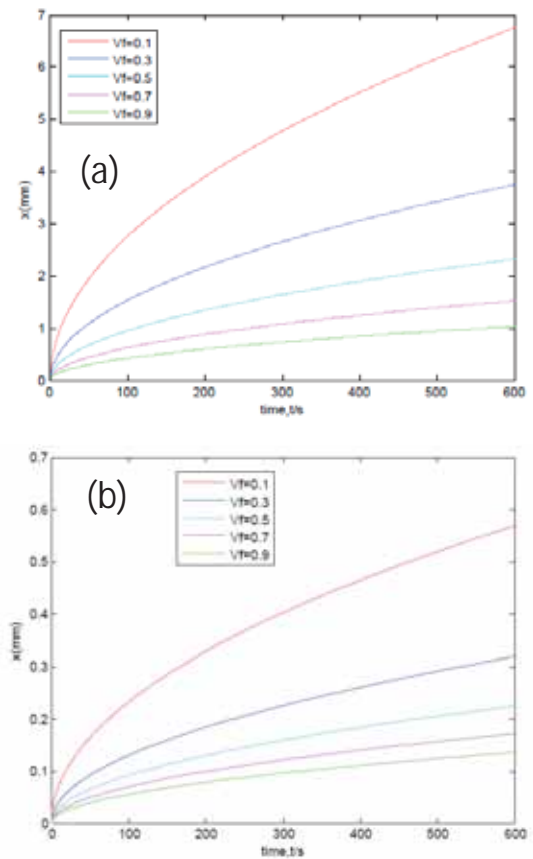


Fig.5. Infiltration distance including the effect of gravity. (a) is calculated in Kozeny-Carmen permeability, and (b) is calculated in Blake-Kozeny permeability.

4. DISCUSSION

4.1 Fluid flow into porous medium

Penetration tends to increase like a logarithmic function and gradually plateaus with progress of flow. Figure.6 shows the comparison between experimental and analytical results for the relation between the infiltration distance and the volume fraction at $t=600$ seconds [1]. It is found that the infiltration distance decreases with increasing volume fraction of alumina for both results.

However, the large discrepancies between experimental and analytical results suggest that capillary action alone is not sufficient to describe the infiltration process.

4.2 Comparison of permeability

Figure.7 shows that the plots calculated with the Kozeny-Carmen and Blake-Kozeny permeability does not correspond. It is also clear that Kozeny-Carmen is closer than the experimental result.

In previous research, Madison [6] states that in the case of low density, the Kozeny-Carmen permeability is more appropriate, since Figure.8 shows the plot of Kozeny-Carmen permeability is similar with that of current study.

On the other hand, Eq.2 and Eq.3 show that Kozeny-Carmen depends on surface area of particle, in other words, a square of particle radius and Blake-Kozeny depends on particle volume, in other words, a cube of particle radius. When particle radius is calculated with an error, the error of Blake-Kozeny might be bigger than Kozeny-Carmen.

In this research, it is appropriated to calculate the infiltration distance with Kozeny-Carmen.

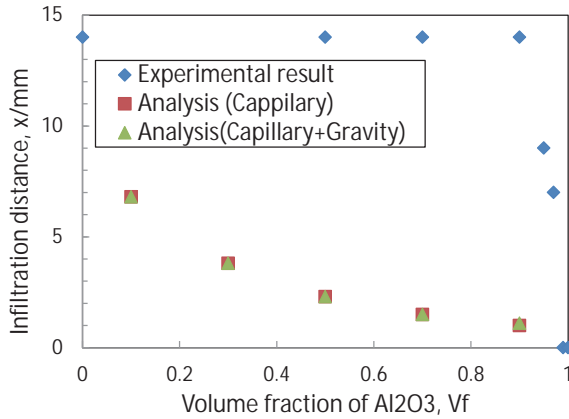


Fig.6. Comparison of experimental result with analytical result in the relation between the infiltration distance and the volume fraction at 600s.

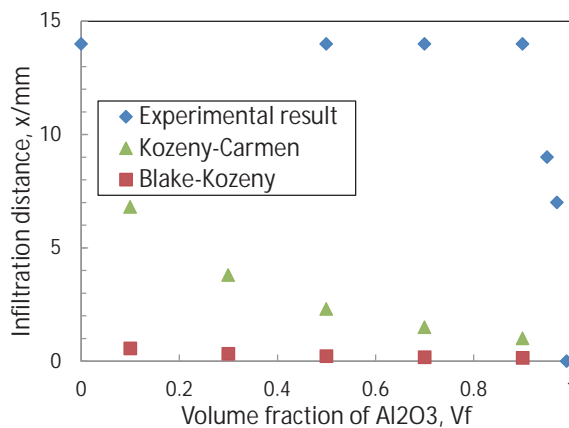


Fig.7. Comparison of the infiltration distance influenced by Kozeny-Carmen and Blake-Kozeny permeability.

4.3 Effect of gravity

In previous research, it was mentioned that the effect of gravity could be negligible. I have confirmed this in analysis, where I find the infiltration distance can be corresponded well. Penetration is that the gravity section is 10^{-5} times as less as the capillary pressure.

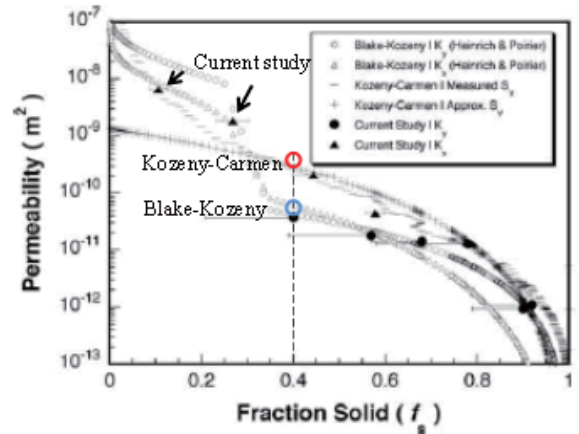


Fig.8. Calculated permeability plotted as a function of solid volume fraction with modified Kozeny-Carmen and Blake-Kozeny

4.4 Validity of definition, Nmix

The calculation of Nmix is difficult and therefore the choice of Nmix was approximated from the experimental images. Analytical results were far from those of experimental suggesting that a value of Nmix=0.4 is inaccurate. It is important to note that according to Figure.3, if Nmix is assumed smaller, analytical distance might increase to better match experimental results. It is essential to improve Nmix close to the real value.

The accuracy of the model can be further improved by considering fluid flow in a 3D array of particles and the change of viscosity that is influenced by structure. If the volume fraction of titanium increases, strength of composite increases, and if that of titanium is less, the wettability between molten magnesium decreases. For such an additional factor, the accuracy of analysis might improve more and more for the next step.

5. CONCLUSION

A new approach for analysis of fluid flow in different kinds of micro-particles was developed by applying Darcy's law with original assumptions. Penetration tends to change time and the relationship between penetration and time is logarithmic.

The results show that the penetration distance decreases as the volume fraction of alumina is increased (volume fraction of titanium decreased). Since titanium improves the wettability between molten magnesium and alumina particle, it makes sense that the infiltration distance decreases. As seen in Fig. 6, this phenomenon is well described by capillary action alone and the experimental and analytical results are in qualitative agreement.

However, in terms of the value, analytical results show values that are much less than experimental results. Therefore, it is essential to improve the assumption of

capillary action as the main driving force by considering another factor like the shape of the pore structure.

6. ACKNOWLEDGEMENTS

I would like to show my greatest appreciation to Prof. Katsuyo Thornton who provided carefully considered feedback and valuable comments. I would also like to express my gratitude to my family for their moral support and warm encouragements. Finally, I would like to express my gratitude to JUACEP for their financial support.

7. REFERENCES

- [1]. Makoto KOBASHI, Effect of preform processing conditions on microstructure and properties of Al₂O₃,Ti particle dispersed Mg matrix composite fabricated by pressureless infiltration method (2010)
- [2]. Alberto Scurati, Influence of Morphology and Packing Properties on the Permeability of Fine Particle Agglomerates
- [3]. Reza Masoodi, Hua Tan, and Krishna M. Pillai, Darcy's Law-Based Numerical Simulation for Modeling 3D Liquid Absorption into Porous Wicks
- [4]. Ping Shen, Dan Zhang, Qiao-Li Lin, Lai-Xin Shi, and Qi-Chuan Jiang, Wetting of polycrystalline α -Al₂O₃ by molten Mg in Ar atmosphere (2010)
- [5]. Masashi Kawakami, Hisashi Imai, Junko Umeda, Hidetoshi Fujii, Wettability of pure Ti by molten pure Mg droplets, Katsuyoshi Kondoh (2010)
- [6]. J. Madison, J. Spowart, D. Rowenhorst, L.K. Aagesen, K. Thornton, T.M. Pollock, Modeling fluid flow in three-dimensional single crystal dendritic structures

DEVELOPMENT OF A VIBRATION EXCITATION SYSTEM FORCED ON PIEZOELECTRIC ELEMENTS

Hiroki Shigematsu

Graduate School of Engineering, Nagoya University
h_shigematsu@nuem.nagoya-u.ac.jp

Supervisor: Bogdan Eupreanu

Department of Mechanical Engineering, University of Michigan
epureanu@umich.edu

ABSTRACT

For excitation of the structure, the model which uses piezoelectric elements has defined. The model is mainly divided into two parts, clamp part and piezoelectric part. We use simple steel beam as vibration objective. By clamping the specimen and adding voltage to piezoelectric elements, we excite specimen. In this report, we searched modal shapes of the whole model, model without specimen, and specimen. And by changing properties of the specimen, we searched worst vibrate case of the model. And we proposed suppression method of the clamp by adding piezoelectric patch on the upper part of the clamp.

1. BACKGROUND

To measure the forced response of structures with complex geometry, appropriate experimental methods are required to provide excitation. Some of the current practices utilize speakers or provide mechanical excitation via pressure waves. However, this method is not practical for excitations at high frequencies due to the large amount of power required by the speaker system. The large power is available, but it comes at the cost of large size, which makes the acoustic approach impractical for structures with complex geometry.

An Alternate approach is the use of stingers to provide direct forces to the excited structure. However, these methods require contact between the excitation (stinger) to the structure being tested. Hence, the properties of the structure may be changed due to its interaction with the stinger.

An alternate, novel concept has been defined by Professor Eupreanu to address these issues. The novel concept is based on use of piezoelectric stacks to provide excitation. The concept calls for these stacks to be incorporated into a clamping mechanism that will place the piezoelectric stacks in contact with the structure (at two contact points on opposite sides of the structure) so that their

applied forces are collinear, equal, opposite, and (as much as possible) perpendicular to the surface of the structure at the contact points. The concept also calls for a thin force sensor to be attached to the ends of the piezoelectric stacks where they come in contact with the structure.

2. OBJECTIVE

My research objective is simulation of vibrational suppression of the structure using ANSYS, a engineering simulation software based on FEM. A computer model must be developed prior to the clamp, and computational results must be obtained prior to building the clamp. Also, a system for suppressing vibration of the excitation clamp must be designed and its operation must be simulated. The clamp provides excitation (vibration) by using piezoelectric stacks but to measure accurate response from specimen, (the structure which we want to know the forced response) it is necessary to suppress the clamp which provides excitation.

This research's specific target is to search bending shapes of the model especially upper jaw and suppress the vibration by adding piezoelectric patch to upper jaw part.

3. INTRODUCTION OF MODEL

We use ANSYS, a engineering simulation software based on FEM, to simulate the model. Fig.1 and Fig.2 shows the generated simulation model by ANSYS. Fig.3 shows the prototype model. The model is consist of aluminium alloy(upper jaw and body), stainless steel (bolts and cylinder), piezoelectric elements, and structural steel (specimen). Fig.4 shows the model with piezoelectric patch to suppress upper part of the clamp.

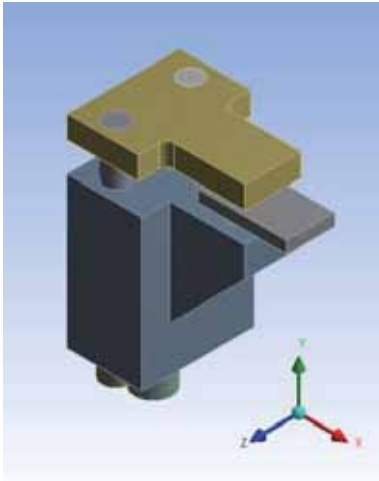


Fig.1 Whole model 1

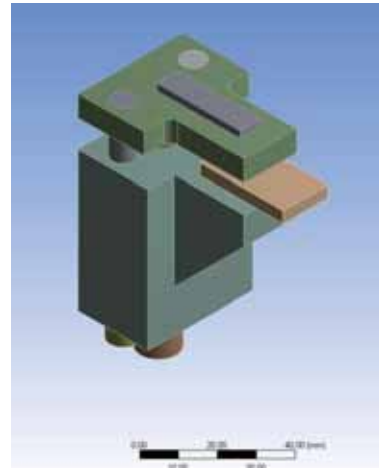


Fig.4 Model with piezoelectric patch

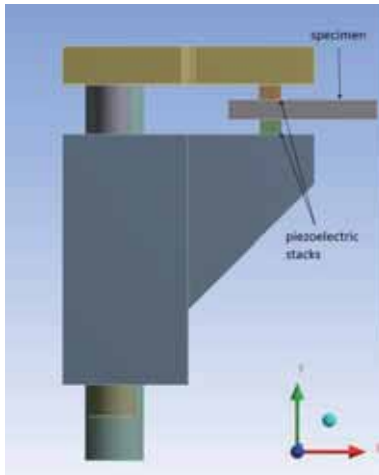


Fig.2 Whole model 2



Fig.3 Prototype model

4 MODAL AND HARMONIC ANALYSIS OF MODEL

4.1 MODAL ANALYSIS OF WHOLE MODEL

I simulated modal analysis of the whole model. I added 100[V] voltage at piezoelectric stacks both upper and lower ones to excite specimen. I got the mode shape of the 15 pieces in order from low frequency. Fig.5~Fig.7 shows the picked total displacement results of mode analysis. I picked up the shapes which both specimen and upper jaw moved much.

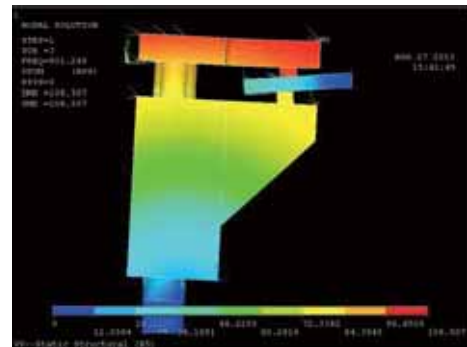


Fig.5 Modal shape at 901[Hz]

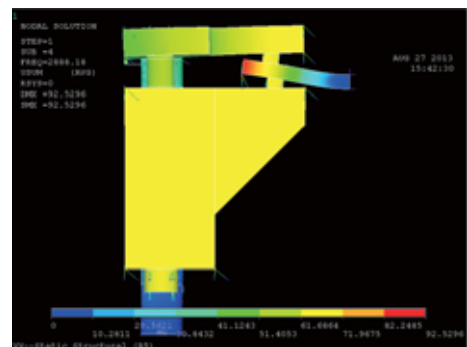


Fig.6 Modal shape at 2881[Hz]

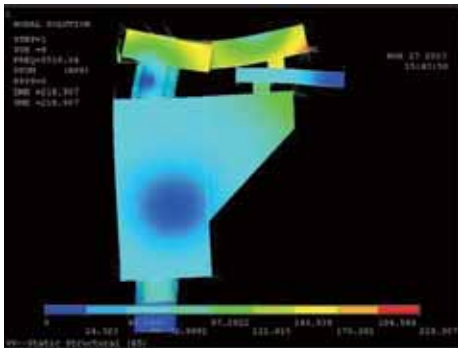


Fig.7 Modal shape at 14058[Hz]

4.2 MODAL ANALYSIS OF SPECIMEN

At the previous section, desired modal shape's resonance frequency was higher than target frequency range. Then I checked the modal shapes of the specimen by reducing its density. Fig. shows specimen's first modal shape, and resonance frequency was 8049.6[Hz]. The yielded resonance frequency was so high that I reduced young's modulus of the specimen(structural steel) by 1/100. Fig shows the first modal shape of the specimen by changing the young's modulus. And the resonance frequency was 359.99[Hz]. I could yield reasonable frequency value.

Table.1 Specimen's property and its first modal shape frequency

density	E(Young's modulus)	Resonance frequency of first mode[Hz]
1/5	original	8049.6
original	1/100	359.99

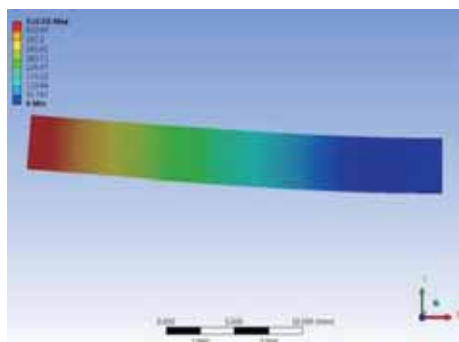


Fig.8 First modal shape of the specimen

4.3 HARMONIC ANALYSIS RELATED TO RESONANCE FREQUENCY OF THE SPECIMEN

I did harmonic analysis of the whole model to yield peak displacement of the model. Fig.9 shows the picked points. Fig.10 ~Fig.12 shows displacement of the picked points. There were no peak around 359[Hz], resonance frequency of the specimen. Then I changed frequency range and Fig.13 ~Fig.15 also shows displacement of the picked points. There can be found peak displacement around 837[Hz].

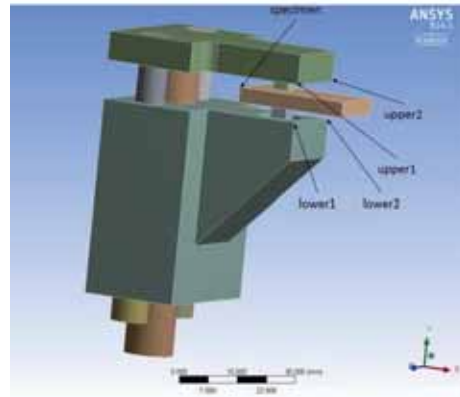


Fig.9 Picked points of the model

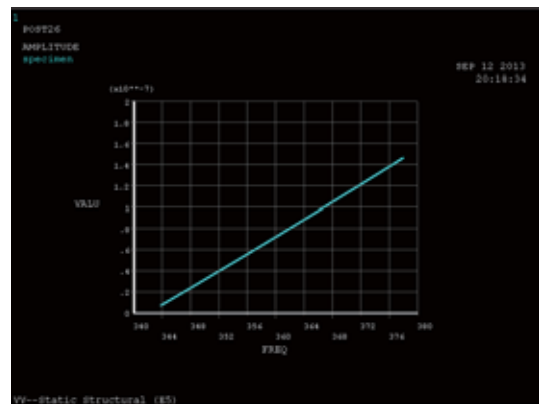


Fig.10 Displacement of the specimen(334~377[Hz])

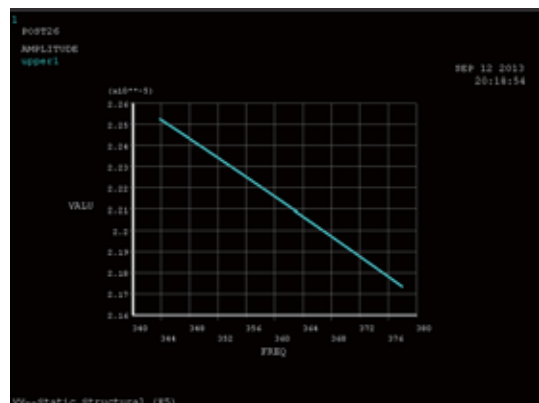


Fig.11 Displacement of upper1(334~377[Hz])

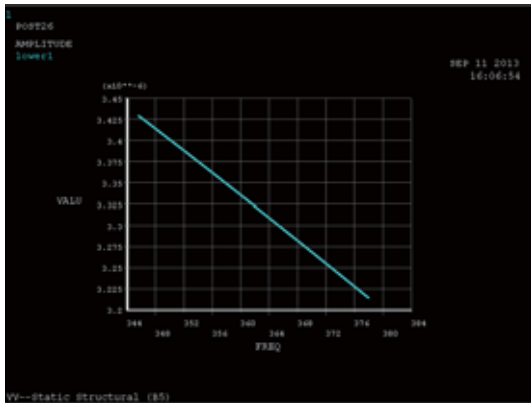


Fig.12 Displacement of lower1(334~377[Hz])

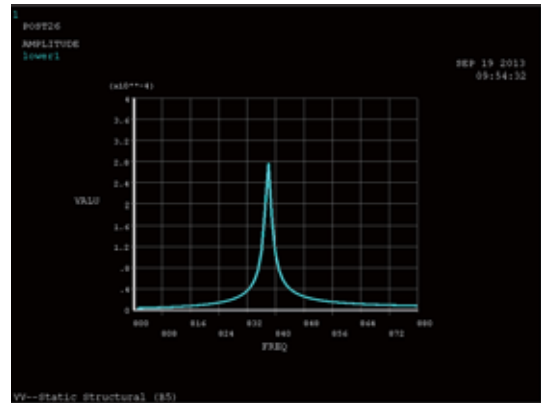


Fig.15 Displacement of lower1(800~880[Hz])

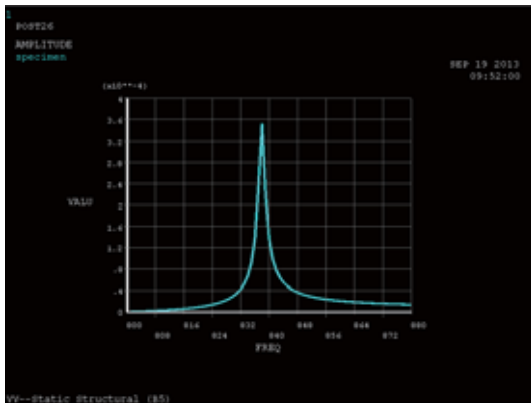


Fig.13 Displacement of specimen(800~880[Hz])

4.4 MODAL ANALYSIS WITHOUT SPECIMEN

I checked the modal shapes of the whole model without specimen. In this modal analysis, prestress are not added and connection between bolts and upper jaws, bolts and bodies are changed to be bonded. I picked up some modal shapes which upper jaw moves much. Fig.16~Fig.18 shows picked up modal shapes.

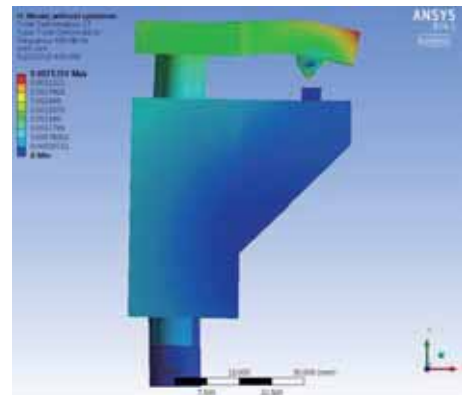


Fig.16 Modal Shape without specimen(650[Hz])

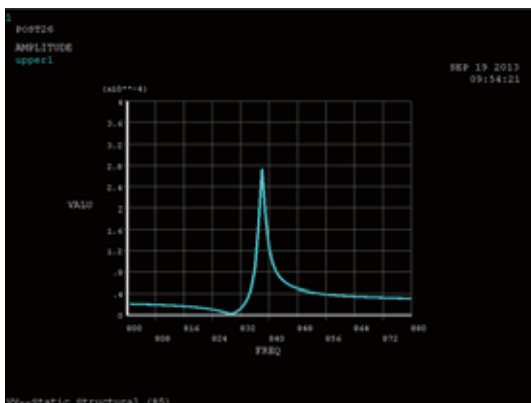


Fig.14 Displacement of upper1(800~880[Hz])

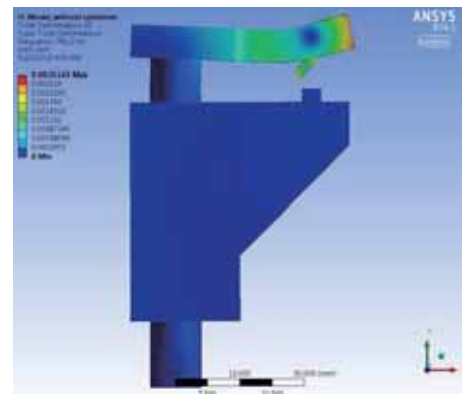


Fig.17 Modal Shape without specimen(742[Hz])

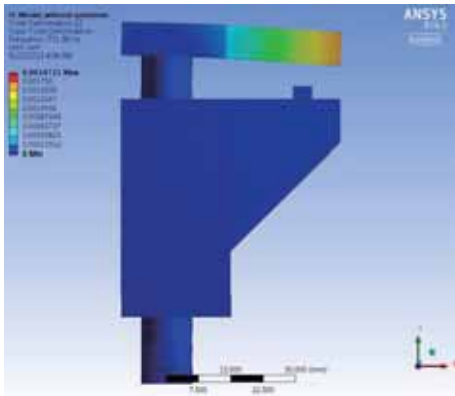


Fig.18 Modal Shape without specimen(771[Hz])

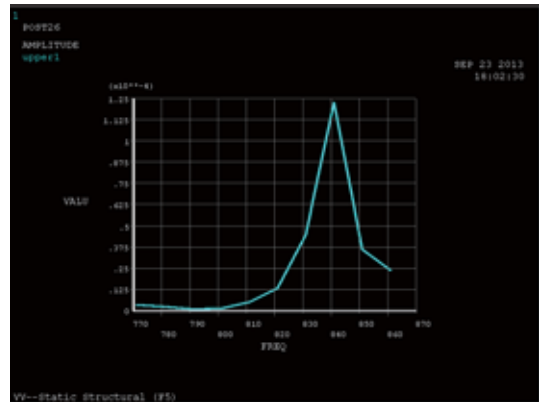


Fig.21 Displacement of lower1(871~861[Hz])

4.5 WORST CASE ANALYSIS

From previous section, I got a modal shape without specimen and I matched specimen's first modal shape at the frequency. I implemented harmonic analysis of whole model using the results of previous section. I expected that I get worst deformation case at 771[Hz] because both only specimen and whole model without specimen have their own modal shape around 771[Hz]. Fig.19 ~ Fig.21 shows displacements of picked points. Fig. and Fig. shows shapes of the whole model at picked frequency. The peak displacement occurred at around 838[Hz].

4.6 CHEKING MOVEMENTS OF THE PATCH

In this section, I show movements of the piezoelectric patch to suppress the upper part of the model. I added 100[V] voltage to horizontal direction of Fig.22. And frequency of input voltage is 838[Hz].

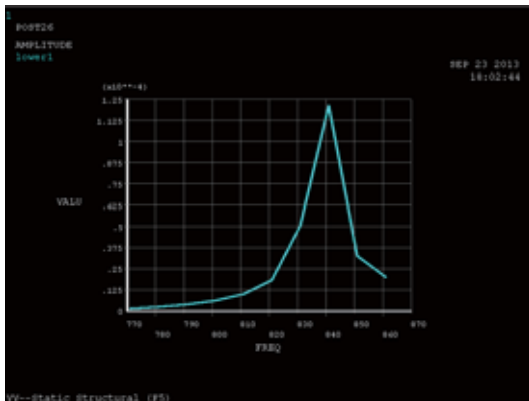


Fig.19 Displacement of specimen(871~861[Hz])

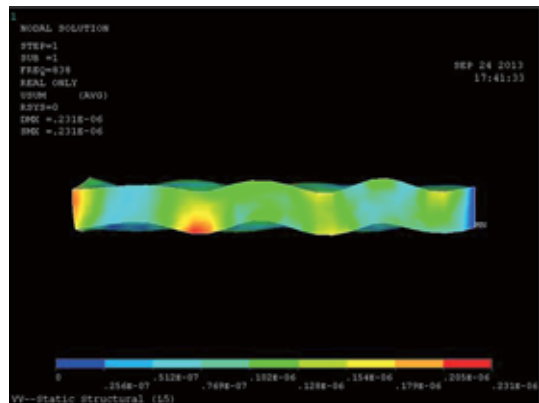


Fig.22 Displacement of piezoelectric patch(838[V])

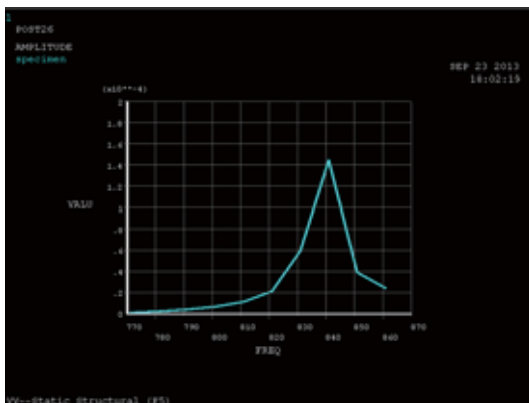


Fig.20 Displacement of upper1(871~861[Hz])

5 DISCUSSION

In section 4.1, I did modal analysis of the whole model and checked desired shapes to suppress but the frequency was higher than target frequency range. Then I changed density and Young's modulus of the specimen to reduce its own resonance frequency. And I simulated harmonic analysis of the whole model using property changed specimen to yield desired shapes in lower and near resonance frequency of the specimen. But Fig.10 ~Fig.12 shows there were no peak around specimen's resonance frequency. I considered that was because effects of the clamp and prestress were so bigger than specimen itself and specimen was too soft by changing the specimen's property.

Then I did modal analysis without specimen and picked the desired modal shape and its frequency. Fig. shows its shape and frequency. After that I tuned specimen's E to fit its

first modal shape's frequency as frequency which was found by modal analysis without specimen. Then I did harmonic analysis of the whole model around the frequency to get worst case vibration shape. But Fig.19 ~Fig.21 shows that peak occurred at around 838[Hz]. That frequency is almost same as the harmonic analysis's results before changing specimen's property.

Although changing property of the specimen, the peak displacement's frequency were almost same. From this results, it is considered that there is much dependence on resonance frequency of the clamp. But clamp's resonance frequency was around 771 [Hz], it is not same as peak frequency of harmonic analysis of the whole model (838[Hz]). Then I considered that there was some errors to simulate modal analysis without specimen and correct frequency of modal shape without specimen is around 838[Hz].

In section4.6, I checked the movements of the piezoelectric patch by adding 838[Hz], 100[V] voltage. I expected to shrink and expand to horizontal direction in Fig.22 but it moved like twisting. I also tried to do at the lower frequency such as 100[Hz], then the patch moved desired direction. The reasons for this result is considered that the 838[Hz] frequency was close to piezoelectric patch's resonance frequency. But by changing frequency higher than 838[Hz], also weird response occurred. Then I thought there are some modal shapes from certain frequency and movements of the patch was depended on that shape at high frequency range.

ACKNOWLEDGEMENTS

I would like to express the deepest appreciation to my Prof. Bogdan Epureanu who has shown the attitude and the substance of a genius. He also taught and led me not only on research but also general life during this short term. I would like to thank Enos Song who worked with me as a same research member. His knowledge helped me a lot especially using the FEM software. And I also would like to thank all members of Epureanu research group. They helped me a lot to stay comfortable in the lab.

In addition, I also thank University of Michigan, Nagoya university, and JUACEP office to offer such a great opportunity and financial aids.

TAPERED ETCH PROFILE

Shunji Shibata

Department of Mechanical Engineering, Graduate School of Engineering, Nagoya University
shibata.shunji@h.mbox.nagoya-u.ac.jp

Supervisor: Euisik Yoon

Mechanical Engineering, University of Michigan
epureanu@umich.edu

Undisclosed

EVALUATION OF AURICULAR BIOMECHANICAL PROPERTY BY FEM

Shun Tamamura

Department of Biomechanics Engineering, Nagoya University, Japan
Tamamura.shun@h.mbox.nagoya-u.ac.jp

Supervisor: Prof. Scott Hollister

Biomedical Engineering, University of Michigan
scottho@umich.edu

ABSTRACT

Several treatments exist for reconstruction of under developed auricle because of microtia, anotia, trauma, and so on. However, these options have challenges and drawbacks respectively. Tissue engineering has been proposed as an alternative to these current treatments. Using scaffolds made by biodegradable materials is given as one of the tissue engineering method. It is important to understand the mechanical properties of normal auricular tissue in order to develop superior and suited scaffold. This study aimed to evaluation of auricular properties with results of human and porcine auricle data in previous research by finite element method software. I created unconfined compressive tests model using Mooney-Rivlin material and performed simulation of these. I could got relationship strain versus reaction force respectively.

Undisclosed

CALIBRATION OF A STRAIN GAUGE FOR FORCE MEASUREMENT IN A PALATAL EXPANDER

Takayuki Yamada

Department of Micro-Nano Systems Engineering, Nagoya University, Japan
Yamatataka3320@gmail.com

Supervisor: Yogesh Gianchandani

Electrical Engineering and Computer Science, University of Michigan
yogesh@eecs.umich.edu

ABSTRACT

“Palatal expander” is an orthodontic appliance which has been used in the treatment of maxillary deficiency. The forces produced during rapidly maxillary expansion by a palatal expander vary from patient to patient. This work investigates the use of force sensors in conjunction with microprocessors and wireless data telemetry for individualized results. Our group is responsible for implementation of a transducer to measure the expansion forces. In this study, I successfully obtained the relationship between force and sensor outputs.

Undisclosed

CHARACTERIZATION OF MOLDED SUPERHYDROPHOBIC SURFACES

Takafumi Hattori

Department of Mechanical Science and Engineering, Graduate School of Engineering, Nagoya University
hattori@ume.mech.nagoya-u.ac.jp

Supervisor: Chang-Jin "CJ" Kim

Mechanical and Aerospace Engineering Department, Henry Samueli School of Engineering and Applied Science
University of California, Los Angeles (UCLA)
cjkim@ucla.edu

ABSTRACT

Important challenges in the research and development of superhydrophobic (SHPo) surfaces include low-cost fabrication of large areas. In terms of regular pattern manufacturing, hot embossing is known as a promising mass production method due to its low cost, high speed, and high throughput. To help mass production of SHPo surfaces, we experimentally examined the effects of the processing parameters for thermoplastic hot embossing using a micromachined silicon mold. By developing a technique to obtain cross-sectional images of the molded product, we confirmed the shrinkage of the molded pattern from the master pattern was minimal. The height of the molded microstructures was only 3.6 % smaller than that of the original master pattern, encouraging further development.

Undisclosed

How split Bregman can apply for non-negative matrix factorization

Yoko Okuda

Department of Computer Science and Engineering, Graduate School of Engineering, Nagoya University

y-okuda@na.cse.nagoya-u.ac.jp

Supervisor: Professor Stanley Osher

Department of Mathematics, University of California, Los Angeles

sjo@math.ucla.edu

ABSTRACT

Dimensionality reduction is widely used in the signal processing, computational machine learning and other applications. For this problem non-negative matrix factorization is needed and it changed to l_1 -regularized convex optimization problems, which have received much attention recently because of the introduction of computer sensing. It allows images and signals to be reconstructed from small amounts of data. One of efficient methods for this problem is "split Bregman". During my stay at UCLA, I focused on studying "split Bregman" method. This paper first describes convex optimization for Lagrange and duality. Then Bregman and split Bregman method are introduced. Finally one of their applications, hyperspectral image, is applied to non-negative matrix factorization and this problem is changed for convex optimization solving by split Bregman.

1. INTRODUCTION

Dimensionality reduction has been widely studied in the signal processing and computational learning communities. One of the major drawbacks of virtually all popular approach for dimensionality reduction is the lack of physical meaning in the reduced dimension space. Rank revealing QR factorization, which I study in my undergraduate, is the one of the efficient method to reduce the dimension. However, it does not take non-negative constraint in account. Non-negative factorization is applied for convex optimization

problem and it is solved by split Bregman or alternating minimization approach. In 1966, Bregman iterative method is introduced by L. M. Bregman [2]. Bregman iteration was first used in image processing by Osher et al. in [11] in 2005 and split Bregman is defined by Tom Goldstein and Stanley Osher [8] in 2009.

This paper is organized as follows. First, convex optimization and how to solve this problem by Lagrange and duality is described in section 2. In section 3 Bregman iterative method and split Bregman method are described and finally one of its applications, hyper spectral image for non-negative matrix factorization, is introduced.

2. CONVEX OPTIMIZATION

In this section optimization problem and convex optimization problem is described. And then lagrange and duality is introduced.

2.1. OPTIMIZATION PROBLEM

A mathematical optimization problem, or just optimization problem, has the form

$$\begin{aligned} & \text{minimize } f_o(x) \\ & \text{subject to } f_i(x) \leq b_i, i = 1, \dots, m \end{aligned}$$

Here the vector $x = (x_1, x_2, \dots, x_n)$ is the optimization value of the problem, the function $f_0: \mathbf{R}^n \rightarrow \mathbf{R}$ is the objective function, the functions $f_i: \mathbf{R}^n \rightarrow \mathbf{R}, i = 1, \dots, m$ are the (inequality) constraint functions, and the constants b_1, \dots, b_m are the limits, or bounds, for the constraints. A vector x^* is called optimal or a solution of this problem if it has the smallest objective value among all vectors that satisfy the constraints: for any z with $f_1(z) \leq b_1, \dots, f_m(z) \leq b_m$, it follows that $f_0(z) \geq f_0(x^*)$.

2.2. CONVEX FUNCTION

A convex optimization problem is one in which the objective and constraint functions are convex, which means they satisfy the inequality

$$f_i(\alpha x + \beta y) \leq \alpha f_i(x) + \beta f_i(y)$$

for all $x, y \in \mathbf{R}^n$ and all α, β with $\alpha + \beta = 1, \alpha \geq 0, \beta \geq 0$.

If the objective and constraint functions f_0, \dots, f_m are linear, i.e., satisfy

$$f_i(\alpha x + \beta y) = \alpha f_i(x) + \beta f_i(y)$$

for all $x, y \in \mathbf{R}^n$ and all $\alpha, \beta \in \mathbf{R}$. This problem is called linear program.

2.3. LAGRANGE AND DUALITY

An optimization problem is considered in the standard form:

$$\begin{aligned} & \text{minimize } f_0(x) \\ & \text{subject to } f_i(x) \leq b_i, i = 1, \dots, m \\ & \quad \quad \quad h_i(x) = 0, i = 1, \dots, m \end{aligned} \quad (1)$$

with variable $x \in \mathbf{R}^n$.

The basic idea in Lagrangian duality is to take the constraints in (1) into account by augmenting the objective function with a weighted sum of the constraint functions.

Lagrangian is defined by $L: \mathbf{R}^n \times \mathbf{R}^m \times \mathbf{R}^p \rightarrow \mathbf{R}$ associated with the problem (1) as

$$L(x, \lambda, \nu) = f_0(x) + \sum_{i=1}^m \lambda_i f_i(x) + \sum_{i=1}^p \nu_i h_i(x)$$

with $\text{dom}L = \mathcal{D} \times \mathbf{R}^m \times \mathbf{R}^p$ where $\mathcal{D} = \bigcap_{i=1}^m \text{dom} f_i \cap \bigcap_{i=1}^p \text{dom} h_i$. λ_i is the Lagrange multiplier associated with the i th inequality constraint $f_i(x) \leq 0$; similarly ν_i is also the Lagrange multiplier associated with the i th equality constraint $h_i(x) = 0$. The vectors λ and ν are called the dual variables or Lagrange multiplier vectors associated with the problem (1).

The Lagrange dual function (or just dual function) $g: \mathbf{R}^m \times \mathbf{R}^p \rightarrow \mathbf{R}$ is defined as the minimum value of the Lagrangian over x : for $\lambda \in \mathbf{R}^m, \nu \in \mathbf{R}^p$,

$$\begin{aligned} g(\lambda, \nu) &= \inf_{x \in \mathcal{D}} L(x, \lambda, \nu) \\ &= \inf_{x \in \mathcal{D}} (f_0(x) + \sum_{i=1}^m \lambda_i f_i(x) + \sum_{i=1}^p \nu_i h_i(x)) \end{aligned}$$

When the Lagrange is unbounded below in x , the dual function takes on the value $-\infty$. Since the dual function is the pointwise infimum of a family of the affine functions of (λ, ν) , it is concave, even when the problem (1) is not convex. The dual function yields lower bounds on the optimal value p^* of the problem (1): For any $\lambda \geq 0$ and any ν ,

$$g(\lambda, \nu) \leq p^*. \quad (2)$$

This important property is easily verified. Suppose \tilde{x} is a feasible point for the problem (1), i.e., $f_i(\tilde{x}) \leq 0, h_i(\tilde{x}) = 0$, and $\lambda \geq 0$. Then it follows that

$$\sum_{i=1}^m \lambda_i f_i(\tilde{x}) + \sum_{i=1}^p \nu_i h_i(\tilde{x}) \leq 0,$$

since each term in the first sum is nonpositive, and each term in the second term is zero, and therefore

$$L(\tilde{x}, \lambda, \nu) = f_0(\tilde{x}) + \sum_{i=1}^m \lambda_i f_i(\tilde{x}) + \sum_{i=1}^p \nu_i h_i(\tilde{x}) \leq f_0(\tilde{x}).$$

Hence

$$g(\lambda, \nu) = \inf_{x \in D} L(x, \lambda, \nu) \leq L(\tilde{x}, \lambda, \nu) \leq f_0(\tilde{x}).$$

Since $g(\lambda, \nu) \leq f_0(\tilde{x})$ holds for every feasible point \tilde{x} , the inequality (2) follows. This section is referred from [1].

3. SPLIT BREGMAN

Split Bregman is applied from Bregman method [2].

3.1. BREGMAN METHOD

In 1996, an iterative method of finding the common point of convex sets is introduced by L.M. Bregman. This method can be also applied to the approximate solution of problems in linear and convex programming.

Suppose some family of closed convex sets A_i , $i \in I$ where I is some set of indices are given in a linear topological space X . And also assume that $R = \bigcap_{i \in I} A_i$ is not empty. It is required to find some point of the intersection of the sets A_i . Let $S \subset X$ be some convex set such that $S \subset R \neq \emptyset$. Then $D(x, y)$, defined over $S \times S$, is considered and satisfies the following conditions.

- i. $D(x, y) \geq 0, D(x, y) = 0$ if and only if $x = y$.
- ii. For any $y \in S$ and $i \in I$, a point $x = P_{iy} \in A_i \cap S$ exists such that $D(x, y) = \min_{z \in A_i \cap S} D(z, x)$.

This point x is called the D-projection of the point y onto the set A_i .

- iii. For each $i \in I$ and $y \in S$, and the function $G(z) = D(z, y) - D(z, P_{iy})$ is convex over $A_i \in S$.
- iv. A derivative $D_x(x, y)$ of the function $D(x, y)$ exists when $x = y$, while $D_x(y, y) = 0$ dfgdkgdkgjd
i.e. $\lim_{t \rightarrow 0} (D(y + tz, y)/t) \leftrightarrow 0$ for all $z \in X$.
- v. For each $z \in R \cap S$ and for every real number L the set $T = \{x \in S | D(z, x) \geq L\}$ is compact.
- vi. If $D(x^n, y^n) \rightarrow 0, y^n \rightarrow y^* \in \bar{S}$ (\bar{S} is the closure of the set S) and the set of the elements of the series $\{x^n\}$ is compact, then it follows that $x^n \rightarrow y^*$.

The following iterative process is considered.

1. take an arbitrary point $x^0 \in S$.
2. if the point $x^n \in S$ is known, we select in some way the index $i_n(x^n) \in I$ and we find the point x^{n+1} which is the D-projection of the point x^n onto the set $A_{i_n(x^n)}$.

These are examples of the function $D(x, y)$.

1. $D(x, y) = (x - y, x - y)$.
2. $D(x, y) = f(x) - f(y) - (\nabla f(x), x - y)$ where $f(x)$ is a strictly convex differentiable function.

Assume the problem is

$$\min_u E(u) + \lambda H(u)$$

where $E(u)$ and $H(u)$ are convex functions and Bregman distance is defined by

$$D(u, v) = E(u) - E(v) - (p, u - v)$$

where p is the gradient of the function E .

The algorithm of Bregman iterative to solve this problem is the followings.

$$u^{k+1} = \min_u D(u, v) + \lambda H(u)$$

It follows that

$$u^{k+1} = \min_u E(u) - \langle p^k, u - u^k \rangle + \lambda H(u) \quad (3)$$

$$p^{k+1} = p^k - \nabla H(u^{k+1}) \quad (4)$$

3.2. SPLIT BRTEGMAN

The Bregman method is applied to solve the general l_1 -regularized optimization problem like

$$\min_u \Phi(u) + \lambda H(u) \quad (5)$$

where $|\cdot|$ denotes the l_1 -norm and both $|\Phi(u)|$ and $H(u)$ are convex functions. Many important problems in imaging science and other computational areas can be posed as l_1 -regularized problem. Assume that $\Phi(u)$ is differentiable function.

The key for the idea of split Bregman is to "decouple" the l_1 and l_2 portions of the energy in (5). The following problem is considered instead of considering (5).

$$\min_{u,d} |d| + H(u) \quad \text{such that } d = \Phi(u).$$

This problem is clearly equivalent to (5). To solve this problem, first convert it into an unconstrained problem as the following.

$$\min_{u,d} |d| + H(u) + \frac{\lambda}{2} \|d - \Phi(u)\|_2^2.$$

To enforce the constraint condition it follows into the Bregman formulation (3) and (4).

$$(u^{k+1}, d^{k+1}) = \min_{u,d} D_E^p(u, u^k, d, d^k) + \frac{\lambda}{2} \|d - \Phi(u)\|_2^2.$$

It follows that

$$(u^{k+1}, d^{k+1}) = \min_{u,d} E(u, d) - \langle p_u^k, u - u^k \rangle - \langle p_d^k, d - d^k \rangle + \frac{\lambda}{2} \|d - \Phi(u)\|_2^2.$$

$$p_u^{k+1} = p_u^k - \lambda(\nabla\Phi)^T(\Phi(u^{k+1}) - d^{k+1}).$$

$$p_d^{k+1} = p_d^k - \lambda(d^{k+1} - \Phi(u^{k+1})).$$

It also follows that following simply two-phase algorithm.

$$(u^{k+1}, d^{k+1}) = \min_{u,d} |d| + H(u) + \frac{\lambda}{2} \|d - \Phi(u) - b^k\|_2^2.$$

$$b^{k+1} = b^k + (\Phi(u^{k+1}) - d^{k+1}).$$

4. NON-NEGATIVE MATRIX FACTORIZATION

A convex model for factoring data matrix X into a non-negative product AS , with a sparse coefficient matrix S , is proposed in [7]. In this paper, they show a frame work for dimensionality reduction, based on matrix factorization and sparsity theory, and they use the data itself for the low dimensionality representation, thereby guaranteeing the physical fidelity.

Many different techniques for dimensionality reduction have been proposed, for instance, rank revealing QR factorization in [4] and [5]. The idea of this method is to find a column permutation of the data matrix such that the first few columns as well as conditioned as possible. However, this this method does not take non-negativity constraint. In [7] they propose a new convex method to factor a non-negative data matrix X into a product AS , for which S is non-negative and sparse and the columns of A coincide with columns form the data matrix X by split bregman or alternating minimization approach. These two methods have the same idea and its connection is discussed in [6]. This model is described as follows.

Assume there exists an index set I such that the columns X_i of X are the bases for $i \in I$. Under the assumption of non-negativity linear

mixing of signals, this means that any column X_j in X can be written as

$$X_j = \sum_{i \in I} X_i T_{i,j},$$

for coefficients $T_{i,j} \geq 0$. The problem is that the coefficients $T_{i,j}$ as well as the index set I are unknown. Hence, it follows to start by using all columns in X to describe X itself, i.e. for coefficients $T \geq 0$ for which

$$X = XT. \quad (7)$$

The equation (7) has many solutions, however the desired representation uses as few columns of X as possible, i.e. only the bases. Since not using the j^{th} row of T be zero, it can be reformulated the detection problem of the basis as finding a solution to (7) such that as many rows of T as possible are zero. Mathematically,

$$\min_{T \geq 0} \|T\|_{\text{row-0}} \quad \text{such that } XT = X$$

where $\|T\|_{\text{row-0}}$ denotes the number of non-zero rows. The columns of X that correspond to non-zero of the minimizer of T of (8) are the desired bases which define the lowest dimensional subspace where the data resides. Since the problem (8) are not convex, it can be relaxed the formulation by replacing $\|T\|_{\text{row-0}}$ by the convex $l_{1,\infty}$ norm $\|T\|_{1,\infty} = \sum_i \max_j |T_{i,j}|$. The l_1 part should encourage the sparsity. $\text{\textcircled{X}}\text{par}$

After data reduction by clustering [10] and make selection model, overall the proposed convex model is given by

$$\min_{T \geq 0} \zeta \sum_i \max_j (T_{i,j}) + \langle R_w \sigma C_w, T \rangle + \frac{\beta}{2} \|(YT - X_s)C_w\|_F^2.$$

This problem is solved by split Bregman. In [7] they apply for the hyperspectral image as one of

its application. And [3] describes the basic idea of image processing.

5. CONCLUSION AND FUTURE TASKS

I learned what the split Bregman is and how to apply for non-negative matrix factorization. I also implemented for split Bregman and I could see how it works by myself. After I go back to Japan, I would like to try to apply this idea for another application of data mining.

ACKNOWLEDGMENTS

First and foremost, I would like to express my great appreciation to everyone who supports me.

First I would greatly appreciate Prof. Stanley Osher, who supervised me during this program. Thank you very much for supervising me at UCLA for six months. It is a great honor for me and I could learn a lot of things from him. I would appreciate to teach me kindly many valuable things. Thank you very much. I am very happy.

I would like to thank the graduate advisor at math department, Ms. Maggie Albert. She kindly helps me to spend a great life in UCLA. I greatly appreciate to answer many questions kindly and give me a lot of valuable advice. Her help makes me be dedicated to study for me.

I would also thank to Dr. Ernie Esser, UC Irvine. He gives me the code for the program and data. I also appreciate to reply of my questions and give me valuable knowledge. Thank you very much.

I would like to express my great appreciation to Prof. Jenn-Ming Yang at UCLA, Prof. Yang Ju, Prof. Noritsugu Umehara and Prof. Yasumasa Ito at Nagoya University, who are coordinator of this program. Thank you very much for giving me the great opportunity and supporting

me. And I would also appreciate to Ms. Tomoko Kato and Ms. Chiharu Yada. Before I came here they also kindly helped and supported me. Their support makes me to focus on my work and life here. Thank you very much.

I also appreciate the members of Zhang's laboratory in Nagoya University. Prof. Shao-Liang Zhang and Associate Professor Shinji Imahori discuss my work on skype for many times and they give me valuable advice for my work. When I get a trouble, they also kindly helped me and I got a great answer. Assistant Professor Takafumi Miyata helped me to install software and he also kindly support me. Thank you very much. Their secretly Ms. Yumi Kobayashi supports me for my documentation process during my stay, especially, to attend the meeting in U.S. I am dedicated to my work better because of my work. The students in Zhang's laboratory also do a lot of tasks instead of me and I would appreciate their great help.

Finally I would appreciate everyone I met here. They are greatly kind and nice to me. I have a great time with them.

REFERENCES

- [1] Stephen Boyd and Lieven Vandenberg, *Convex optimization*, Cambridge University press, Cambridge, UK (2004).
- [2] L. M. Bregman, *The relaxation method of finding the common point of convex sets and its application to the solution of problems in convex programming*, USSR Computational Mathematics and Mathematical Physics, 7 (1967), pp. 200-217.
- [3] Kenneth R. Castleman, *Digital image processing*, Englewood Cliffs, N.J. (1979)
- [4] Tony F. Chan, *Rank revealing qr factorization*, Linear Algebra Appl., 88/89 (1987), pp.67-82.
- [5] Tony F. Chan and Per C. Hansen, *Some application of the rank revealing qr factorization*, SIAM. J. Sci. Stat. Comput., 13 (1992), pp.33-44.
- [6] Ernie Esser, *Applications of Lagrange-based alternating direction methods and connections to split Bregman*, Tech. Rep., (2009), UCLA CAM Report [09-31].
- [7] Ernie Esser, Michael Moller, Stanley Osher, Guillermo Sapiro and Jack Xin, *A convex model for non-negative matrix factorization and dimensionality reduction on physizal space*, IEEE Transactions on image processing, 21 (2012) pp. 3239-3252.
- [8] Tom Goldstein and Stanley Osher, *The split bregman method for l1-regularizes problems*, SIAM J. Imaging Sciences, 2 (2009), pp. 323-343.
- [9] Gene H. Golub and Charles F. Van Loan, *Matrix computations*, Third edition, The Johns Hopkins University Press, Baltimore and London (1996).
- [9] Teofilo F. Gonzalez, *Clustering to minimize the maximum intercluster distance*, Theoretical Computer Science 38 (1985), pp.293-306.
- [10] Stanley Osher, Martin Burger, Donald Goldfarb, Jinjun Xu, and Wotao Yin, *An iterative reguralization method for total variation-based image restoration*, Multiscale Model. Simul., 4 (2005), pp.460-489.
- [11] Wotao Yin and Stanley Osher, *Error forgetting of Bregman iteration*, Springer, Journal of Scientific Computing, Volume 54, (2013), pp684-695.

MODELING FOR A NANO-PRECISION SYSTEM

Hiroshi Fuji

Graduate School of Engineering, Nagoya University
h_fuji@nuem.nagoya-u.ac.jp

Supervisor: Tsu-Chin Tsao

Mechanical and Aerospace Engineering Department, University of California Los Angeles
ttsao@seas.ucla.edu

Abstract

In this research, the system identification of the nano-precision stage is conducted. This research focuses on modelling the wafer holder of the Multi-Axis Positioning System (MAPS). To attain the accurate positioning, the model accuracy is indispensable. The model has been built according to the first-principle modelling but the model doesn't correspond well with its actual behaviour. Models built in a theoretical way often has some differences from the real model because the actual behaviour of the system can be affected by many causes which we can't expect. This research builds the model by using the black-box identification method. As the black-box identification method is a purely data-driven modelling method, the model built by the method is expected to correspond well with the actual behaviour.

1. Introduction

Transistor density has been increasing steadily. As feature size continues to decrease, the need for higher precision increases. The most common form of nano-manufacturing in the semiconductor industry is optical lithography. Reducing feature size, using photo lithography, is limited in part by diffraction of light. To overcome the diffraction limitation many resolution enhancements such as mask design techniques, correct for diffraction.

The international roadmap for semiconductors predicts that extreme ultraviolet lithography (EUV) is the most leading candidate to achieve ≤ 22 nm in the future and nano-imprint lithography (NIL) is not far behind. Imprint lithography is a technique where pattern transfer occurs by physically pressing the mask and wafer together and is therefore not limited by diffraction. Due to the ability to stamp a large area, such as the whole wafer, NIL can reduce fabrication steps and lower cost. The manufacturing system that is presented in [1], the Multi-Axis and Positioning System (MAPS), was designed in part to implement NIL.

Precision motion control is becoming incredibly more important in the areas of nanotechnology. Lithography, for one, is requiring greater precision as transistor density

continues to increase. Permanent magnet synchronous linear motors (PMSLM), or brushless motors, are among the most prevalent in precision machines due to their long-range travel, high force density, and high precision and accuracy. Lack of mechanical coupling needed, versus rotary motors, and in conjunction with an air bearing eliminate many disturbances such as backlash and friction.

The dynamic model of the wafer holder of MAPS, was built according to the white-box identification method, but the model does not correspond well with its actual behaviour. To attain the accurate positioning, the model accuracy is very important. The model therefore needs to be rebuilt in a proper way.

2. Theory and method

2.1 Multi-Axis Positioning System (MAPS)

MAPS, as shown in figure 2.1 and 2.2, is composed of a 6 degree-of-freedom (DoF) wafer holder and a 3 DoF module holder, both of which move relative to the base. The module can be chosen for a desired task, such as atomic force microscopy or imprint lithography.

The 6 DoF wafer holder, referred to as the platen (see figure 2.3), is propelled in all degrees of freedom by four linear permanent-magnet synchronous motors. Each 3-phase linear motor was designed to produce two orthogonal forces, in-plane and out-of-plane, by using a Halbach magnet array instead of the standard magnet array, which will be described in the coming section.

2.2 In-plane motion of the platen

Although the platen has 6 degree-of-freedom, only in-plane motion is considered in this paper. As we assume that the platen is a linear system, the model of the platen's in-plane motion can be considered independently of the model of the platen's out-of-plane motion. The dimensions of the platen corresponding figure 2.3 are shown in table 2.1. In [1], the



Fig. 2.1 Photo of MAPS system showing the platen, structure frame, and bridge

model of the platen was built by using the white-box identification method. Each parameter was estimated separately, and the model was built according to Newtonian methods using those parameters. But the model does not explain the system correctly.

Table 2.1 Dimensions of the platen

Variable	Value (mm)	Description
R_m	188	radius to linear motor
R_d	197	radius to eddy current dumper
D_c	95	distance between cap probes
d	40	distance between interferometers

The platen's in-plane motion is modeled as a system of decoupled mass-spring-damper systems:

$$G: M\ddot{\mathbf{X}} + B\dot{\mathbf{X}} + K\mathbf{X} = \mathbf{F} \quad (2.1)$$

where

$$M = \mathbf{diag} \begin{pmatrix} m \\ m \\ I_z \end{pmatrix} \quad (2.2)$$

$$B = \mathbf{diag} \begin{pmatrix} 2b \\ 2b \\ 4R_m^2 b \end{pmatrix} \quad (2.3)$$

$$K = \mathbf{diag} \begin{pmatrix} 2k \\ 2k \\ 4R_m^2 k \end{pmatrix} \quad (2.4)$$

2.3 Halbach brushless linear motors

The platen is actuated by four linear motors and will be described in this section. Figure 2.4 shows the Halbach brushless linear motor. The Halbach array produces a levitation force independent of the thrust force, where standard array produces only thrust, and has an increased magnetic field by $\sqrt{2}$. The motor law describing the

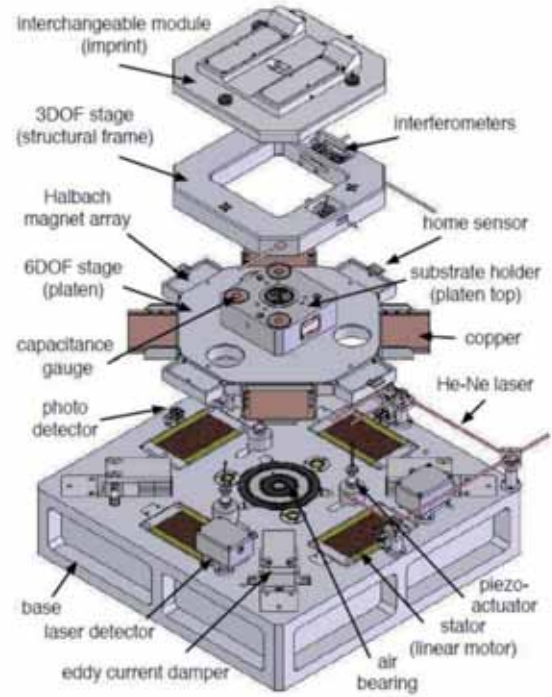


Fig. 2.2 Detailed exploded view of MAPS showing all the actuators and sensors

relationship between the generated forces and the supplied current is

$$f_{xk} = \begin{bmatrix} a \sin(\omega x_k + \phi) \\ a \sin(\omega x_k + \phi + \pi/3) \\ a \sin(\omega x_k + \phi + 2\pi/3) \end{bmatrix} \begin{bmatrix} i_{1k} \\ i_{2k} \\ i_{3k} \end{bmatrix} \quad (2.5)$$

$$= \mathbf{S}_{xk}^T(x_k) \mathbf{i}_k$$

x_k is the k th magnet array's relative position to its stator, and the parameters are listed in the table 2.2. In [2] the Halbach brushless linear motors were described in more detail.

Table 2.2 Motor parameters

Variable	Value
a	2.4167 N-A ⁻¹
ω	217.4 rad-m ⁻¹
ϕ	-3.1087 rad

2.4 ARX model identification

System identification methods are roughly divided into three groups: the white-box system identification, the grey-box system identification and the black-box system identification. The white-box system identification is also called the first-principle modeling. It is used when we know the parameter of each component and the model can be built according to Newton's law. The black-box system identification is used when we do not know the parameters of the model, and those parameters are estimated from inputs and outputs. Grey-box system identification is a method which combines the white-box system identification and the black-box system identification. It is used when some

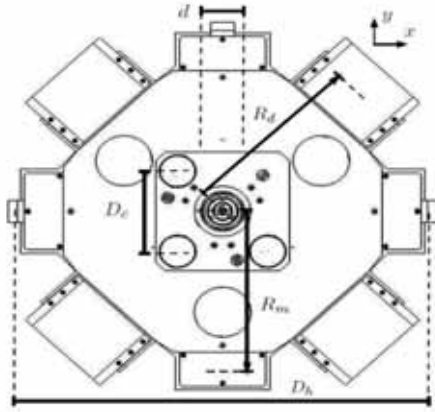


Fig. 2.3 The platen 6 DoF wafer holder

parameters of the system are known but the other parameters are unknown.

The actual behavior of a system is often different from its theoretical model because there are many unexpected factors in the real control. Models which are built by the white-box system identification or the grey-box system identification often have some errors because they are based on the theoretical way. We focus on the black-box system identification. It uses actually collected data to estimate parameters, therefore it is expected that the model built by this method corresponds well with the actual system. We use the ARX model identification [3] to conduct the black-box system identification.

To apply the ARX model identification to estimating the parameters of the system, the differential equation (2.1) needs to be converted to the difference equation. Only the conversion about x is described here, but the same process can be applied to y and θ . With the approximations

$$\dot{x} = \frac{x(n+1) - x(n-1)}{2\Delta t} \quad (2.6)$$

$$\ddot{x} = \frac{x(n+1) - 2x(n) + x(n-1)}{\Delta t^2} \quad (2.7)$$

the differential equation about x

$$m\ddot{x} + b\dot{x} + kx = f_x \quad (2.8)$$

is converted to the difference equation

$$x(n) = a_1x(n-2) + a_2x(n-1) + a_3f_x(n-1) \quad (2.9)$$

where

$$a_1 = -\frac{2m - b\Delta t}{2m + b\Delta t} \quad (2.10)$$

$$a_2 = \frac{4m - 2k\Delta t^2}{2m + b\Delta t} \quad (2.11)$$

$$a_3 = \frac{2\Delta t^2}{2m + b\Delta t} \quad (2.12)$$

If we can estimate a_1 , a_2 and a_3 , we can derive the parameters m , b and k from the equations (2.10-12). By defining ϕ , θ as:

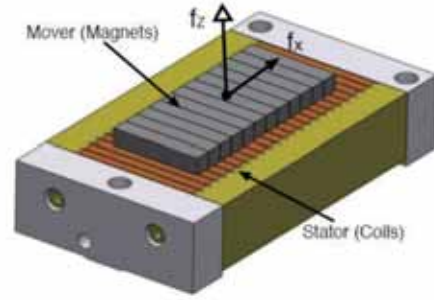


Fig. 2.4 Linear motor components

$$\phi(n) = [x(n-2) \ x(n-1) \ f_x(n-1)] \quad (2.13)$$

$$\theta = [a_1 \ a_2 \ a_3]^T \quad (2.14)$$

the equation (2.9) can be described as:

$$x(n) = \phi(n)\theta \quad (2.15)$$

When a series of inputs $x(0), x(1), \dots, x(N)$ are collected, we can get $N-2$ sets of equations from the equation (2.15):

$$\begin{bmatrix} x(2) \\ x(3) \\ \vdots \\ x(N) \end{bmatrix} = \begin{bmatrix} \phi(2) \\ \phi(3) \\ \vdots \\ \phi(N) \end{bmatrix} \theta \quad (2.15)$$

By defining the two matrixes in the equation (2.15) as:

$$\mathbf{X} = \begin{bmatrix} x(2) \\ x(3) \\ \vdots \\ x(N) \end{bmatrix} \quad (2.16)$$

$$\Phi = \begin{bmatrix} \phi(2) \\ \phi(3) \\ \vdots \\ \phi(N) \end{bmatrix} \quad (2.17)$$

the equation (2.13) can be described as:

$$\mathbf{X} = \Phi\theta \quad (2.18)$$

When the parameters are completely correct, the equation (2.18) is realized. With the estimated parameters $\hat{\theta} = [\hat{a}_1 \ \hat{a}_2 \ \hat{a}_3]$, however, some error occurs. We define the error vector as:

$$\mathbf{e} = \mathbf{X} - \Phi\hat{\theta} \quad (2.19)$$

where

$$\mathbf{e} = \begin{bmatrix} e(2) \\ e(3) \\ \vdots \\ e(N) \end{bmatrix} \quad (2.20)$$

A set of parameters which minimize the errors are considered to be good parameters. To estimate the parameters, we derive $\hat{\theta}$ which minimizes the square norm of the error vector \mathbf{e} . The square norm of the error vector \mathbf{e} is

$$\begin{aligned} \|\mathbf{e}\|^2 &= \{\mathbf{X} - \Phi\hat{\theta}\}' \{\mathbf{X} - \Phi\hat{\theta}\} \\ &= \mathbf{X}^T \mathbf{X} - 2\mathbf{X}^T \Phi \hat{\theta} + \hat{\theta}^T \Phi^T \Phi \hat{\theta} \end{aligned} \quad (2.21)$$

When the first-order differentiation of $\|e\|^2$ about $\hat{\theta}$ is zero, the minimum of $\|e\|^2$ is realized:

$$\frac{d\|e\|^2}{d\hat{\theta}} = -2\mathbf{X}^T\Phi\hat{\theta} + 2\hat{\theta}^T\Phi^T\Phi = 0 \quad (2.22)$$

So the optimal parameters are derived by this equation:

$$\hat{\theta}^* = (\Phi^T\Phi)^{-1}\Phi^T\mathbf{X} \quad (2.23)$$

3 Results

3.1 Validation

We made a program that estimates the parameters from inputs and outputs. In order to estimate the parameters precisely, the program needs to be validated. We did some validations to make sure that the program works correctly.

First, we made a differential equation solving program. It uses ode45 function in Matlab to solve the differential equations of the dynamic model of the platen. When 3 inputs (f_x, f_y, f_θ) are put to the solver, it outputs the platen's motion. The results are calculated by using the theoretical model of the platen where the ideal parameters are used. By using the inputs and the outputs from the solver, we checked if the parameter estimation program estimates the given parameters.

Impulse inputs were put to the theoretical model of the platen and the outputs were collected (see figure 3.1). The sampling rate of these data was 5000 Hz. We tested the parameter estimation program by using these inputs and outputs. Table 3.1 shows the parameters of the platen's theoretical model and table 3.2 shows the estimated parameters. Comparing the estimated parameters with the parameters of the theoretical model, it can be seen that the program estimates the good parameters. From this result, it can be said that the parameters estimated by the program are dependable.

Table 3.1 Parameters of the theoretical model of the platen

	x, y	θ
m	6.6000 [kg]	0.13370 [kg-m ²]
b	638.80 [N-s-m ⁻¹]	25.391 [N-s-m]
k	1313.5 [N-m ⁻¹]	92.847 [N-m]

Table 3.2 Estimated parameters

	x, y	θ
m	6.63375 [kg]	0.13503 [kg-m ²]
b	638.76 [N-s-m ⁻¹]	25.389 [N-s-m]
k	1313.6 [N-m ⁻¹]	92.852 [N-m]

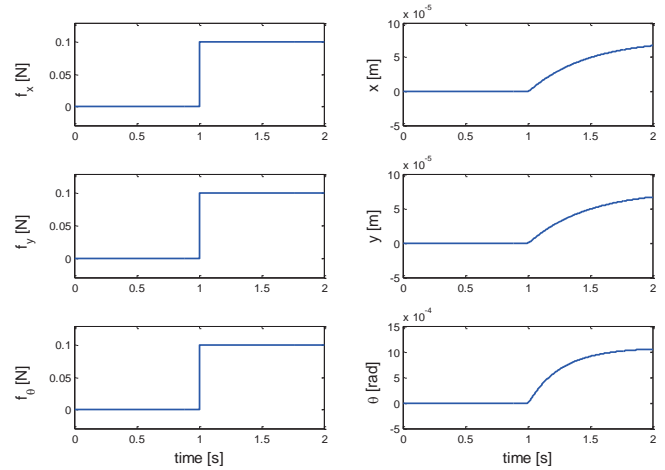


Fig. 3.1 Force inputs and position outputs of the theoretical model of the platen

3.2 Parameter estimation

We estimated the parameters of the dynamic model of the platen by using the parameter estimation program described above with actual inputs and outputs. Impulse input to x, y, θ was put to the platen separately. The actual inputs from the controller are not forces but voltage inputs to each motor. To use the parameter estimation program, these voltage inputs need to be converted to local forces using the voltage-current conversion $i_{ik} = Kv_{ik}$ and the equation (2.5). K is a constant amplifier gain. Then they are converted to global forces $\mathbf{F} = [f_x f_y f_\theta]^T$ by this equation:

$$\mathbf{F} = \begin{bmatrix} -1 & 0 & 1 & 0 \\ 0 & -1 & 0 & 1 \\ -R_m & -R_m & -R_m & -R_m \end{bmatrix} \begin{bmatrix} f_1 \\ f_2 \\ f_3 \\ f_4 \end{bmatrix} \quad (3.1)$$

With these equations, global forces can be derived from voltage inputs.

We put the voltage inputs, shown in figure (3.2-4), to the platen, and got the platen position outputs, shown in figure (3.5-7). From these data, we estimated the parameters of the platen. First we converted the voltage inputs to global forces, and the results are shown in figure (3.8-10). These forces are fluctuating in the beginning part to hold the platen at the center, and those parts were truncated when deriving global forces. With the global forces, the parameters were estimated, and those parameters are shown in table 3.3.

Table 3.3 Estimated parameters from the actual data

	x, y	θ
m	12.654 [kg]	-2.2370 [kg-m ²]
b	2068.9 [N-s-m ⁻¹]	-4949.9 [N-s-m]
k	2364.4 [N-m ⁻¹]	1003.6 [N-m]

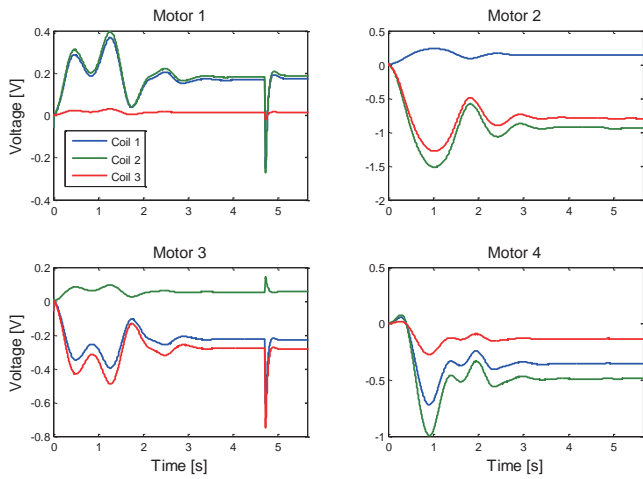


Fig. 3.2 Voltage inputs to each motor when putting f_x step input

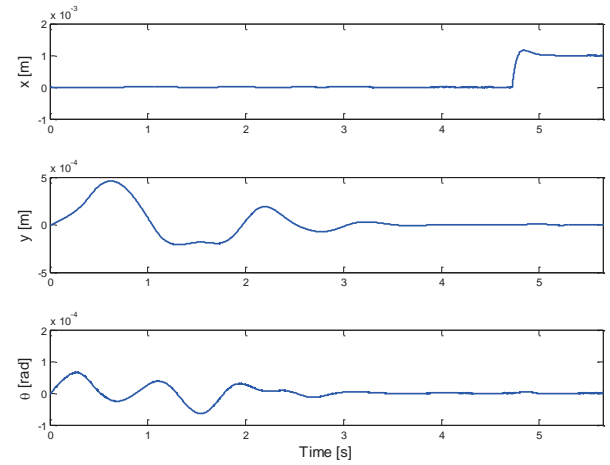


Fig. 3.5 Platen position outputs when putting f_x step input

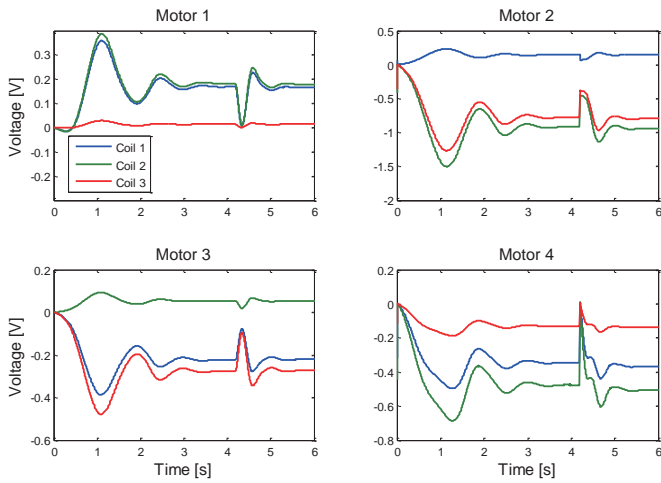


Fig. 3.3 Voltage inputs to each motor when putting f_y step input

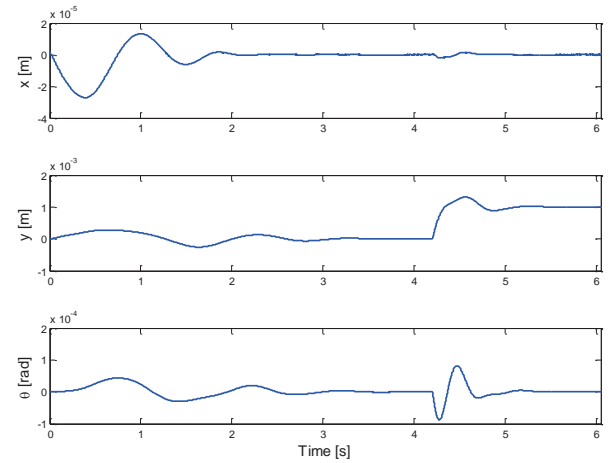


Fig. 3.6 Platen position outputs when putting f_y step input

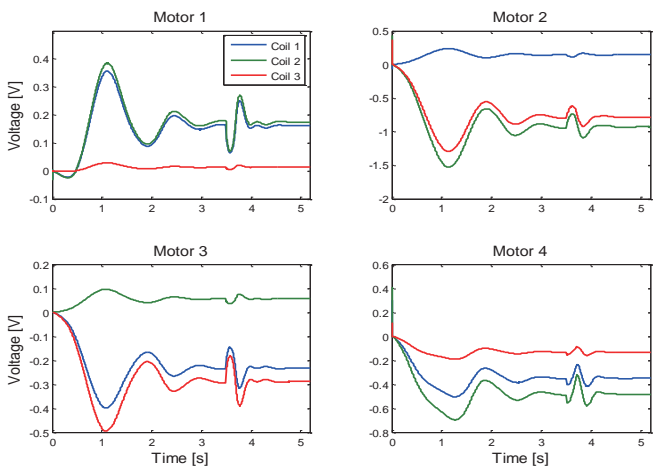


Fig. 3.4 Voltage inputs to each motor when putting f_θ step input

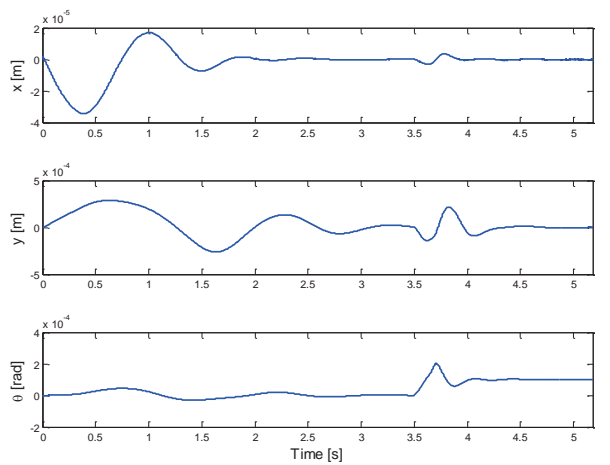


Fig. 3.7 Platen position outputs when putting f_θ step input

4. Discussion

The estimated parameters in table 3.3 do not seem reasonable. As the program was validated in the previous section, it can be said there was some sort of problem in deriving global forces. One possibility is that the parameters in the table 2.2 were different from those in the controller. Another possibility is that the order of 3 voltage inputs to each motor do not correspond with the order in the controller. Those possibilities should be considered to conduct parameter estimation correctly.

After the system identification, it is a very important phase to evaluate the parameters with data which was not used for system identification. However we couldn't evaluate the parameters due to the problem in deriving global forces.

The sampling rate of the data in this paper was 5000 Hz, and its validity is not considered in this paper. The sampling rate significantly affects the precision of the parameter estimation. When there are not enough data points, the parameter estimation is not precise. When there are too many data points, effects of noise gets significant. Therefore the sampling rate needs to be considered to improve the parameter estimation.

5. Conclusion

To identify the dynamic model of the platen, we estimated the parameters using the ARX model identification method. We made a parameter estimation program and its function was validated. With the program, we estimated the parameters from the actual inputs and outputs. There were however some problem deriving global forces from voltage inputs to each motor, and we could not estimate the parameters correctly. The validation of the voltage-force conversion is needed to solve this problem.

Acknowledgements

I would like to show my greatest appreciation to Yen Chi Chang who offered continuing support and constant encouragement. I would also like to thank Prof. Tsu-Chin Tsao for giving me this great opportunity.

References

- [1] Shalom Dovber Ruban. *Modeling, Control, and Real-Time Optimization for a Nano-Precision System*. PhD dissertation, University of California Los Angeles, 2010.
- [2] Mark Williams. *Precision Six Degree of Freedom Magnetically-Levitated Photolithography Stage*. PhD thesis, Massachusetts Institute of Technology, 1998.
- [3] Philipp Reist. *Black Box System Identification: Time Domain*, Institute for Dynamic Systems and Control, www.idsc.ethz.ch/Course/signals_and_systems/lectureNotes11.pdf, accessed September 12, 2013

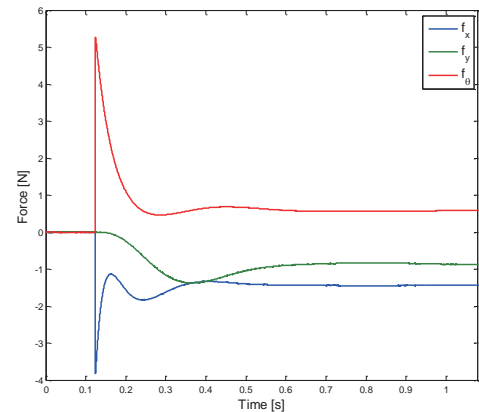


Fig. 3.8 Global forces when putting f_x step input

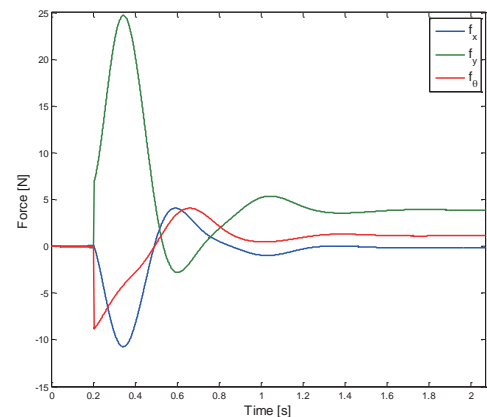


Fig. 3.9 Global forces when putting f_y step input

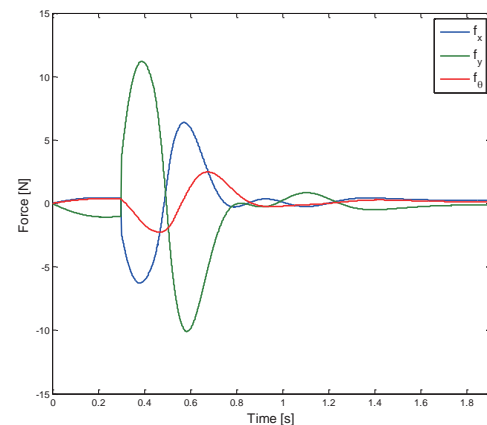


Fig. 3.10 Global forces when putting f_z step input

NUMERICAL SIMULATION OF WAVE PROPAGATION IN COMPOSITE STRUCTURES

Shinichi Hayashi

Graduate School of Engineering, Nagoya University
s_hayashi@nuem.nagoya-u.ac.jp

Supervisor: Ertugrul Taciroglu

Department of Civil & Environmental Engineering, University of California, Los Angeles
etacir@ucla.edu

ABSTRACT

The vibration-based identification of damage in a structure is one of the widely used non-destructive techniques. The numerical approach for identification of a scatter within a heterogeneous media was suggested by Jung et al. In this study, under the purpose of the verification of Jung's method against the experimental data, we analyze the wave propagation in composite structures. The composite sandwich structure consisted of a woven composite plate and an aluminium honeycomb core was considered. The numerical simulation using finite element method was carried out for a two-dimensional plane-strain model of the transversely isotropic plate. These results of several numerical experiments show that the clearly Rayleigh wave propagation and the same trend with respect to the distance from the source location.

1. INTRODUCTION

Advanced composites are being increasingly used in aircraft and aerospace structures. Despite their high structural efficiency, composite materials are often susceptible to hidden defects which if undetected, may cause sudden catastrophic failure of the entire structure. For that reason, the non-destructive evaluation (NDE) methodology of the detection and characterization of damage in composite structures is needed. Various methods of NDE (i.e., ultrasonic testing, radio graphic analysis and electrical impedance tomography) are used experimentally. These techniques that use the response of structures under dynamic excitation without any systematic modeling, however, are not suited to an accurate reconstruction of the scatter's locations and sizes, particular in composite structures because of reflected waves from interfaces and boundary. Thus the need of model-based studies and robust computational techniques is widely recognized in the NDE community.

Recently, computational approaches combining the extended finite element method (XFEM) and gradient-based minimization under a divide-and-conquer strategy was

suggested by Jung et al [1]. The proposed damage identification method consists of three parts: (i) the divide-and-conquer for bypassing the multiple local minimum; (ii) the dynamic XFEM for forward analyses of propagating waves [2]; (iii) the gradient-based optimization for the minimization of the error norm between the measured and simulated responses collected multiple sensors. In his study [1], several numerical simulations are carried out for some example problems to identify a single scatter (e.g., a crack, a void, an inclusion) using the synthetic data computed for a hypothetical target scatter as the measured response. These results of several numerical experiments clearly show that the proposed approach is very effective and accurate to the identification of various types of scatters. However the simulation using the experimental data is not carried out.

In this study, under the purpose of the verification of Jung's method against the experimental data, we analyze the wave propagation in the composite structure. Based on the experimental study of wave propagation in composite structure [3-5], we execute numerical simulation.

2. EXPERIMENTAL DATA

In this study, we use the experimental data carried out by Mal et al [3-5]. They carried out numerical simulation and laboratory experiments about the interaction of guided waves with defects in a honeycomb composite sandwich structure with and without damage. In this section, the brief explanation of the experimental setup and honeycomb composite sandwich structure is described.

2.1. EXPERIMENTAL SETUP

The general experimental setup used in the Mal's test is shown in Fig. 1. Several broadband transducers are placed precisely on the composite surface. Only two transducers are placed on the composite structure surface to obtain data from transducer with prescribed position. Several identical broadband PZT transducers are used as transmitters and receivers of the waves. A five-cycle sinusoidal wave generated by an arbitrary waveform generator is used as the input to the source transducer. The ultrasonic signal is

digitized and recorded directly in a digital oscilloscope. The input source has the following form:

$$(t) = \frac{1}{2} \left[1 - \cos\left(\frac{2\pi ft}{5}\right) \right] \sin(2\pi ft), \quad (1)$$

where f is the central frequency in cycles.

2.2. THE ELASTIC PROPERTIES OF THE COMPOSITE SANDWICH STRUCTURE

The honeycomb composite plate consists of a 12.7mm thick aluminum honeycomb core sandwiched between two 1.78mm thick 2/2 twill carbon fiber composite face sheets

(Fig. 2). Due to low frequency used in their work, both materials can be assumed to be a transversely isotropic with a common symmetry axis normal to the plate. The elastic properties of the composite plate and the honeycomb are given in Table. 1.

Fig. 3 shows the top view of distribution of transmitter and receiver sensors on the sandwich plate. The red spots represent source locations whereas the blue spots represent the receiver locations. The row containing S1 as source is assumed to be the undamaged region. The vertical displacements on the surface of the plate were obtained at location R2 to R7

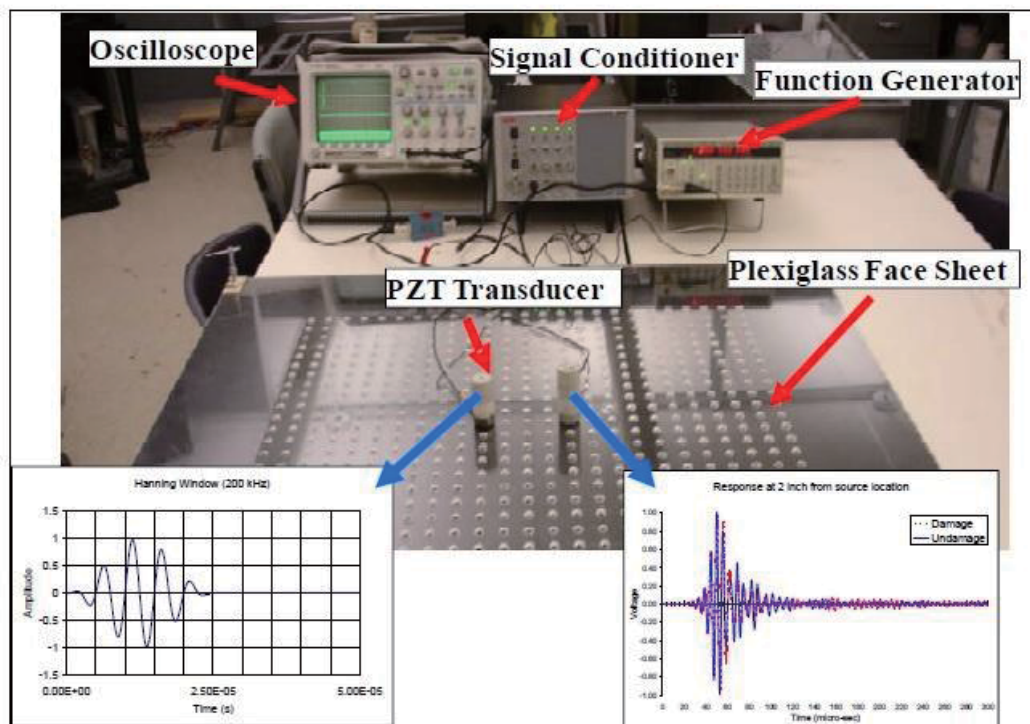


Fig. 1. Experimental setup and sample recorded signals.

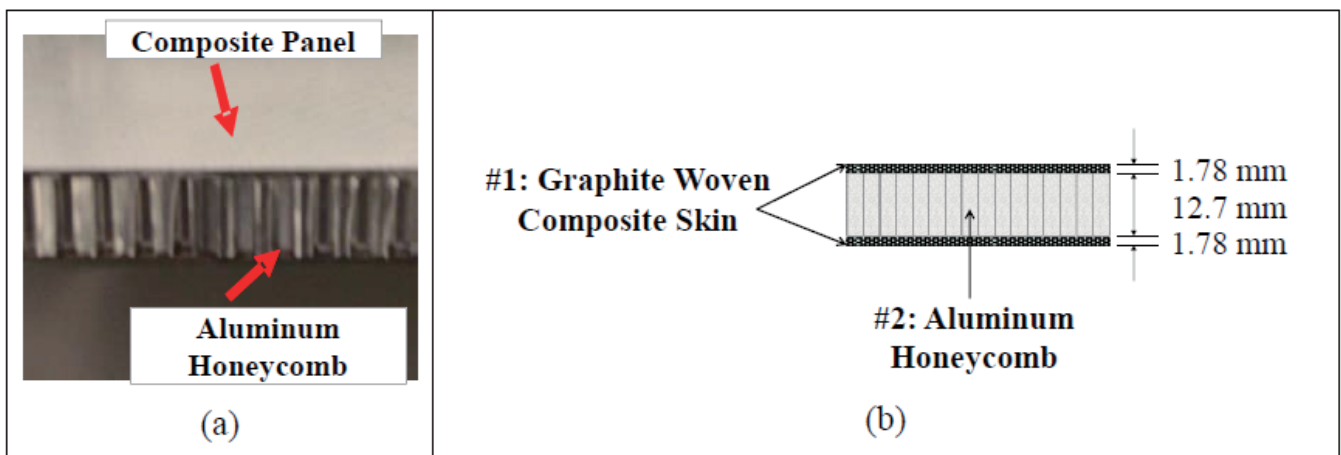


Fig. 2. (a) 2/2 twill woven carbon fiber composite panel and aluminium honeycomb sandwich structure, (b) test specimen dimension.

Table. 1. The properties of the twill woven carbon fiber composite skin and aluminum honeycomb core [4].

	E_{11}, E_{22} [GPa]	E_{33} [GPa]	G_{12} [GPa]	G_{13}, G_{23} [GPa]	ν_{12}, ν_{21}	ν_{31}, ν_{32}	ν_{13}, ν_{23}	ρ [kg/m ³]
Composite skin	38.8	9.77	14.77	2.94	0.3137	0.0816	0.324	1276
Al honeycomb	3.43×10^{-3}	2.99	8.6×10^{-4}	0.413	1	0.33	3.79×10^{-4}	114.1

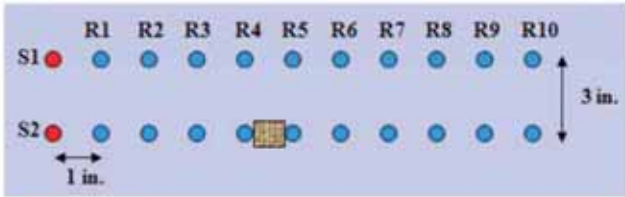


Fig. 3. Source is fixed at S and receiver is moved from R2 to R7.

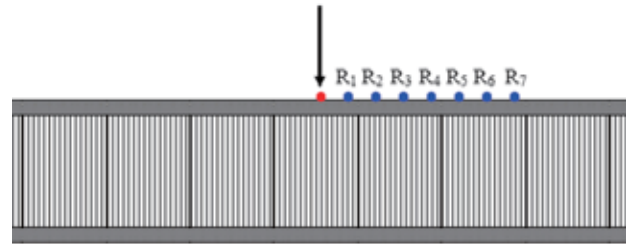


Fig. 4. Schematic of the 2D model of sandwich structure

4. NUMERICAL EXPERIMENTS

4.1. NUMERICAL MODEL

A finite element simulation is carried out in a plane-strain model of the transversely isotropic plates. Fig. 6 shows the schematic of the 2-D model with applied vertical source and receiver locations. The vertical displacements on the surface of the plate were obtained at sensor's location R2, R3, R4 and R5. The nodal points near the experimental sensor's location are selected as numerical sensor's locations and they are 0.0504mm, 0.0762mm, 0.1056mm and 0.1266mm from the loading source location respectively. Guided wave propagation was activated in the sandwich structure using a waveform given by Eq. (1) with central frequency 200 kHz. Fig. 5 shows a narrow band pulse in (a) time domain and (b) frequency domain.

4.2. NUMERICAL RESULTS

Fig. 6 displays the snapshot of the vertical displacement of the two-dimensional specimen. It clearly shows Rayleigh wave propagation along the top and bottom surface.

Also, the normalized vertical displacements obtained numerically at each receiver location due to a five-cycle sine pulse at 200 kHz central frequency are shown in Fig. 7-8 and the experimentally obtained time-voltage surface response in Mal's test [3] are shown in Fig. 9. There is discrepancy between numerical results and experimental one, however it shows same trend with respect to the distance from the source location. It is thought that the main reasons of the discrepancy are (i) the original loading signal is used, and (ii) the sensor's locations are not same as actual positions. The original loading source is modified by various components of the test setup before it is transmitted as a force on the specimen.

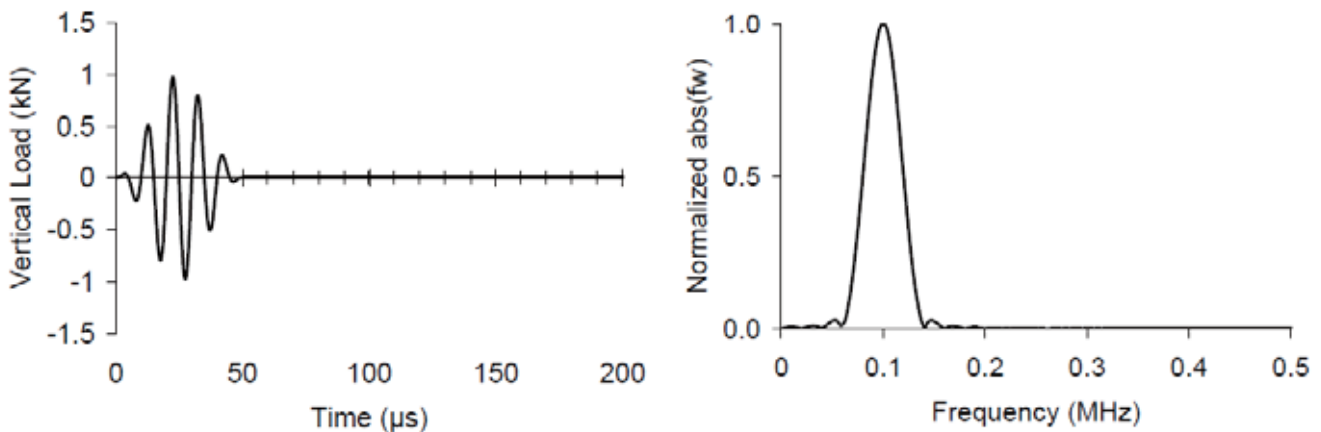


Fig. 5. A narrow band pulse with central frequency 200 kHz in (a) Time domain (left) and (b) Frequency domain (right).

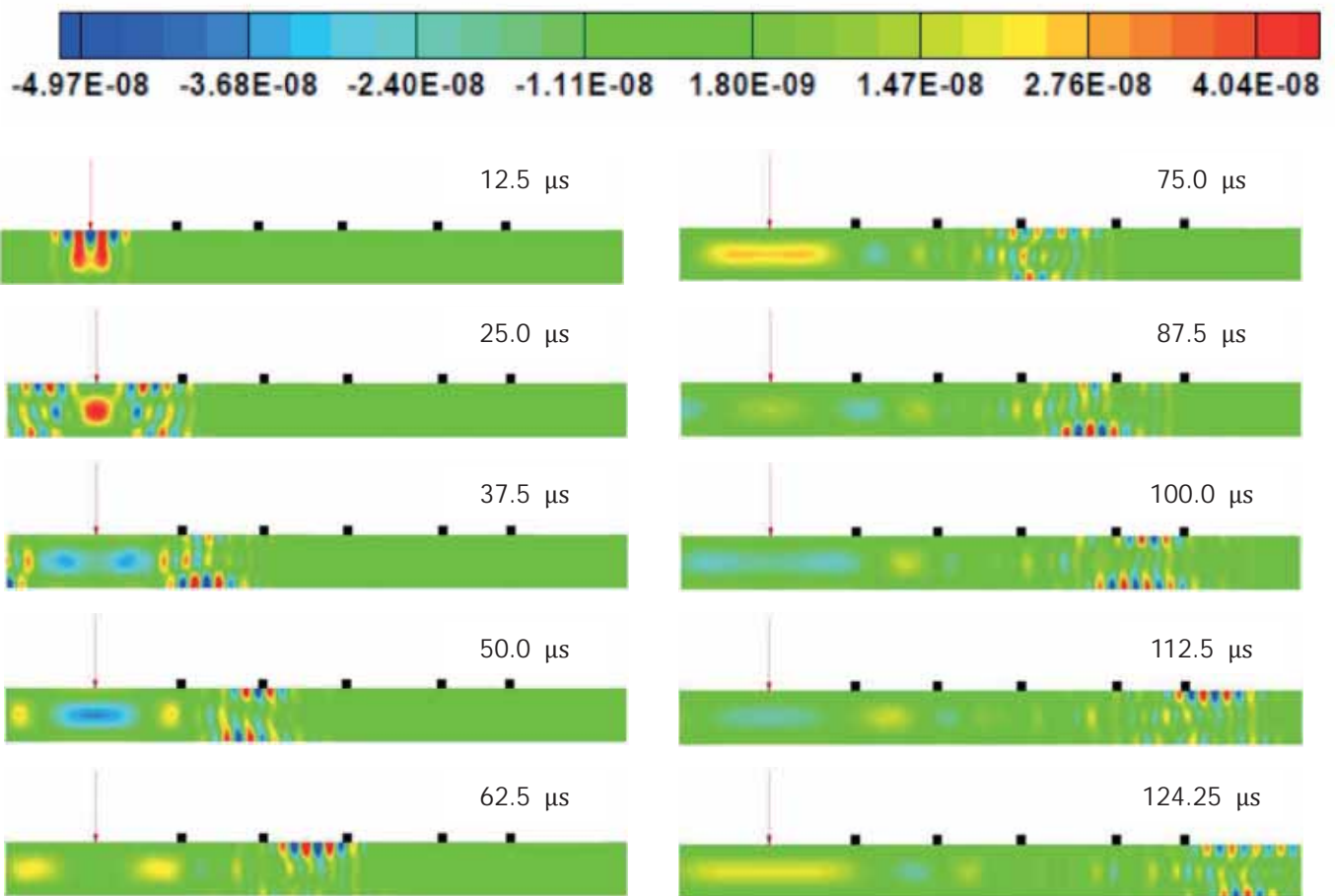


Fig. 6. Contour plot of vertical displacement in a sandwich structure at time intervals for 12.5 μs to 125μs
(■: sensor's location, from left R1, R2, R3, R4, R5).

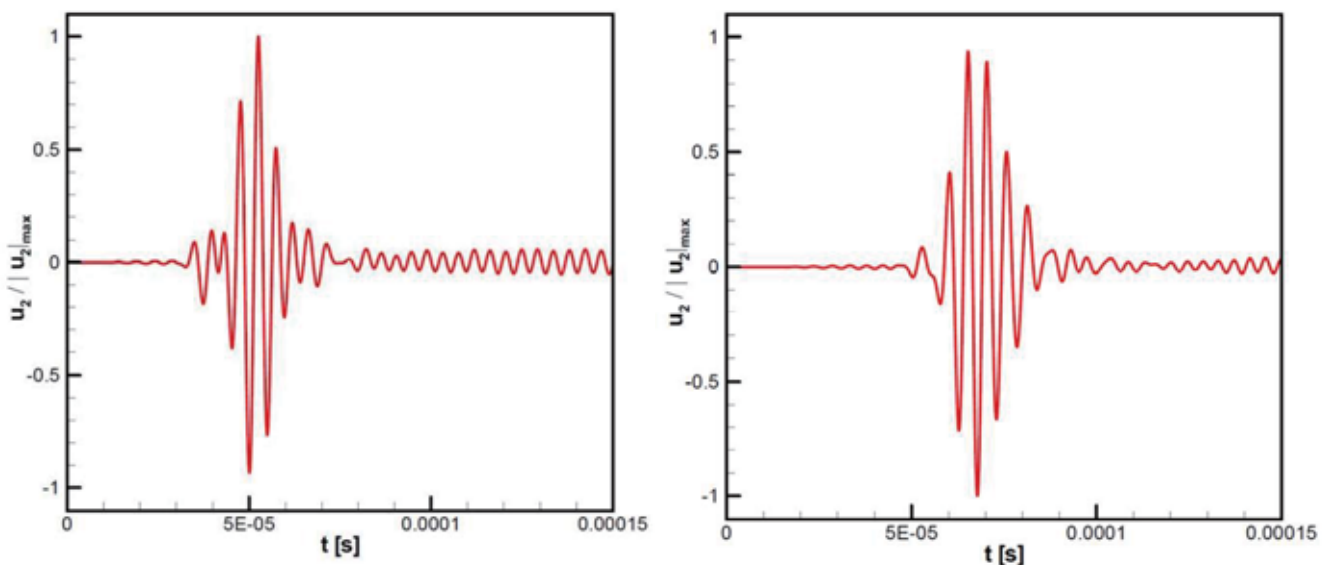


Fig. 7. Normalized vertical displacements with respect to time at sensor's location (a) R2 and (b) R3.

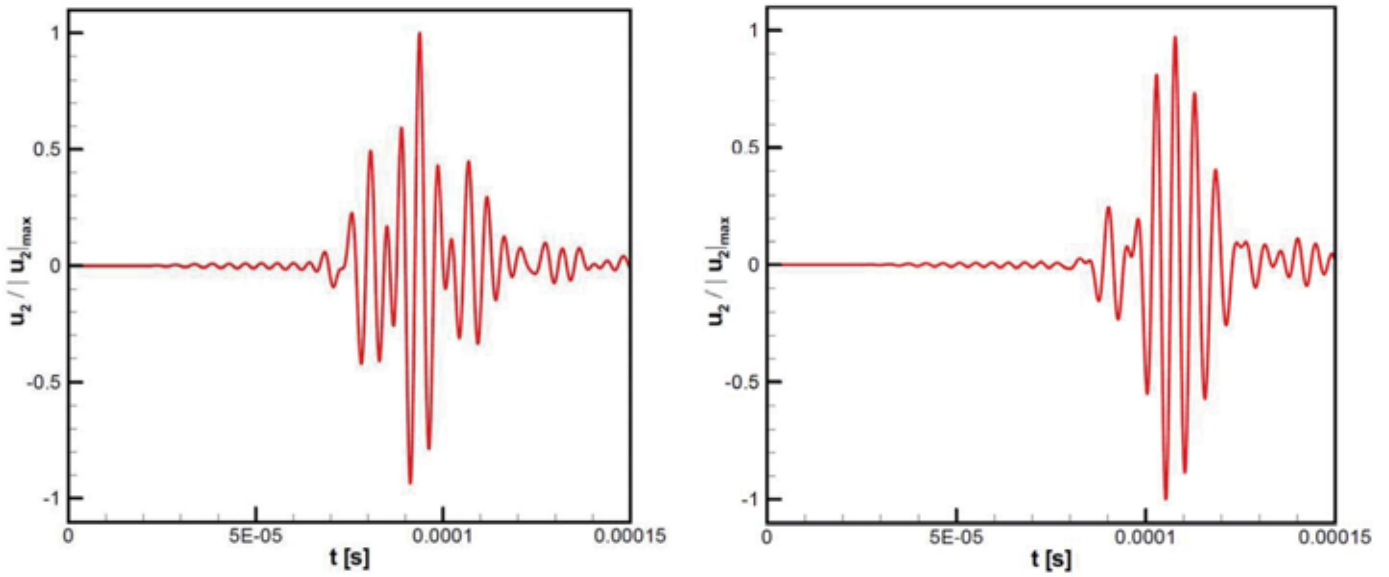


Fig. 8. Normalized vertical displacements with respect to time at sensor's location at (a) R4 and (b) R5.

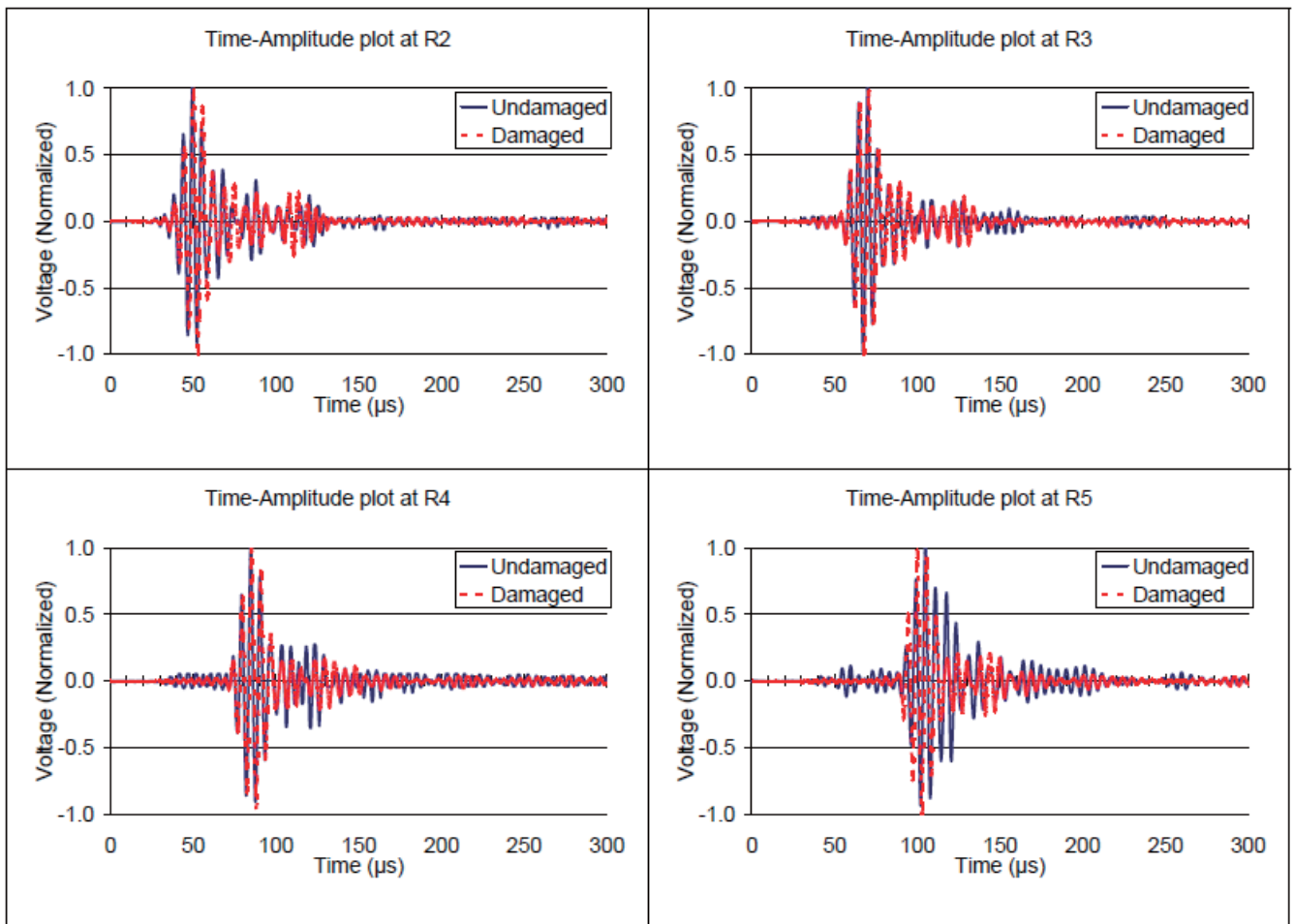


Fig. 9. Received signals in the sandwich structure at 200 kHz central frequency obtained experimentally [3].

5. CONCLUSIONS

The wave responses obtained numerically from the composite sandwich structure that consisted of a woven composite panel and an aluminium honeycomb core are analyzed. The simulations carried out using finite element method for a two-dimensional plane-strain model of the transversely isotropic plate provided a clearly Rayleigh wave propagation, however there was the little discrepancy between the numerical results and experimental ones. It is thought that the same sensor's positions and the modified input signals lead to the improvement of the difference between numerical and experimental results. Nevertheless, it shows same trend with respect to the distance from the source location.

The current study focuses on the wave propagation in composite structure without damages. To verification of Jung's method against the experimental data, we need to analyze the wave propagation in composite structure with a disbond between the composite plate and the aluminium core.

ACKNOELEDGEMENTS

I would like to express my profound and appreciation to my advisor Professor Ertgurl Taciroglu. I am also grateful to Jaedal Jung for his help during my research.

REFERENCES

- [1] Jung, J., Jeong, C. and Taciroglu, E., Identification of a scatter embedded in elastic heterogeneous media using dynamic XFEM, *Comput.Methods Appl. Mech. Engrg.* 259, 50-63 (2013)
- [2] Abdelaziz, Y. and Hamouine, A., A survey of the extended finite element. *Computers and Structures*, 86, pp. 1141-1151 (2007).
- [3] Baid, H. and Mal, A., Detection of damage in a composite structure using guided waves. PhD Dissertation, University of California, Los Angeles (2012).
- [4] Mal, A., Ricci, F., Samajder, H and Baid, H., NDE of composite structures using ultrasonic guided waves. *Health Monitoring of Structural and Biological Systems*, Vol. 8695 (2013)
- [5] Samajder, H., Bais, H., Fabrizio, R. and Mal, A., Lamb waves in a honeycomb composite sandwich plate, *Health Monitoring of Structural and Biological Systems*, Vol. 8695 (2013)

EFFECT OF PROTEIN CHARGE ON ADSORPTION TO APATITE AND CELL VIABILITY

Sakina Kondo

Graduate School of Engineering, Nagoya University
Kondou.sakina@b.m-box.nagoya-u.ac.jp

Supervisor: Benjamin M. Wu

Department of Bioengineering, Graduate School of Engineering, University of California, Los Angeles
benwu@ucla.edu

ABSTRACT

Previous studies suggest that protein plays a significant role in “rescuing” cell viability as a mediator at the cell-apatite interface. Furthermore it is known that surface charge is one of many apatite properties that may directly modulate protein adsorption. Here, we attempt to investigate the influence of protein charge on cell viability. Proteins having different charge were coated on apatite, then protein adsorption and cell viability on the protein-coated apatite was measured. Albumin which has negative charge at physiological pH, is the best at “rescuing” cell viability on the protein-coated apatite while lysozyme, which has positive charge, is poor in “rescuing” cell viability. Both the presence of a mediator at the cell-apatite interface and negative charge of the mediator may be important for cell viability on apatite surface.

Undisclosed

Impact tolerance of metal, composites, and FMLs

Kazuki Miyazaki

Graduate School of Engineering, Nagoya University
miyazaki@ume.mech.nagoya-u.ac.jp

Supervisor: Professor Jenn-Ming Yang

Materials Science and Engineering Department, University of California Los Angeles
jyang@ucla.seas.edu

ABSTRACT

This work presents the results of an experimental investigation concerning the impact tolerance of metal (aluminum), fiber composites (glass/epoxy) and Fiber Metal Laminates (GLARE5-2/1). The Alloy and Glare were purchased and the glass/epoxy composite was fabricated through wet layup. Impact experimental tests were conducted through an impactor to characterize the types and extent of the damages observed for the types of material subjected to the same impact velocity.

Drop-weight impacts were applied at a variety of energy levels to inflict barely visible impact damage, clearly visible impact damage, and penetration damage. The results showed that GLARE laminates exhibit superior impact tolerance when compared with the monolithic 2024-T3 aluminum alloy and glass/epoxy composites.

1. INTRODUCTION

A fiber-metal laminate (FML) such as GLARE is a hybrid composite consisting of layers of thin aluminum and fiber-reinforced epoxy composite. The most widely used metal for FML is aluminum, and the fibers are Kevlar or glass. FMLs are used in aircraft structures [1–6] because they offer many benefits such as low weight, high notch strength, flame resistance, excellent impact resistance, and good damage tolerance [7]. Also, the corrosion resistance is excellent because the composite layers can prevent moisture ingress between the metal layers [7]. Furthermore, FMLs retain the conventional workshop practices of metals such as easy machining, forming, and mechanical fastening abilities, as well as substantial ductility and metal-based damage inspection methods [8]. Therefore, FMLs can be a large part of material for the next generation of aircraft (fig.1). Some of the most important safety issues concerning structural applications in transportation are impact resistance, damage

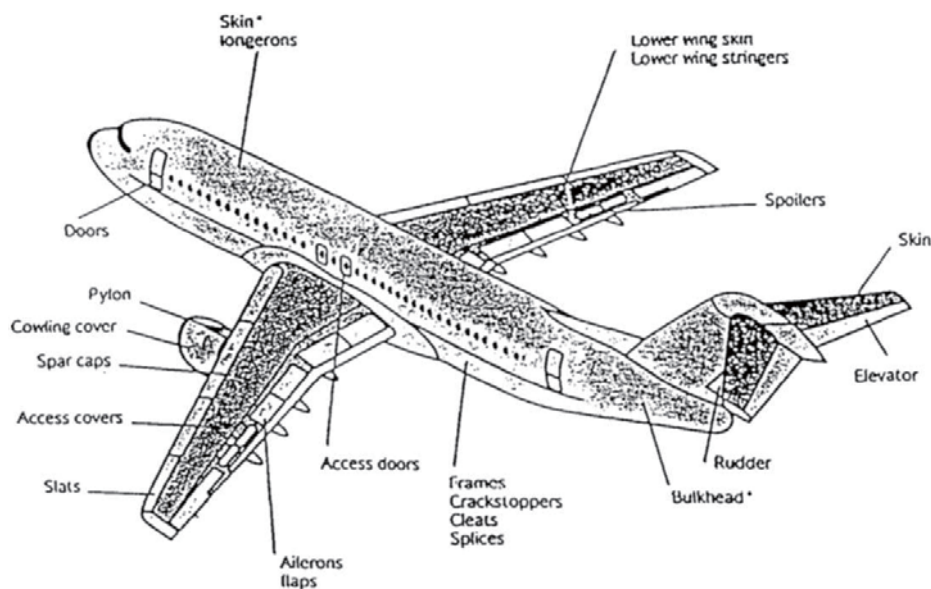


Fig.1 Candidate areas for Aerospace ARALL and GLARE [9]

tolerance, and durability after impact. Impact damage of aircraft structures can be caused by collision between service cars or cargo vehicles and the structure, dropped tools during maintenance, hails, bird strikes, and lightning strikes [9]. Previous researchers have demonstrated that fiber-metal laminates are not as susceptible as traditional composites to the formation of extensive internal damage under impact loading. FMLs offer improved fracture toughness and comparable damage tolerance over monolithic metallic materials [1, 9]. The present report investigates the impact tolerance of GLARE laminates and the result was compared with monolithic 2024-T3 aluminum alloy and fiber composites (glass/epoxy) that has the same thickness as GLARE laminates.

2. EXPERIMENTAL PROCEDURES

2.1 MATERIALS AND SPECIMENS

GLARE 5-2/1 and monolithic 2024-T3 aluminum alloy were provided by Aviation Equipment, Inc. (Costa Mesa, CA). Figure 1 shows the configuration of GLARE laminates used in the present experimental investigation. A GLARE 5-2/1 laminate consists of two layers of 2024-T3 aluminum alloy and one layer of (0°/90°/90°/0°) glass/epoxy composite.

The total laminate thickness was 1.562 mm. On the other hand, the average thicknesses of the aluminum 2024-T3 sheets was 1.60 mm. All specimens were about 76 mm long and 76 mm wide. The figures of all specimens are shown in Fig. 3(a)-(c).

2.2 MANUFACTURING COMPOSITES

Glass/epoxy composites coupons were fabricated to compare with the Glare 5-2/1 and the monolithic 2024-T3 aluminum alloy. The composite was made of glass fiber and epoxy resin. The epoxy resin was EPON Resin 826 with EPIKURE W Curing Agent to cure the epoxy resin. The composites consisted of 12 layers of the glass fiber sheet to produce a composite around 1.5~1.7 mm thick. Figure 4 shows the procedures of manufacturing glass/epoxy composites.

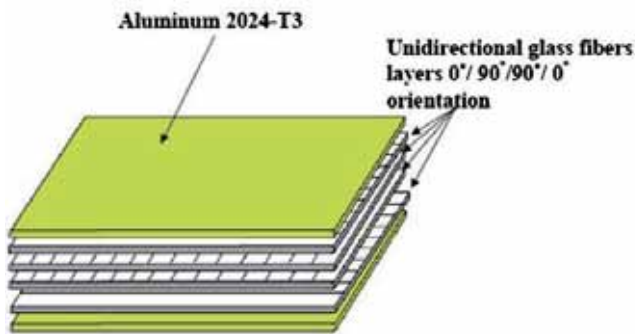


Fig. 2 Configuration of GLARE 5-2/1

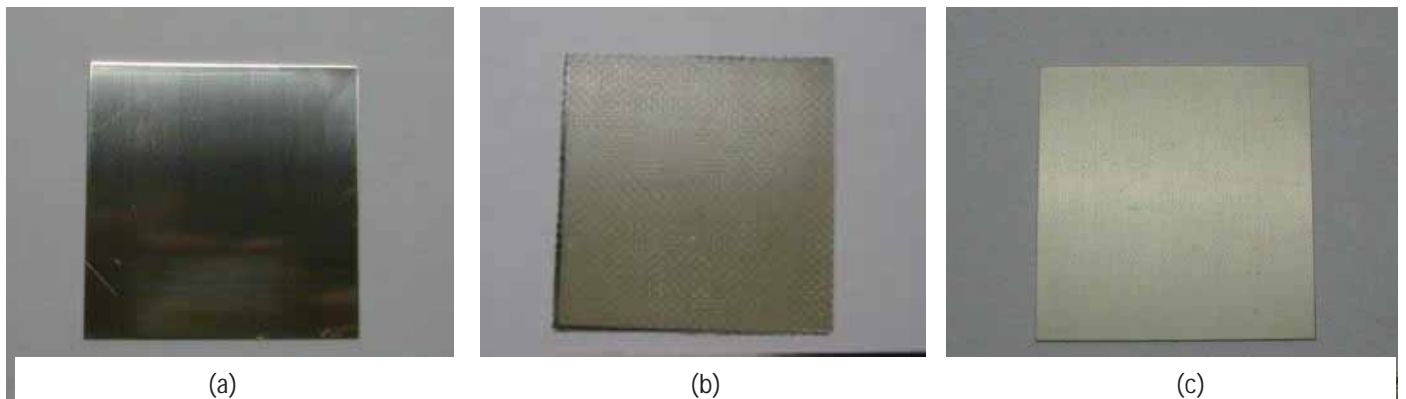


Fig. 2 The figure of (a) 2024-T3 aluminum alloy, (b) the fiber composite (glass/epoxy) and (c) the GLARE 5-2/1 laminate



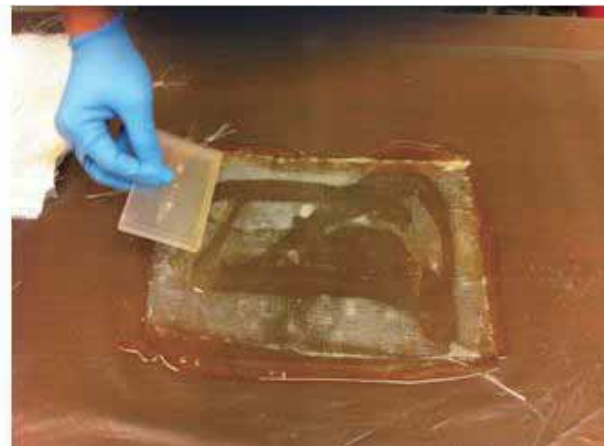
① 200g of the epoxy resin and 52g of the curing agent to the cup.



② Epoxy and curing agent is mixed well with a magnetic stir bar. Then the epoxy is degassed to remove air bubbles that can cause defects in the composite.



③ Woven glass fiber is cut into 30 cm by 20 cm rectangular sheets.



④ Twelve sheets of glass fiber is impregnated with the epoxy resin and stacked together.



④ Vacuum bagging is used to remove excess resin. The illustration of the components of the bag is shown in Fig. 5



⑥ Finally the composite is hot press for 3 hours at 60°C and more 3 hours at 150°C to cure the laminates. The hot press is shown in fig. 6. After curing, take it from the bag.

Fig.4 The procedures of manufacturing glass/epoxy composites

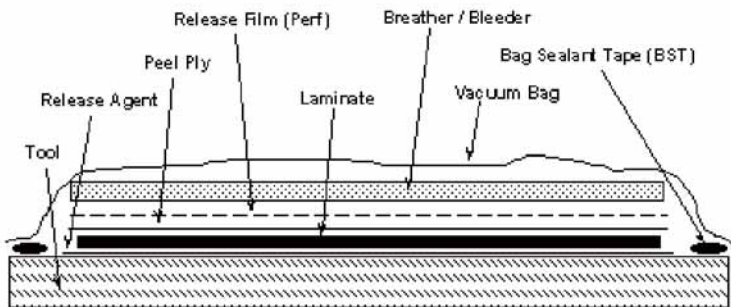


Fig.5 The illustration of the components of the bag [10]



Fig.6 The hot press

2.3 IMPACT TESTING

Low-velocity impact tests were conducted on a Dynatup Model 8250 drop-weight impact tower at impact velocities up to 13.4 m/s. It is shown in fig.7. The 2024-T3 aluminum sheet and the glass/epoxy composite were used for comparison with the GLARE laminates. The data during an impact testing were collected by a National Instrument data acquisition system (NI-DAQ6341) with a photodiode velocity detector. After just applying impact, the pneumatic rebound breaks are activated to push up and hold the impactor assembly in place so that the specimen is not subjected to multiple impacts. Diverse impact energies were obtained by adjusting the dropping height in low-velocity impact tests. One specimen was tested at each different height. During impact testing, the load cell senses the reaction force from specimen. After impact testing, the specimens were carefully removed to investigate the status of damage. For impact, the specimen was clamped between two steel plates. They had a circular opening with a 52 mm diameter at the center. A steel rod of 12.7 mm in diameter with a semispherical end was used with a mass of 3.58 kg or 6.31 kg as an impactor. In this report, the impact energies of the test are 5 J, 10 J, 15 J, 20 J, 25 J and 40 J.

3. RESULT AND DISCUSSION

3.1 IMPACT BEHAVIOR (5 J)

The samples after the impact test (5 J) are shown in fig. 8(a)-(c). They all were dented at the impact points. Figure 9 shows the impact load as a function of time. They all can tolerate impact energy of 5 J because all lines of the load in Fig.8 are regular in shape.

3.2 IMPACT BEHAVIOR (10 J)

The samples after the impact test (10 J) are shown in fig. 10(a)-(c). They all were dented at the impact points and the dents became bigger. Figure 11 shows the impact load as a function of time during 10J impact events. This figure shows the load of all became heavier than that at the impact energy of 5 J and they all can tolerate the impact energy of 10 J by the same token.

3.3 IMPACT BEHAVIOR (15 J)

The samples after the impact test (15 J) are shown in fig. 12(a)-(c). They all were dented at the impact points and the dents became bigger. Figure 13 shows the impact load as a function of time. This figure shows the load of the aluminum and GLARE laminate became heavier than that at the impact energy of 10 J and only the glass/epoxy composite can't tolerate impact energy of 15 J because a precipitous decrease of the load were observed at 2800 μ s in fig.13 and it means the glass/epoxy composite reached the fracture beyond the elastic deformation zone. We think it is because the lack of bond strength between layers occurred delamination.

3.4 IMPACT BEHAVIOR (20 J)

The samples after the impact test (20 J) are shown in fig. 14(a)-(c). They all were dented at the impact points and the dents became bigger. Furthermore a crack was observed on the aluminum on the nonimpacted side (fig.15). Figure 16 shows the impact load as a function of time. This figure shows the load became higher than that of the impact energy of 15 J and only the glass/epoxy composite had penetration damage under impact energy of 20 J by the same token.

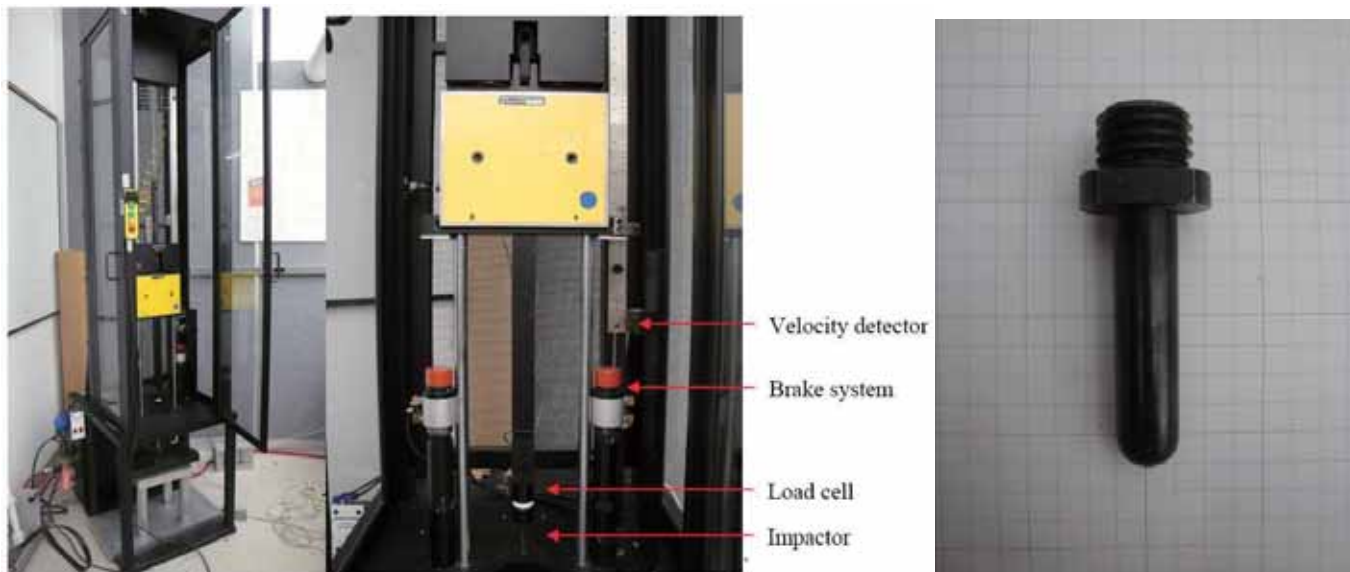


Fig.7 The Dynatup Model 8250 weight drop tower

3.5 IMPACT BEHAVIOR (25 J)

The samples after the impact test (25J) are shown in fig. 17(a)-(c). The glass/epoxy composite was penetrated at the impact point. The aluminum and the GLARE laminate were dented at the impact points and the dents of them became bigger. Furthermore crack damages were observed on the aluminum and the GLARE laminate on the nonimpacted side (fig.18). Especially, the crack damage on the GLARE laminate occurred along the 0° and 90° fiber directions. It means that, as expected, the impact damage spread out along the fiber directions. Figure 19 shows the record of load history during the impact. The load history shows a clear damage behavior after the peak load in impact events.

3.6 IMPACT BEHAVIOR (40 J)

The samples after the impact test (40 J) are shown in fig. 20(a), (b). They all were penetrated at the impact points. Figure 21 shows the record of the load at that time. This figure shows they all can't tolerate impact energy of 20 J.

4. CONCLUSIONS

The low-velocity impact tolerance for 2024-T3 aluminum alloys, glass/epoxy composites, and GLARE 5-2/1 laminates have been investigated experimentally. The different levels of damage (dent, crack and penetration) were induced by varying the impact energy. Monolithic Aluminum shows good ductility, indicating that there is high energy absorption. The Glass fibers composites show immediate damage through delamination or through penetration. However when the GLARE laminates were tested, the GLARE exhibited better impact tolerance than the monolithic aluminum and glass fiber composite. The combined properties of energy absorption of Aluminum and the stiffness of the glass fiber composite, allowed the GLARE to absorb greater impact while exhibiting higher modulus.

ACKNOWLEDGEMENT

This work was supported by Jenn-Ming Yang's Laboratory at UCLA. I would like to express my gratitude to Prof. Jenn-Ming Yang for his generous support for my fulfilling work at UCLA. Po-Ching Yeh is UCLA Post-Doctoral Research Scientist. Without his guidance and persistent help, this report would not have been possible. And also, I would like to appreciate Edward Chang's help with preparing for the experiment and Jonathan Quan's support for writing this report.

REFERENCES

- [1] Wu, G., and Yang, J. M., 2005, "The Mechanical Behavior of GLARE Laminates for Aircraft Structures," *Journal of the Minerals Metals and Materials Society*, **57**(1), pp. 72–80.
- [2] Vermeeren, C. A. J. R., 2003, "An Historic Overview of the Development of Fiber Metal Laminates," *Appl. Compos. Mater.*, **10**(4/5), pp. 189–205.
- [3] Krishnakumar, S., 1994, "Fiber Metal Laminates—The Synthesis of Metals and Composites," *Mater. Manuf. Processes*, **9**(2), pp. 295–354.
- [4] Volt, A., Vogelesang, L. B., and de Vries, T. J., 1999, "Towards Application of Fiber Metal Laminates in Larger Aircraft," *Aircraft Engineering and Aerospace Technology: An International Journal*, **71**(6), pp. 55–57.
- [5] Vogelesang, L. B., and Vlot, A., 2000, "Development of Fibre Metal Laminates for Advanced Aerospace Materials," *J. Mater. Process. Technol.*, **103**(1), pp. 1–5.
- [6] Afaghi-Khatibi, A., Ye, L., and Mai, Y. W., 2003, "Hybrids and Sandwiches," *Comprehensive Composite Materials*, **2**, pp. 249–290.
- [7] Asundi, A., and Choi, Alta Y. N., 1997, "Fiber Metal Laminates: An Advanced Material for Future Aircraft," *J. Mater. Process. Technol.*, **63**(1/3), pp. 384–394.
- [8] Vermeeren, C. A. J. R., 2003, "An Historic Overview of the Development of Fiber Metal Laminates," *Appl. Compos. Mater.*, **10**, pp. 189–205.

[9] Wu, G., 2007, "The Impact Properties and Damage Tolerance and of Bidirectionally Reinforced Fiber Metal Laminates," *J. Mater. Sci.*, **42**, pp. 948–957.

[10] "Vacuum Bagging: Basics,"
<http://composite.about.com/od/aboutcompositesplastics/l/aa000109.htm>

[11] Hyoungseock Seo, H. T. Hahn and Jenn-Ming Yang, 2008, "Impact Damage Tolerance and Fatigue Durability of GLARE Laminates," *Journal of Engineering Materials and Technology*, **130**, 041002-1–041002-6.

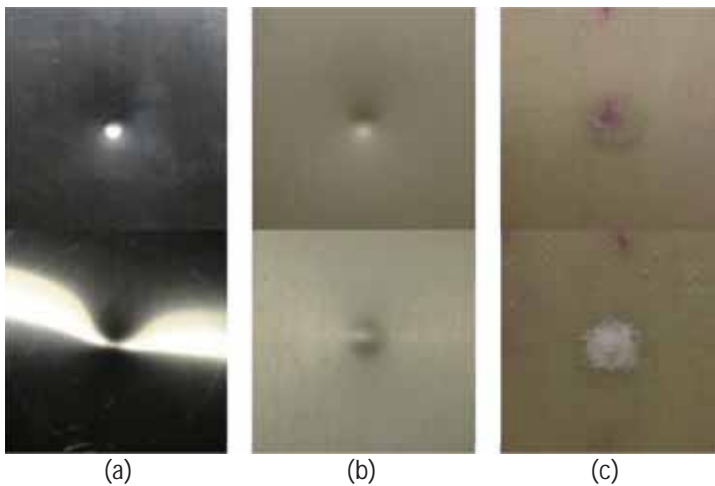


Fig. 8 The figure of (a) 2024-T3 aluminum alloy, (b) the fiber composite (glass/epoxy) and (c) the GLARE 5-2/1 laminate after the impact test (5 J)

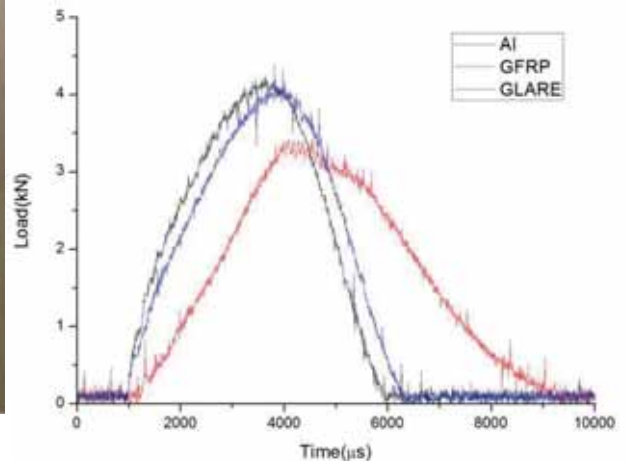


Fig. 9 The impact load as a function of time (5 J)

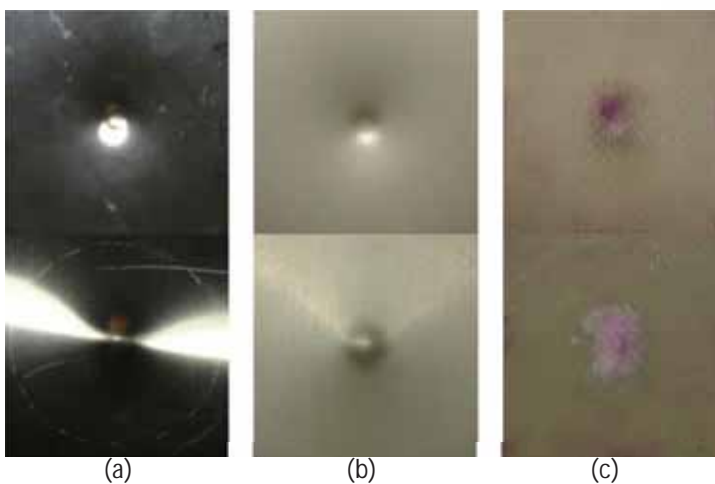


Fig. 10 The figure of (a) 2024-T3 aluminum alloy, (b) the fiber composite (glass/epoxy) and (c) the GLARE 5-2/1 laminate after the impact test (10 J)

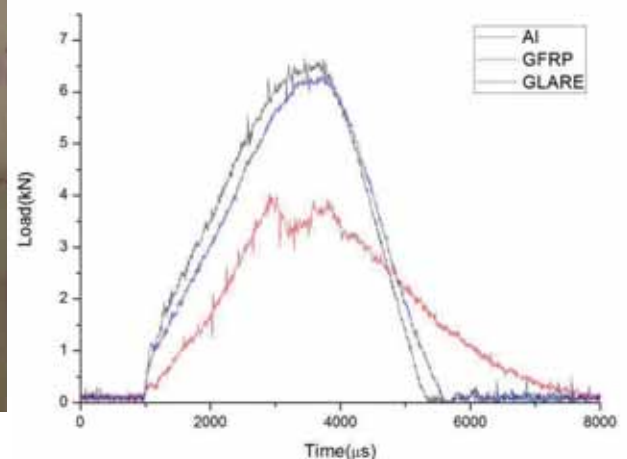


Fig. 11 The impact load as a function of time (10 J)

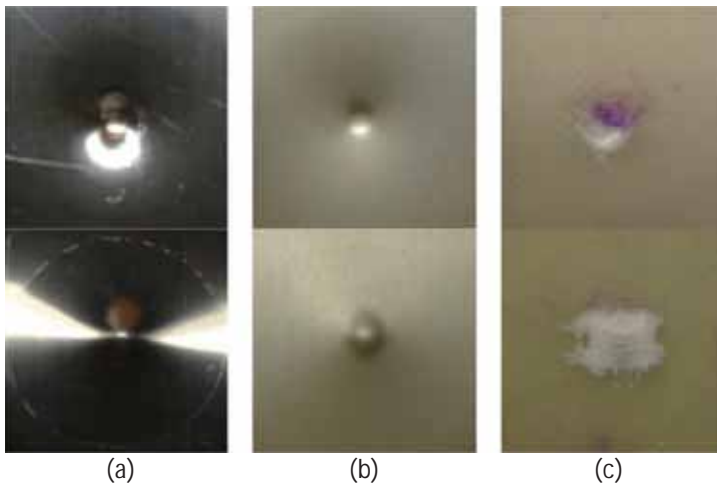


Fig. 12 The figure of (a) 2024-T3 aluminum alloy, (b) the fiber composite (glass/epoxy) and (c) the GLARE 5-2/1 laminate after the impact test (15 J)

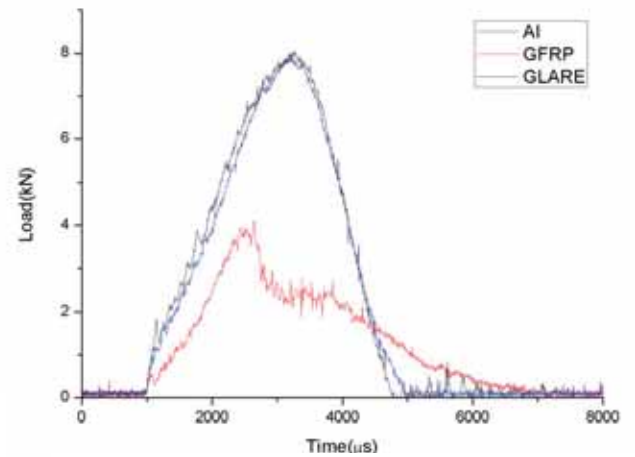


Fig. 13 The impact load as a function of time (15 J)

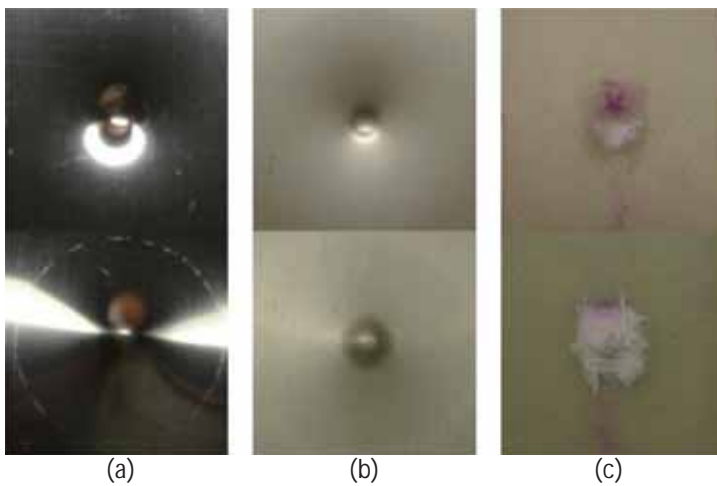


Fig. 14 The figure of (a) 2024-T3 aluminum alloy, (b) the fiber composite (glass/epoxy) and (c) the GLARE 5-2/1 laminate after the impact test (20 J)



Fig. 15 The crack damage on 2024-T3 aluminum alloy after the impact test (20 J)

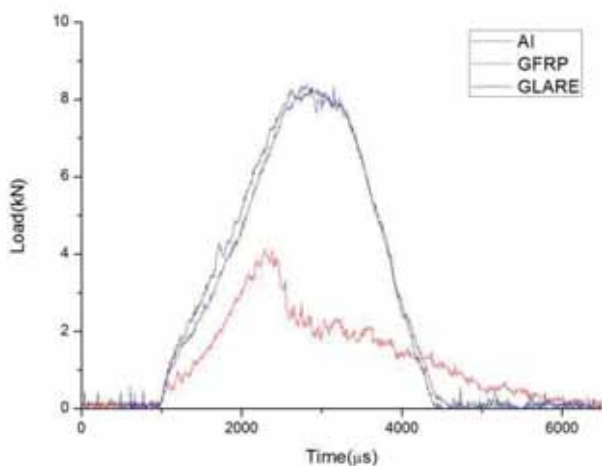


Fig. 16 The impact load as a function of time (20 J)

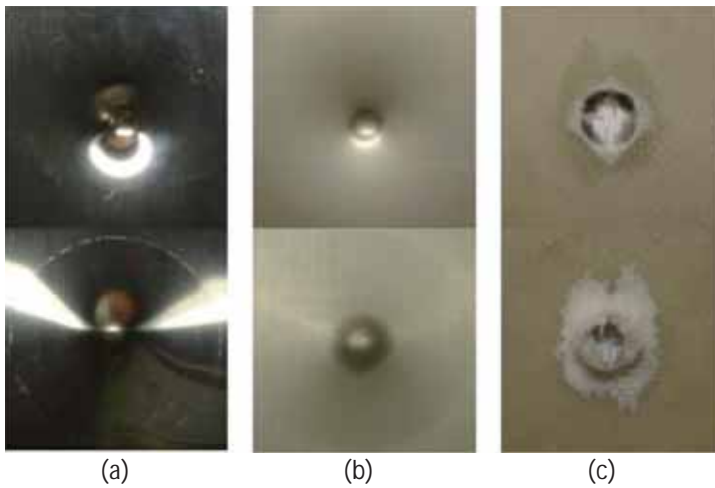


Fig. 17 The figure of (a) 2024-T3 aluminum alloy, (b) the fiber composite (glass/epoxy) and (c) the GLARE 5-2/1 laminate after the impact test (25 J)

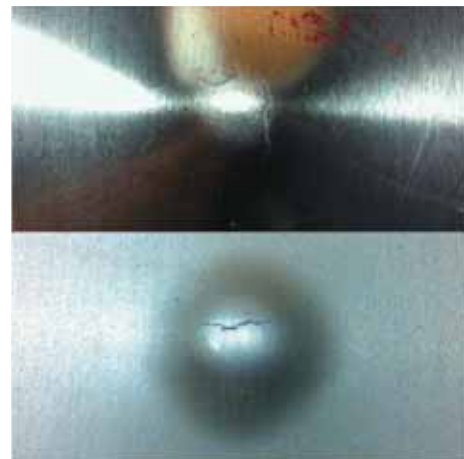


Fig. 18 The crack damage on 2024-T3 aluminum alloy and the GLARE 5-2/1 laminate after the impact test (25 J)

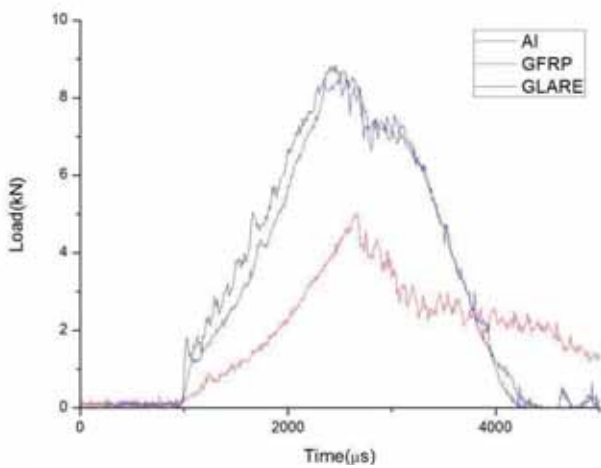


Fig. 19 The impact load as a function of time (25 J)

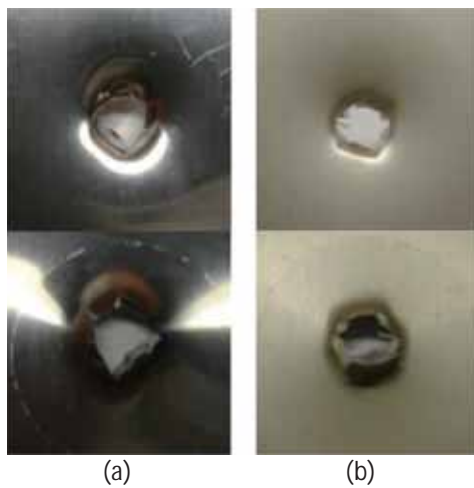


Fig. 20 The figure of (a) 2024-T3 aluminum alloy and (b) the GLARE 5-2/1 laminate after the impact test (40 J)

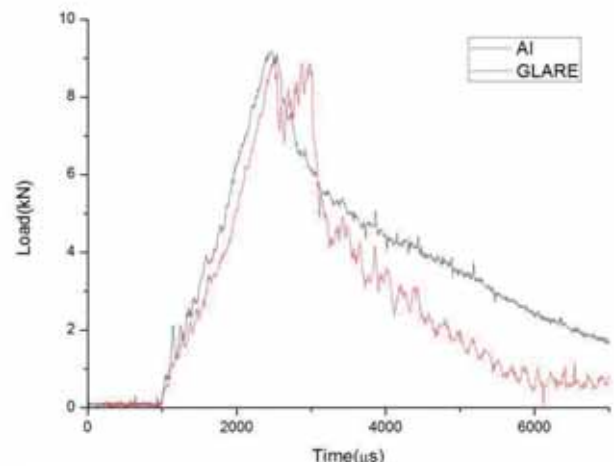


Fig. 21 The impact load as a function of time (40 J)

STUDY ON AN ALUMINUM TWO-PHASE HEAT TRANSFER DEVICE USING IAS FLUID

Shoya Ono

Department of Aerospace Engineering, Graduate School of, Nagoya University
ohno@prop2.nuae.nagoya-u.ac.jp

Supervisor: Ivan Catton

Department of Mechanical and Aerospace Engineering, University of California, Los Angeles
catton@ucla.edu

ABSTRACT

Two phase heat transfer devices such as heat pipes and thermo-syphons are widely used to manage the heat of electronic equipment. In this research, to reduce weight and to improve efficiency, aluminium thermo-syphon using IAS as a working fluid is studied. In the past, it was found that aluminium / IAS which was cooled by a cooling block would work correctly, but a 6 foot length aluminium / IAS thermo-syphon cooled by natural convection failed. The purpose of this study is to figure out the reason the natural convection test failed. In this study, different lengths of natural convection thermo-syphons were tested. These thermo-syphons were made of aluminium (6061) with 3/8 in OD and 0.305 in ID, and inside wall was smooth. As a result, it was discovered that the reason for failure was not the cooling methods but rather the discontinuity of the back flow. Furthermore, it was found that the critical operating length of the thermo-syphon is between 2 and 3 feet.

1. INTRODUCTION

Phase-change heat transfer devices such as heat pipes are used to manage heat of electronic devices. A heat pipe is a two-phase heat transfer device which consists of a sealed working fluid in a pipe. Heat pipes transfer heat from a source passively where the working fluid is evaporated and carried to the other end of the pipe where heat is rejected and liquid is re-condensed. Fluid is returned from the condenser to the evaporator by a variety of methods such as gravity forces or capillary forces. Generally, copper is the most commonly used casing material due to its high thermal conductivity with water which has high heat transfer capacity and safety. However, for space applications where heat transfer devices need to be light weight, copper is an unwise choice due to its high density. Therefore, aluminum is used as a casing material in these applications because its density is more than three times less than copper. However, water cannot be used as a working fluid with aluminum because exposing aluminum to water will oxidize the surface of aluminum and generate aluminum oxide and hydrogen. Hydrogen is a non-condensable gas (NCG) and

will build up in the condenser and block the area available for condensation. This leads to failure of the heat pipe. Therefore, ammonia or methanol are being used as the working fluids in aluminum heat pipes to avoid NCG formation. However, heat transfer capacity of methanol is inferior to water. The performance of a working fluid is represented by the merit number. Merit number is shown by equation (1) [1].

$$M = \frac{\sigma_l h_{fg}}{v_l} \quad (1)$$

The key properties of working fluid are the latent heat of vaporization, surface tension, and liquid viscosity. This number compares the relative performance of heat pipe working fluids, and a high number is required to achieve efficient heat transport. Figure 1 shows merit numbers of various fluids. From this, it can be seen ammonia and ethanol have a lower number compare to water.

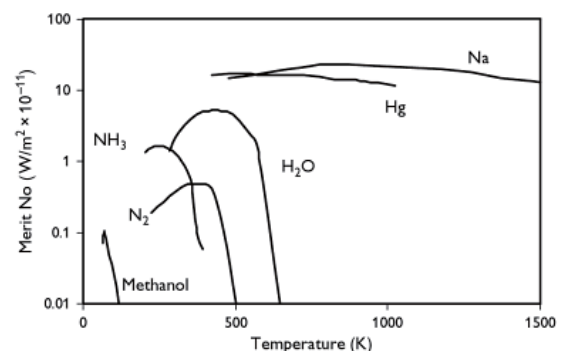


Fig. 1 Merit number of various fluids

In this study, inorganic aqueous solution (IAS) is used as a working fluid in aluminum casing. IAS is complex mix of 9 chemical constituents in aqueous solution. The properties of IAS are similar to water, but IAS reacts with the aluminum surface to create a compact oxide layer, hydrophilic coating and electrochemical reaction which prevent hydrogen gas formation and improve the heat transfer performance. Using an aluminum casing with a water-based fluid such as IAS will improve the performance of light weight heat pipes. More details of IAS are mentioned in the next chapter.

In the past, Thermo-syphons using aluminum and IAS have been fabricated and tested. Thermo-syphons are the simplest phase-change heat transfer devices. In a thermo-syphon, the surface of the tube is smooth and the condensed liquid returned by gravity forces while heat pipes use capillary force to return the condensed liquid using wick. It was confirmed that an aluminum/IAS thermo-syphon can perform as well as a copper-water thermo-syphon.^[2] However, it was also confirmed that an aluminum-IAS thermo-syphon which is cooled on the top by a cooling block using chilled water, can work normally, on the other hand, a 6 foot long aluminum/IAS thermo-syphon cooled by natural convection failed. So, the purpose of this research is to determine the cause.

2. IAS FLUID

IAS fluid shown in figure 2 is an aqueous solution with the 9 chemical constituents shown in Table 1. IAS fluid reacts with an aluminum surface to create a compact oxide layer, hydrophilic coating and electrochemical reaction. The aluminum oxide layer and electrochemical reaction prevent NCG generation. In addition, because the wettability of surface is improved by hydrophilic coating; the heat transfer performance improves. Using IAS with aluminum thermo-syphons, the reactions taking place are shown in equation (2) ~ (15)



Fig. 2 IAS fluid

Table 1 Ions present in IAS

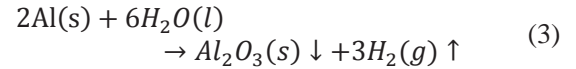
Solution		Suspension
Positive ions	Negative ions	
Na^+	MnO_4^-	$MgCrO_4$ Small solubility
K^+		
Mg^{2+}	$Cr_2O_7^{2-}$	MnO_2 Only after long time
Ca^{2+}		
Sr^{2+}		
Ag^+	CrO_4^{2-}	

a) Water reaction

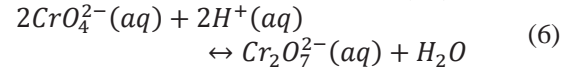
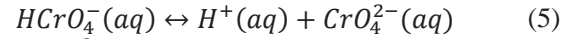
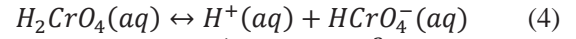


Water self-ionization is shown by equation (2). If water contacts an aluminum surface, the reaction between

the aluminum surface and water is shown by equation (3). In this reaction, hydrogen gas, which is an NCG, is generated and the heat transfer device will fail.

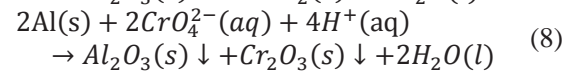
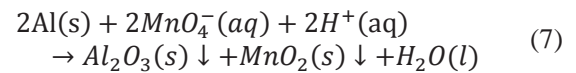


b) Chromium balance



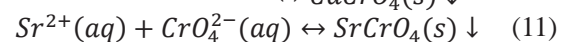
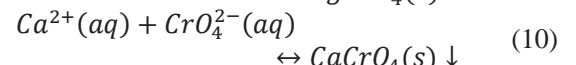
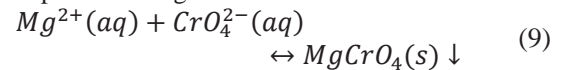
Chromium exists in IAS fluid as chromate acid, hydrogen chromate ion, chromate ion, and dichromate ion. The composition is dependent upon pH number. When the pH number is between 6 and 8, the amount of chromate ions increase.

c) Oxidation



There are two oxidizers, permanganate and chromate, in the IAS fluid. Oxidizers such as permanganate react with aluminum surface and create oxidation on the surface as indicated in equations (7) and (8). This oxidation prevents contact between water and the aluminum surface. In addition, this reactions consumes hydrogen ions, which makes the pH number increase. Therefore, chromate will be generated on the surface. It promotes the generation of a hydrophilic coating shown in the next chapter.

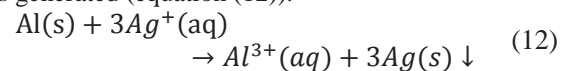
d) Hydrophilic coating



With the concentration of chromates increasing, some hydrophilic chromate salts will be generated as shown in equations (9), (10) and (11). These salts are hydrophilic and will coat the surface with a porous structure. The porous hydrophilic coating will improve the heat transfer performance.

e) Silver effect

The silver ions in IAS react with aluminum, and the silver is generated (equation (12)).



Aluminum oxide is an electric insulator. It protects the chemical reaction and electric connection between aluminum and IAS. In that case, the reaction occurring in the evaporating region is by equations (7) and (8). However, the reaction occurring in the condenser and adiabatic regions is by equation (11). However, silver works as a bridge, connecting aluminum surface and IAS fluid. This makes the

electro-chemical problem between the aluminum surface and IAS fluid. Therefore, the reaction shown in equation (13) occurs in the condenser and adiabatic regions, and the reaction shown in equation (14) and (15) occurs in the evaporating region. In this reaction, the hydrogen ions are transported with liquid back flow from the condenser region to the evaporating region, and the electrons are transported through aluminum and silver from the condenser region to the evaporating region shown in figure 3. Therefore, NCG does not generate.

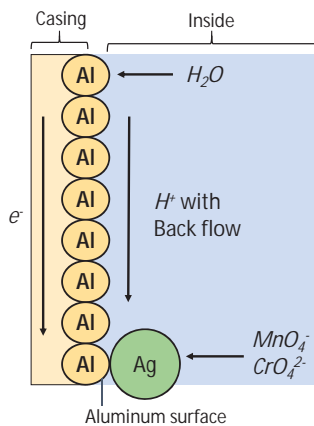
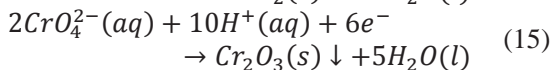
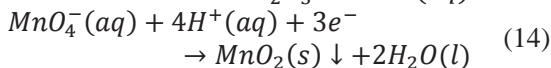
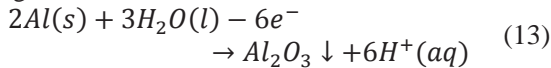


Fig. 3 Effect of silver in electrochemistry circle

3. PROBLEM AND PROPOSED THEORY

In the past, it was observed that aluminum/IAS thermo-syphon with cooling block can work normally. However, an identical thermo-syphon with cooling method changed from a cooling block to natural convection failed. The purpose of this research is to formulate a hypothesis for

the reason of failure and test that hypothesis.

Figure 4 shows the theory proposed in this study. In aluminum/IAS thermo-syphon, the hydrogen ions should be transported from the condenser region to the evaporator region by back flow to allow the electrochemical reactions to occur, shown in equation (13) ~ (15). The thickness of back flow depends on cooling methods and length of thermo-syphon. When the same heat flow is applied, the thickness of the back flow in evaporator region is same between cooling-block method and natural convection. For the cooling-block method, the thickness is constant in the adiabatic region, and the thickness is gradually reduced at condenser region (Fig.4 left). On the other hand, in natural convection method, the thickness is gradually reduced at the upper part of the evaporator (Fig.4 center). Therefore, the thickness of back flow in natural convection is thinner than the thickness of back flow in cooling-block method. So, it is expected that the back flow in natural convection is discontinuous. For a long thermo-syphon using natural convection, it is easier to have a discontinuous back flow. In that case, at the upper side where the back flow remains, the hydrogen ions cannot transfer to evaporator region, water and the aluminum surface react at the region and NCGs are generated. NCGs will block the two phase cycle and it cause the thermo-syphon to fail (Fig.4 right).

4. EXPERIMENT

Thermo-syphon tests were conducted to verify the theory. In these tests, the aluminum/IAS thermo-syphon cooled by natural convection was tested. In these experiments, different length of thermo-syphons were tested. For natural convection, the longer the thermo syphon is the thinner thickness of back flow it will have. So, it is estimated that back flow was easier to disconnect in the long thermo-syphon. From these tests, the relationship between the length of thermo-syphon and our theory was able to be verified.

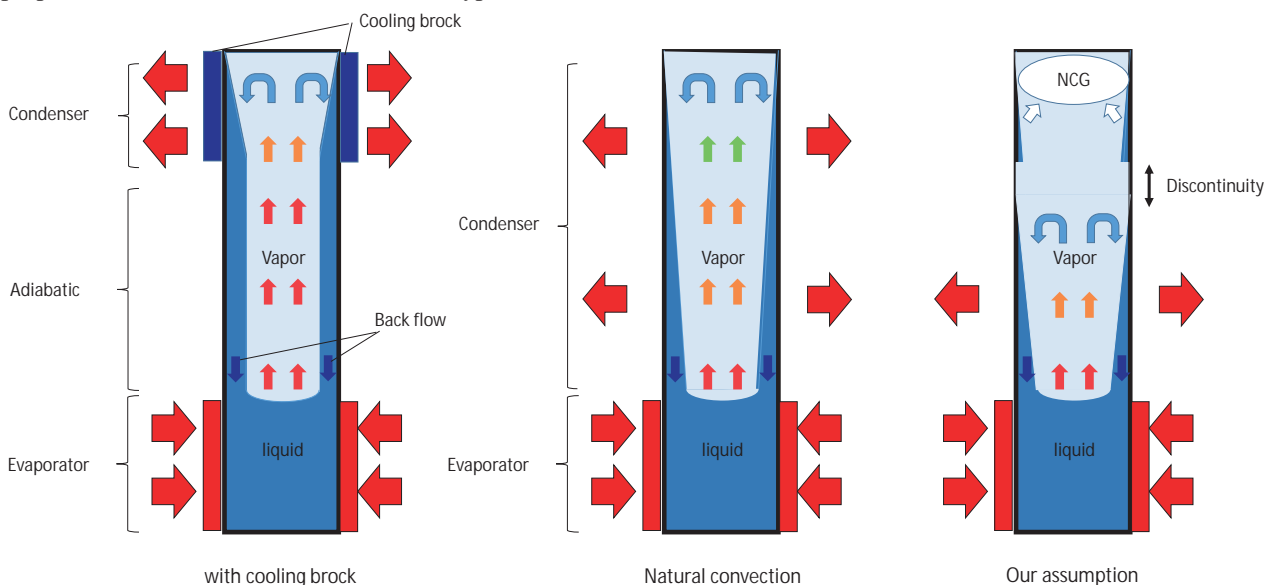


Fig.4 The relationship of cooling methods and back flow and our theory of the fail

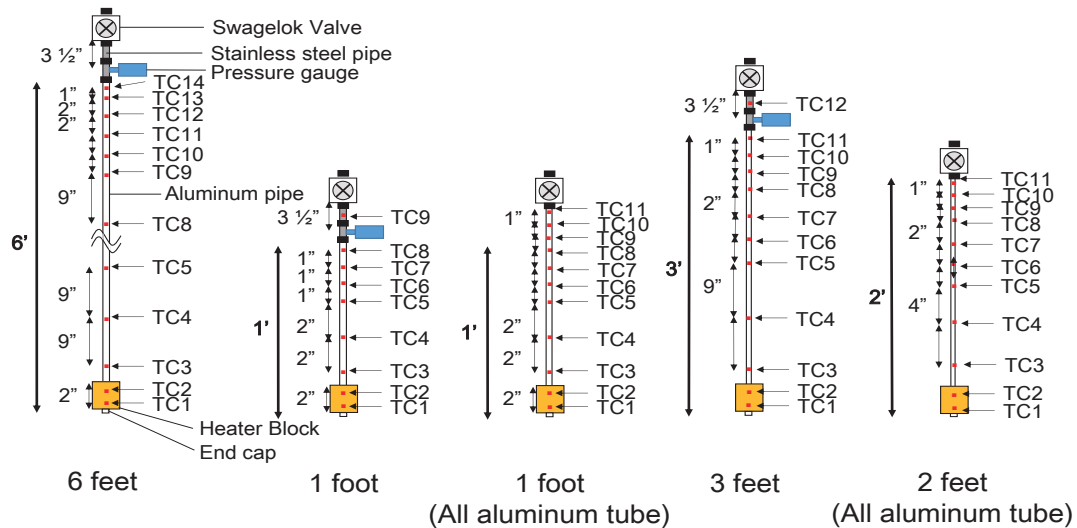


Fig.5 Thermo-syphon and thermocouple location

5. TEST SETUP

In this experiment, five different thermo-syphons were fabricated and tested. All thermo-syphons were made of aluminum (6061) with 3/8 in OD and 0.305 in ID, and inside wall was smooth. The heater block measured 2 in×1.1/4 in×1.1/2 in and was attached to the bottom of the thermo-syphon. The working fluid was IAS and 2.1 ml was charged into the pipe, which is 60% of the evaporator region volume. The temperature was measured by K-type thermocouples. Thermocouples were attached in short intervals at the top of the thermo-syphon to observe the volume of NCG generated. The pressure was also measured during the test. In each test, thermocouple placements, heater and condenser locations, and pressure measurements can be found in figure 5.

6. RESULTS

6.1 6 foot thermo-syphon

Figure 6 shows the test results of the 6 foot thermo-syphon. In this test, 50W heat load was first applied to the heater block, 20 minutes later heat load increased from 50W to 100W. Tube temperature measurements (TC3~14) were observed to be the same for 15 minutes. After 15 minutes, temperatures of TC14 which is located at the top of the thermo-syphon decreased. After that, temperature of TC 13, TC12 and TC11 also decreased. It is expected that NCG was generated and stayed at the top of the tube. After that, heat load was changed from 50W to 100W, and TC11 temperature returned. This is because the tube pressure increased and NCG was compressed. 45 minutes later, the heater temperature jumped up and tube temperatures decreased. It was because of dry out, then, the test was stopped.

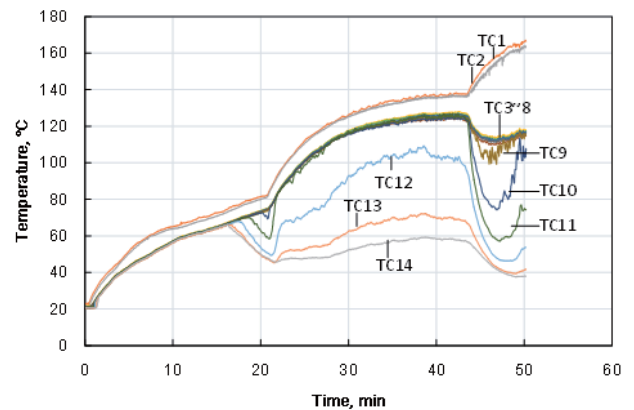


Fig. 6 Test result of 6 foot thermo-syphon

6.2 1 foot thermo-syphon

Figure 7 shows the results of the 1 foot thermo-syphon test. In this test, the heat load was 50W. From this result, it can be found that the thermo-syphon cycle worked for more than 1 hour. From the results of 6.1 and 6.2, it is expected that the reason for failure was not natural convection. However, the top region of this thermo-syphon consists of stainless steel tube, then, it is also expected that the discontinuity happened in this area. Then, a thermo-syphon consisting of only an aluminium tube was made and tested in the next step.

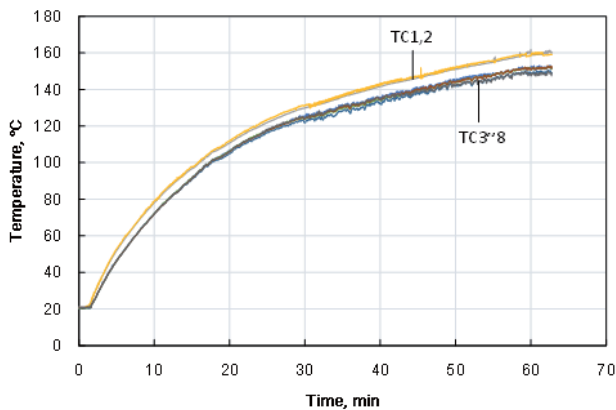


Fig. 7 Test result of 1 foot thermo-syphon

6.3 1 foot thermo-syphon (all aluminum tube)

Figure 8 shows the results of the 1 foot thermo-syphon which consists of only an aluminium tube, without stainless steel pieces for the pressure transducer, shown in figure 5. This tube doesn't use stainless steel, therefore, potential discontinuities in the top region can be identified. In this test, the heat load was 50W. From this result, it can be found that thermo-syphon cycle could work more than 1 hour. Therefore, it is expected that the discontinuity doesn't happen less than 1 foot. In the next step, the maximum length which discontinuity does not occur was verified.

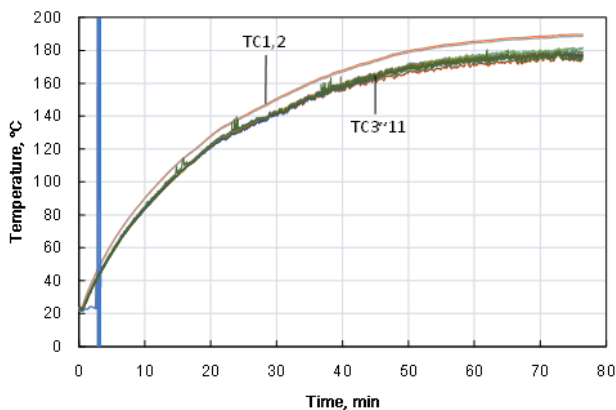


Fig. 8 Test result of 1 foot all aluminium tube

6.3 3 foot thermo-syphon

To find the critical point that discontinuity will occur, a 3 foot thermo-syphon was fabricated and tested. Figure 9 shows the results of this experiment. In this experiment, 50W was applied to the heater. From the results, the temperature of TC12 fell in 15 minutes. This means NCG was generated above this point. 55 minutes later, the temperature of TC11 also fell. After that, the temperature of TC11 was constant. It means no NCG was generated, and, no discontinuity occurred within the tube after the temperature of TC11 fell.

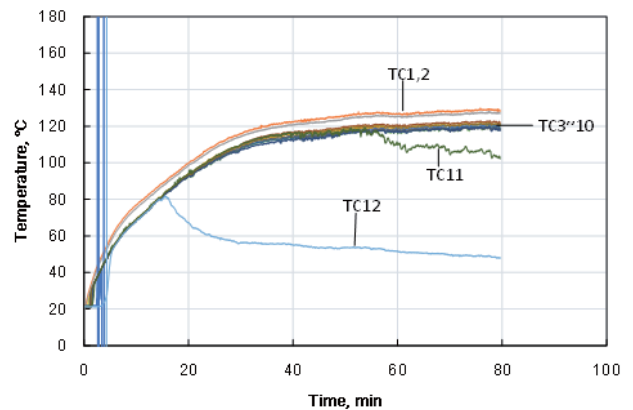


Fig. 9 Test result of 3 foot thermo-syphon

6.3 2 foot thermo-syphon (all aluminum tube)

From these results, it was found that the critical point is between 1 and 3 feet. Therefore, a 2 foot thermo-syphon was fabricated and tested. Figure 10 shows the results of the 2 foot thermo-syphon test. In this test, 50W was applied to the heater and the entire tube consisted of aluminum. It can be found that the 2 foot thermo-syphon worked correctly. From these results, the critical point is determined to be between 2 and 3 feet.

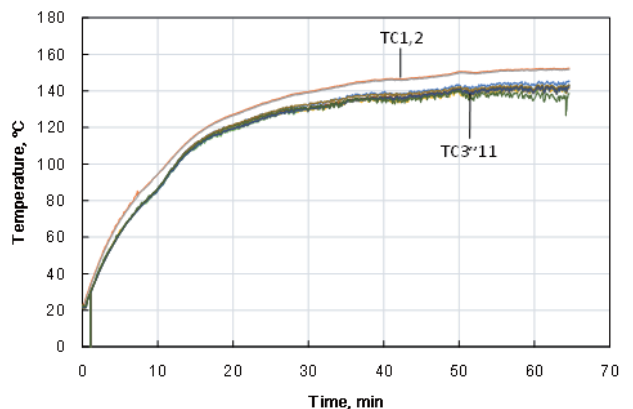


Fig. 10 Test result of 2 foot thermo-syphon

CONCLUSION

In this research the reason for failure of aluminium / IAS thermo-syphons, cooled by natural convection, was verified. In summary, the reason for failure is not natural convection but discontinuity of back flow. It was also found that this discontinuity depends upon the length of the thermo-syphon. In this experiment, the critical point of the length of thermo-syphon was between 2 and 3 feet.

ACKNOWLEDGEMENTS

I appreciate that professor Ivan Catton gave me the opportunity to study in his laboratory. I had a great experience there. I would like to offer my special thanks to Qi Yao. Without his support this report would not have been possible. I appreciate Michael Stubblebine for his help writing this report. I would also like to thank Armin Karimi and express my gratitude for his support as well.

REFERENCES

- [1] Reay, D. and Kew, P., Heat Pipes: Theory, Design, and Applications, 5th ed. Elsevier, Oxford, UK (2006).
- [2] Qi Yao, Mike Stubblebine, Sean Reilly, Ladan Amouzegar, Ivan Catton, "Using an Inorganic Aqueous Solution in Copper and Aluminum Phase Change Heat Transfer Devices", Proceeding of the ASME 2013 International Mechanical Engineering Congress and Exposition, ASME,(2013)

MECHANICAL STIMULATION ON RAT INTESTINAL SMOOTH MUSCLE CELLS TO IMPROVE MATURITY

Supervisor: Benjamin M.Wu

Department of bioengineering,
benwu@ucla.edu

Toshihiro Sato

Graduate School of Engineering, Nagoya University
satou.toshihiro@b.mbox.nagoya-u.ac.jp

ABSTRACT

Many intestinal diseases, such as Crohn's and colitis (or Hirschsprung's), require large portions of the small intestine to be removed for treatment, which can result in Short Bowel Syndrome. Short Bowel Syndrome is currently treated with total parenteral nutrition (TPN) or rarely transplantation. TPN can lead to liver failure and transplantation often leads to immunological problems, leaving a tissue engineering solution to be desired. The inability to engineer clinically relevant functional intestinal tissue remains a major hurdle.

This article describes that we will confirm an improvement in the maturity of smooth muscle cells on the substrate of PDMS that is fibronectin (FBN) coated by adding mechanical stimulation. We examine three markers: myosin heavy chain (MHC), desmin (DES) and smooth muscle actin (SMA) by using PCR and immunostaining.

Improvement of maturity of the smooth muscle cells gives significant progress in tissue engineering and fabrication of artificial the intestine.

1. INTRODUCTION

Intestinal failure (IF) is the actual or impending loss of nutritional autonomy due to gut dysfunction, resulting from: short bowel syndrome(SBS), mucosal defects, motility disorders, trauma, or tumors. SBS is the consequence of massive resection of the small intestine due to Crohn's disease, mesenteric vascular accidents, trauma, volvulus, or surgical complications and results in insufficient functional small bowel for maintaining protein energy, fluid, electrolyte, or micronutrient balance on a normal diet.

It is important to pursue tissue engineering alternatives for diseased tissues. Among other tissues, intestine is composed of smooth muscle which functions to propel intestinal contents towards the rectum by repeated relaxation and contraction. Intestine is not functional without smooth muscle so it is important to understand the characteristics of muscle. Tissue engineering of smooth muscle in vitro for functional tissue replacement in vivo may provide a potential therapeutic solution to this unmet medical need. A major problem is that smooth muscle cells taken from rat intestinal

tissue decrease in maturity rapidly. When cells are present in the body, they have maintained links with the surrounding environment. But after taking out the cells from tissue and digesting in to individual cells, these links are removed and functionality decreases, leading to changes in observable markers. Cells change their characteristics according to environmental factors such as mechanical stimulation.

The objective of this study is to provide mechanical stimulation on rat intestinal smooth muscle cells to improve their maturity. This advancement in SMC maturity and proliferation may lead to an exciting engineering solution for intestinal smooth muscle tissue.

2. EXPERIMENTAL METHOD

2.1 Cell culture

We use smooth muscle cells taken from 5 day old Lewis rat pups. The primary cells are cultured using DMEM included GultaMax, FBS (10%) and ABAM. Media was exchanged once every three days, and cells were kept at 37° Celsius and 10% CO₂ concentration. We took pictures of the cell culture at day 1, day 4, day 7.

2.2 Making PDMS membrane

PDMS was poured in to a mold (Fig.1) and solidified at 65° Celsius before autoclaving for sterilization. the PDMS membrane was coated with Fibronectin(1mg/ml) in order to help smooth muscle cells attach.PDMS membrane dimensions were (Fig.2) 10mm, thick, 75mm long and 2mm high.

2.3 Primary Harvest from Rat Pups

Pups were euthanized by CO₂ overdose before removing the intestine. The muscle layer was gently stripped from the intestine and put in to 1x HBSS with 1x ABAM added. Muscle strips were digested in to cells using a 1mg/ml solution of collagenase IV in HBSS at 37 degrees Celsius for 30 minutes. Finally, cells were seeded at a density of 1x10⁶ cells per scaffold. Cells were grown in a

petri dish on the PDMS membrane for 7 days prior to stretching.

2.4 Bioreactor

We used a bioreactor (Fig.3) to provide smooth muscle cells with cyclic mechanical stimulation. First, the PDMS membrane was firmly fixed on the bioreactor.. Media was added to thoroughly cover the PDMS membrane.

Next step by mounting the motor, the PDMS membrane was strained longitudinally. This movement was controlled with a computer and a custom LabVIEW program. It was maintained in the incubator until completion of cyclic stretch. We determined the max strain to be 10% and the frequency was 1 Hz for the entire 7 days.

2.5 Immunostaining

To evaluate protein expression from smooth muscle cells, immunostaining was performed. First, cells were fixed in formalin for six hours and rinsed in 1x PBS-tween for 5 minutes each. Next, cell membranes were permeabilized with .5% Triton-X for 1 hour and washed with 1x PBS-tween 2 times for 5 minutes again. After rinsing, membranes were incubated in blocking solution (2%BSA, 4% normal goat serum, PBS-tween) for 1 hour. Primary antibody solutions were added following blocking at the following dilutions: Smooth muscle actin (SMA 1:250), Desmin (DES, 1:250) and Myosin (MHC. 1:50) and incubated overnight in the fridge. The next day, membranes were washed 3x5min each in 1x PBS-tween prior to incubation in secondary antibody solution. The secondary solution was diluted in blocking solution and was composed of Goat anti-mouse 488 secondary antibody and phalloidin 594 at ratios of 1:500 and 1:250, respectively. Membranes were incubated for 30 minutes at room temperature and washed 3x5min each in 1x PBS-tween. Lastly, before imaging the scaffolds were transferred onto glass slides and 1 drop of DAPI was added.

2.6 RNA extraction

RNA was extracted with a Qiagen RNeasy kit by adding 400 uL of buffer RLT (lysis buffer) on to samples. Next, 350 ul of lysed cells was pipette into Qiashredder. Standard RNeasy instructions were followed.

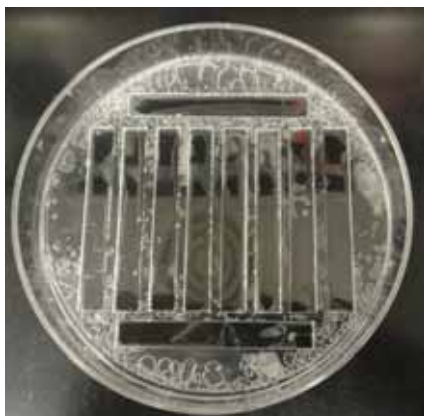


Fig.1 Mold to make PDMS membrane



Fig.2 PDMS membrane

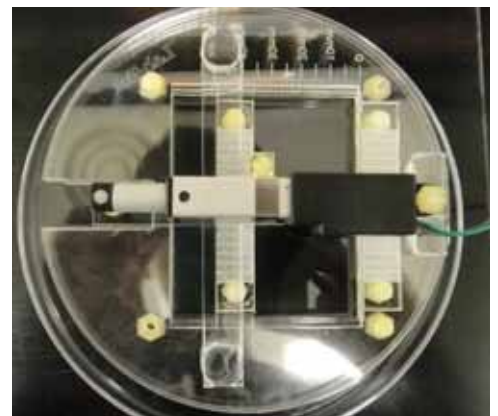


Fig.3 Bioreactor

3. RESULT AND DISCUSSION

The object of this study was to improve cell maturity of cultured rat primary smooth muscle cells with mechanical stimulation.

First of all, we confirmed the attachment and proliferation of cells on the PDMS membrane. We next made a comparison between the membrane coated with fibronectin (FBN) and without it.

Figure 4 shows the result of cell attachment and proliferation. From day 0 to 7, the number of smooth muscle cells on the PDMS membrane coated with FBN increased steadily. On the other hand, adhesion of cell was poor on the PDMS membrane without FBN proving FBN helps smooth muscle cells attach on the membrane.

Next immunostaining and PCR were performed. First, the PDMS membrane was cut into 2 pieces after stretch. Half was used for immunostaining and the other for PCR. Fig.5 - Fig.9 show the results of PCR. Smooth muscle actin (SMA) is a general marker for smooth muscle cells. Desmin (DES) is intermediate maker of maturity. Myosin (MHC) is late marker of maturity. Fig.5 shows relationship of relative mRNA levels and stretch conditions for these 3 markers and Fig.6 shows the relationship of relative mRNA levels and stretch condition in regards to myosin. The control was muscle strips from rat pups.

After 7 days, the relative mRNA levels for mature smooth muscle on stretched membranes were higher than any other result. The second highest condition is that of stretch for 1 day.. In addition, cells grown on membranes improved maturity even without stretching. This validates the hypothesis that smooth muscle cells respond to the surrounding physical environment.

Fig.7, Fig.8 and Fig.9 shows how each factor changes over time regarding the stretch conditions. For all factors, the relative mRNA levels increased while stretching compared to non-stretched controls. On the other hand, they appear to decrease at day 1 and increase at day 7 without stretching, but this result is less certain,

Next we confirmed maturity on the PDMS membrane by using immunostaining. This experimental report shows whether there is any change under stretch and without stretch. Fig.10-Fig.12 shows the result of immunostaining about smooth muscle actin, desmin and myosin. Only SMA exists in abundance on the PDMS membrane at day 1. On the other hand, DES and MHC are not easily visualized implying loss of maturity. At day 1, all samples had low expression except for SMA. By day 7, SMA expression remains constant and DES and MHC expression increases, even without stretch. All three factors increase a lot by day 7. Similarly, orientation along the axis of stretch increases over the course of 7 days on the stretched scaffolds compared to the

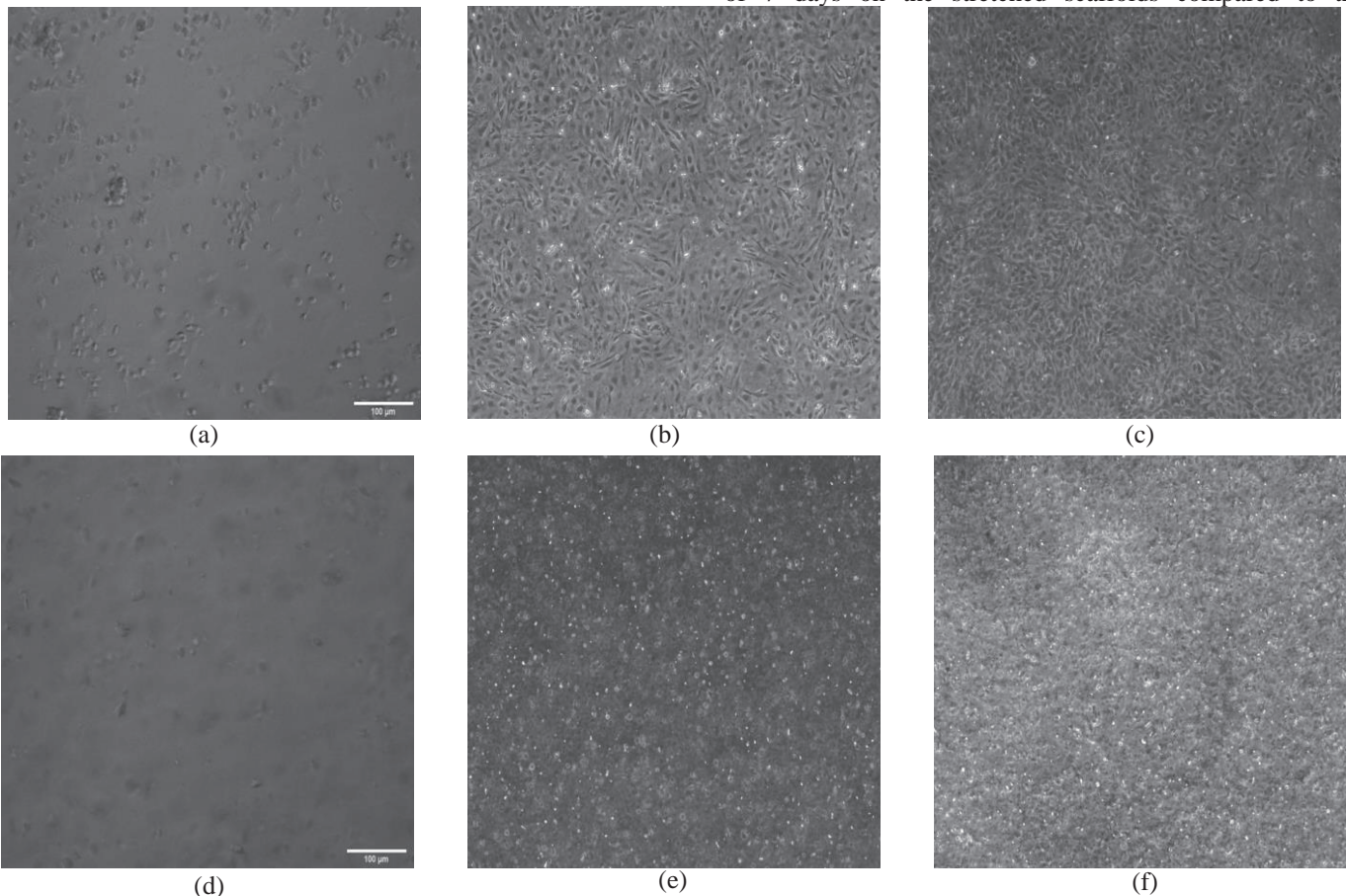


Fig.4 Bright field images of cultured smooth muscle cells on PDMS: (a-c) On the PDMS membrane coated fibronectin and (d-f) on the PDMS membrane without fibronectin.

(a) and (d) are day 0. (b) and (e) are 4 days, (c) and (f) are 7 days post stretch.

unstretched. In particular, MHC is the important factor when determining the maturity. Among these three factors, MHC showed the strongest tendency to increase with mechanical force, so mechanical stimulation is effective in improving the maturity of smooth muscle cells.

In summary, mechanical stimulation is better at improving smooth muscle maturity for 7 days compared to unstretched membranes. When cells are present in the body, they maintain links with the surrounding environment. But after taking out the cells from tissue and digesting in to individual cells, these links are removed and functionality decreases, leading to changes in observable markers. Cells change their characteristics according to environmental factors. Cells are given mechanical stimulation in the body to improve maturity because cells can sense mechanical stimulation.

4. CONCLUSION

The objective of my study is to provide mechanical stimulation on rat intestinal smooth muscle cells to improve their maturity. In this study, we examined cell attachment on the PDMS membrane coated with FBN and without FBN.

improve maturity of smooth muscle cells by examining the expression of proteins.

The best result occurred after giving smooth muscle cells mechanical stimulation for 7 days. This condition increased expression levels the most. By sensing the mechanical stimulation, the cells have been found to undergo various changes, for example, differentiation, recovery, improving maturity and so on. This study shows it is very important for cells to receive mechanical stimulation. But, in this study, the results differed slightly between immunostaining and PCR. Future testing is necessary to improve this result.

Other ways to improve the study design include improving the thickness of the PDMS membrane. . In this study, thickness was 2mm. This value had strength to withstand the expansion and contraction but may have compromised the conduction of strain to the cells. We should find the best boundary thickness between the tolerant strength of the film and the conduction of power to the cells. The second thing is a possibility that the cells are peeling when cutting the DMS membrane into pieces or while stretching, which is easily visualized with a light microscope.

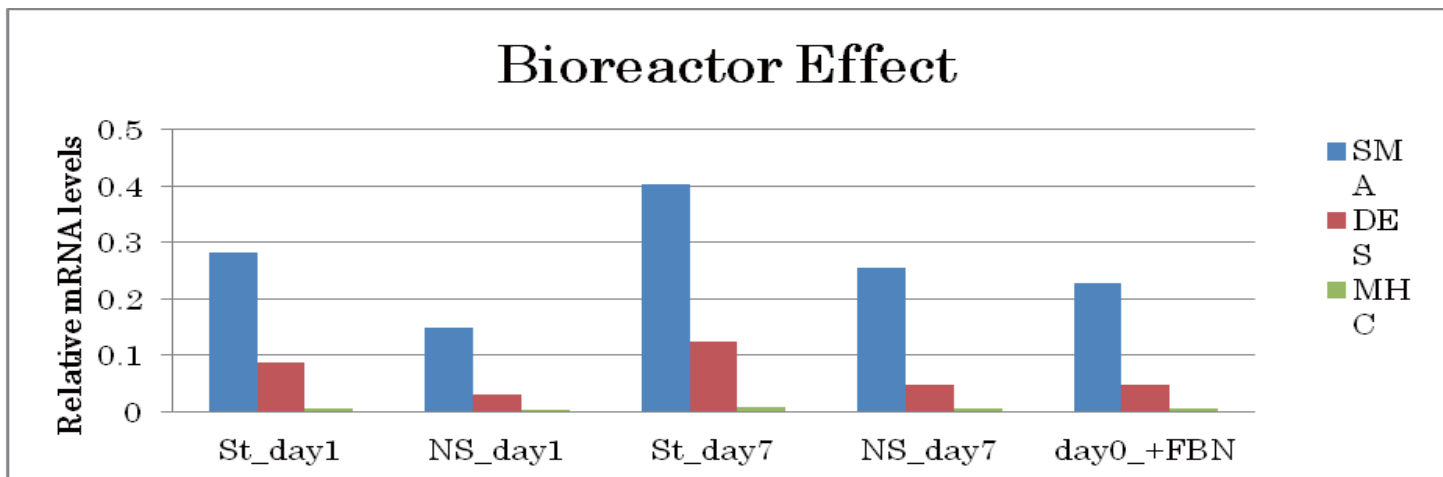


Fig.5 Relationship of relative mRNA levels of smooth muscle actin (SMA), desmin (DES), and myosin heavy chain (MHC) for 0, 1 and 7 days.

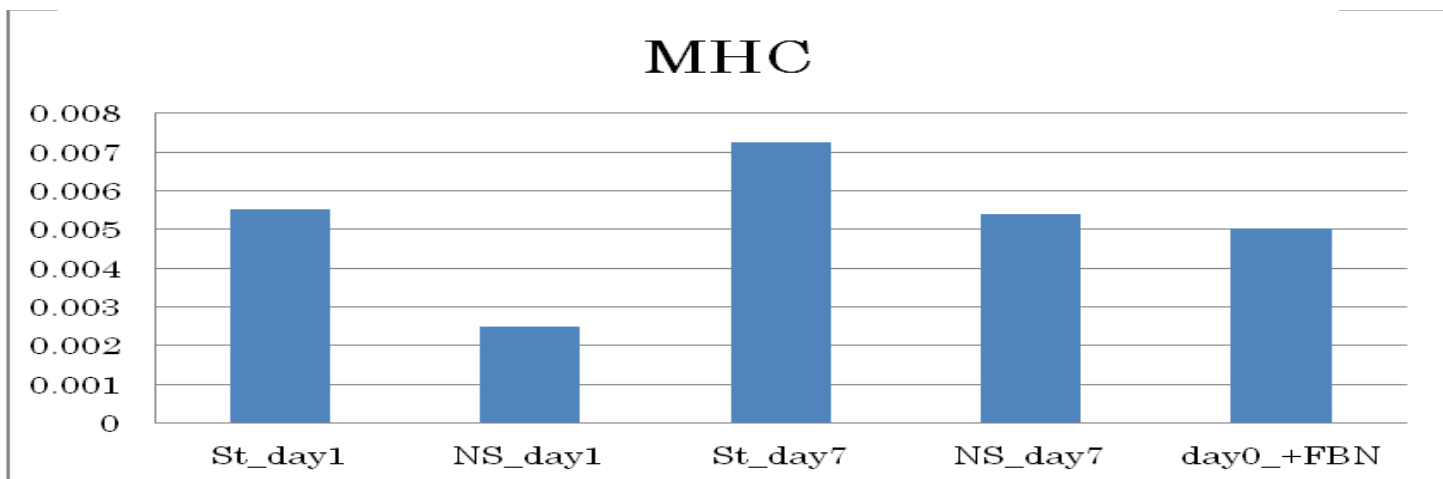


Fig.6 Relationship of relative mRNA levels and duration of stretching about MHC

Next administered mechanical stimulation and aimed to

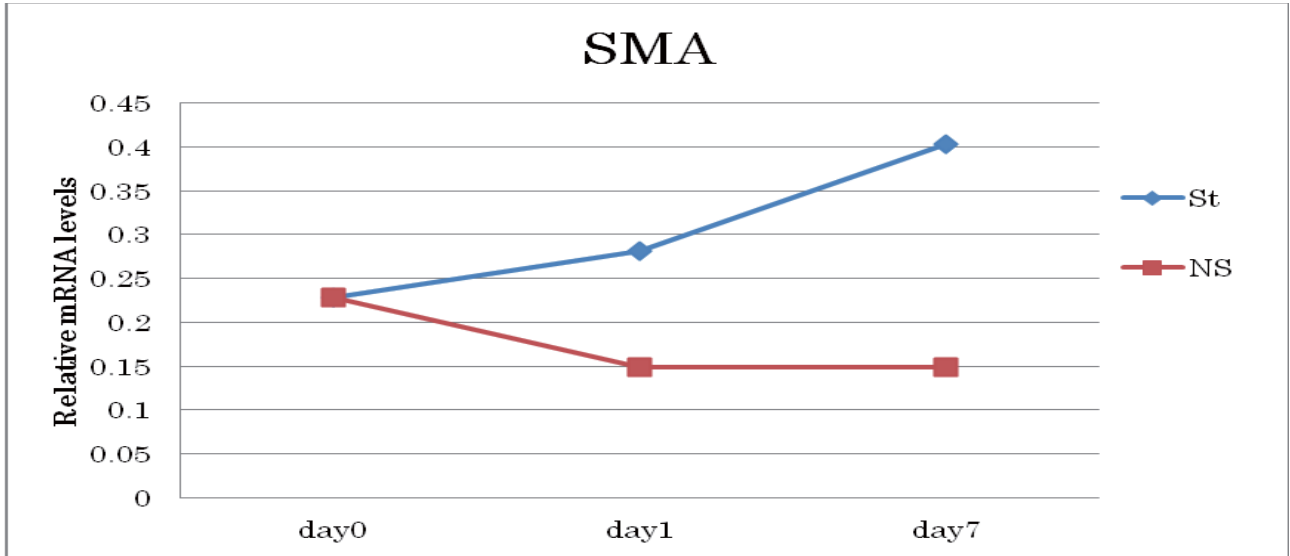


Fig.7 SMA expression in the stretch (St) and no stretch (NS) conditions from 0 to 7 days.

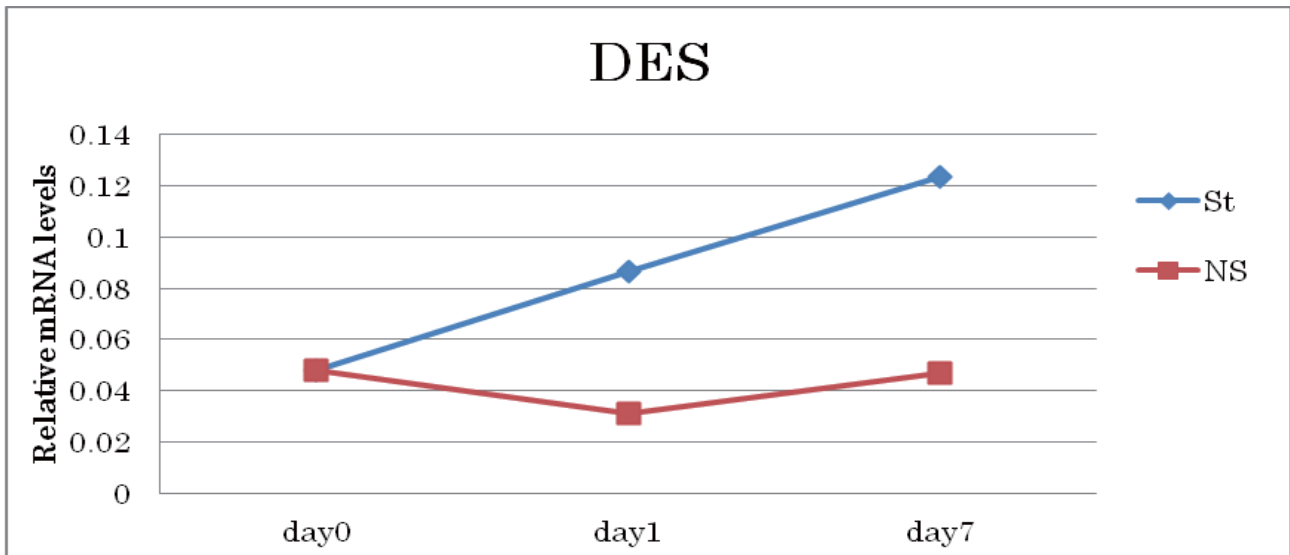


Fig.8 DES expression in the stretch (St) and no stretch (NS) conditions from 0 to 7 days.

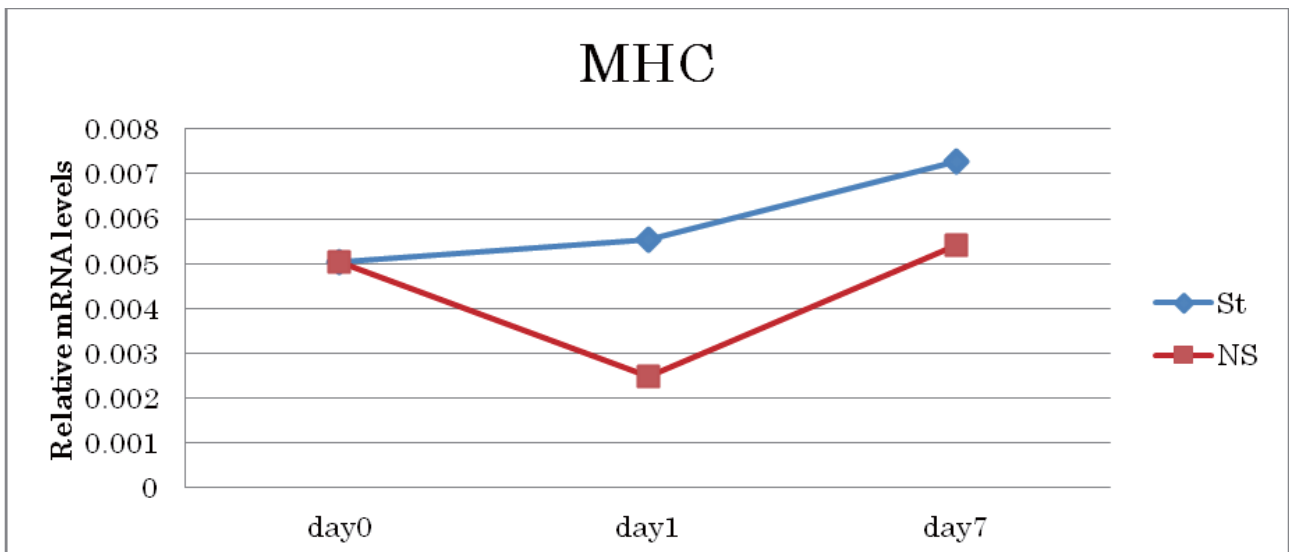


Fig.9 MHC expression in the stretch (St) and no stretch (NS) conditions from 0 to 7 days.

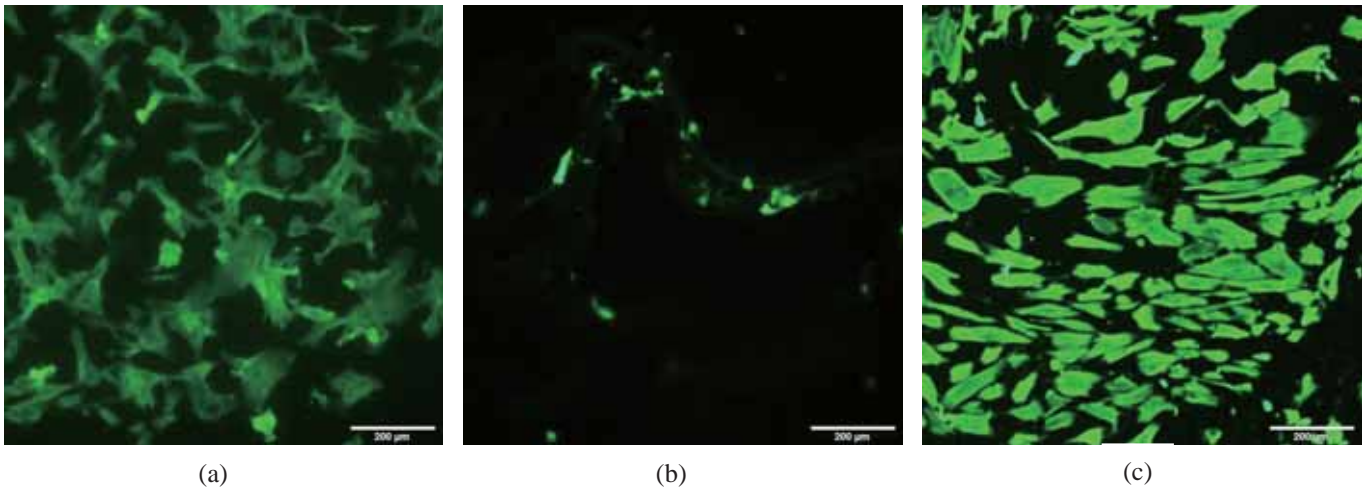


Fig.10 The image of SMA by immunostaining
(a) at day0 (b) at day7 without stretch (c) at day7 after stretch

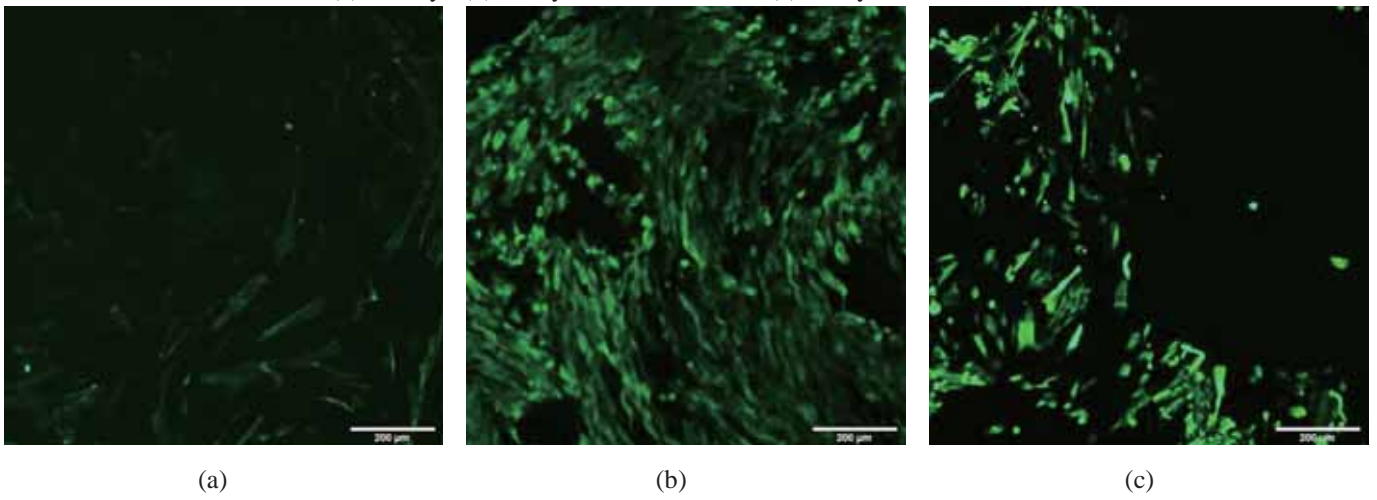


Fig.11 The image of DES by immunostaining
(a) at day0 (b) at day7 without stretch (c) at day7 after stretch

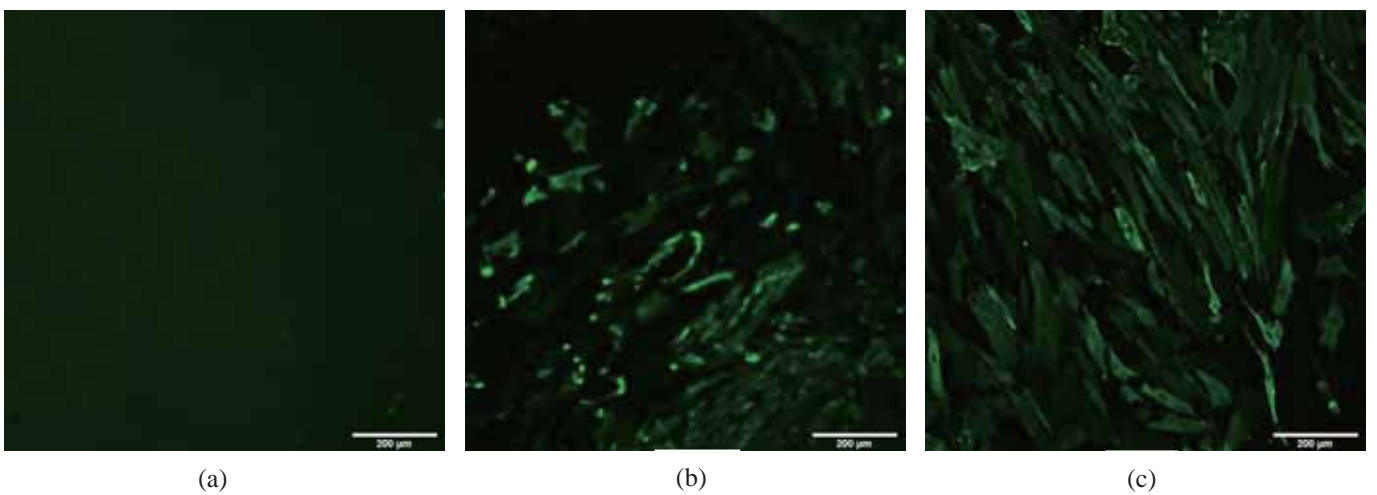


Fig.12 The image of MHC by immunostaining
(a) at day0 (b) at day7 without stretch (c) at day7 after stretch

. Improvements are necessary for greater adhesion of cells to the membrane. This study shows maturity of smooth muscle cells increases by adding mechanical stimulation but has many problems to improve.

5. ACKNOWLEDGEMENT

I am deeply grateful to Professor Benjamin M. Wu. Thank you very much for great experience. I would particularly like to thank Chris Walthers and Masae Kobayashi. They set up an experimental plan by design and helped me also experiment. Without their guidance and persistent help this paper would not have been possible.

REFERENCES

[1] DU GEON MOON, M.D.,* GEORGE CHRIST, Ph.D., JOEL D. STITZEL, Ph.D, ANTHONY ATALA, M.D., and JAMES J. YOO, M.D., Ph.D, Cyclic Mechanical Preconditioning Improves Engineered Muscle Contraction, TISSUE ENGINEERING, volume 14, p473~482

<3> The 7th Workshop on October 9, 2013

The 7th JUACEP Workshop

--- Medium Course / Summer Short Research Course 2013

at University of Michigan and UCLA---

Date & Time: Wed., 9 October, 13:00~

Place: VBL Hall

Timetable:

- 13:00 **Opening address from Prof. Umehara**
- 13:05 - 13:18 **Hiroshi Fuji (Suzuki Lab.)**
“Modeling for a Nano Precision System” (p.88)
- 13:19 - 13:32 **Fumitake Nonoyama (Umehara Lab.)**
“3D-printed Bone-mimicking Material for Orthopedic Surgical Simulation”
(N/A)
- 13:33 - 13:51 **Takafumi Hattori (Umehara Lab.)**
“Characterization of Molded Superhydrophobic Surfaces” (N/A)
- 13:52 - 14:05 **Yoko Okuda (Zhang Lab.)**
“What Split Bregman Can Do for Image Processing” (p.91)
- 14:06 - 14:19 **Kazuki Miyazaki (Umehara Lab.)**
“Impact Tolerance of Metal, Composites, and FMLs” (p.93)
- 14:20 - 14:33 **Toshihiro Sato (Ju Lab.)**
“Mechanical Stimulation on Rat Intestinal Smooth Muscle Cells to Improve Maturity” (p.96)
- 14:33 - 14:45 Break
- 14:45 - 14:58 **Sakina Kondo (Ohtsuki Lab.)**
“Effect of Protein Charge on Adsorption to Apatite and Cell Viability” (N/A)
- 14:59 - 15:12 **Shinichi Hayashi (Matsumoto Lab.)**
“Numerical Simulation of Wave Propagation in Composite Structures” (p.98)

- 15:13 - 15:26 **Shoya Ono (Kasahara Lab.)**
 “Study on an Aluminum Two-phase Heat Transfer Device Using IAS Fluid”
 (p.101)
- 15:27 - 15:40 **Hiroki Shigematsu (Inoue Lab.)**
 “Development of a Vibration Excitation System Forced on Piezoelectric
 Elements” (p.104)
- 15:41 - 15:54 **Takayuki Yamada (Hata Lab.)**
 “Calibration of a Strain Gauge for Force Measurement in a Palatal
 Expander” (N/A)
- 15:55 - 16:08 **Shunji Shibata (Hata Lab.)**
 “Tapered Etch Profile of Silicon” (N/A)
- 16:08 - 16:20 Break
- 16:20 - 16:33 **Akitomo Matsumoto (Tanaka Lab.)**
 “Effects of Soft Tissue Stiffness on Stress Values of Femur Neck” (p.107)
- 16:34 - 16:47 **Shun Tamamura (Tanaka Lab.)**
 “Evaluation of Auricular Biomechanical Property by FEM” (N/A)
- 16:48 - 17:01 **Tomoko Ozawa (Kanetake Lab.)**
 “Analysis of Fluid Flow of Molten Magnesium into Micro-particles”
 (p.110)
- 17:02 - 17:15 **Tomoya Nishiyama (Yamada Lab.)**
 “Kinematics and Compliance Testing Simulation of an Automobile Using
 a Rigid Body Suspension Model” (p.114)
- 17:16 - 17:29 **Yasunori Iijima (Hasegawa Lab.)**
 “Research of Organic Functionalized Silsesquioxanes” (p.117)
- 17:30 - 17:45 **Award Ceremony**
- 18:00 - **Banquet**
 Address from Prof. Matsushita, Dean of Graduate School of Engineering

N/A... not available for publication

Modeling for a Nano-Precision System

Hiroshi Fuji

Backgrounds

Nanomanufacturing



Semiconductor industry
• Need for higher precision increases

Photo lithography
limited in part by diffraction of light

➔ Nano-imprint lithography (NIL)
✓ not limited by diffraction

Multi-Axis Positioning System (MAPS)



(Shalom Dovber Ruben 2010)

Platen (6 DoF wafer holder)

➢ Actuator

- 4 Linear permanent-magnet synchronous motors

3 DoF module holder

➢ Actuator

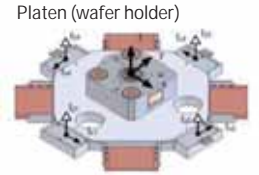
- 3 Piezo-electric actuators

The module can be chosen for a desired task.
(atomic force microscopy, imprint lithography, etc.)

Research objective

To attain accurate positioning

model accuracy is indispensable



(Shalom Dovber Ruben 2010)

To Build an accurate dynamic model of the platen by using a proper modeling method

Method

- ▶ White-box modeling
Use known parameters of each component
Build a model according to some theory
Actual behavior is often different from theoretical model.
- ▶ Black-box modeling
Identify the system from only collected data
doesn't consider any physical law
- ▶ Grey-box modeling
Based in part on some theory
Use collected data to estimate parameters



ARX identification

ARX model identification

• From differential equations to difference equation

$$m\ddot{x} + d\dot{x} + kx = f_x \quad \text{estimate } m, d, k$$

approximations

$$\begin{cases} \dot{x} = \frac{x(n+1) - x(n-1)}{2\Delta t} \\ \ddot{x} = \frac{x(n+1) - 2x(n) + x(n-1)}{\Delta t^2} \end{cases}$$

$$x(n) = a_1x(n-2) + a_2x(n-1) + bf_x(n-1)$$

$$a_1 = -\frac{2m - d\Delta t}{2m + d\Delta t}, a_2 = \frac{4m - 2k\Delta t^2}{2m + d\Delta t}, b = \frac{2\Delta t^2}{2m + d\Delta t}$$

ARX model identification

- Least squares estimation

$$x(n) = a_1 x(n-2) + a_2 x(n-1) + b f_x(n-1)$$

$$\theta = [a_1 \ a_2 \ b]^T$$

$$\phi(n) = [x(n-2) \ x(n-1) \ f_x(n-1)]$$

$$x(n) = \phi(n)\theta$$

$$\begin{bmatrix} x(2) \\ x(3) \\ \vdots \\ x(N) \end{bmatrix} = \begin{bmatrix} \phi(2) \\ \phi(3) \\ \vdots \\ \phi(N) \end{bmatrix} \theta \longrightarrow X = \Phi \theta$$

N : the number of the data

ARX model identification

- Least squares estimation

$$X = \Phi \theta$$

Error vector : $e = X - \Phi \hat{\theta}$ $\hat{\theta} = [\hat{a}_1 \ \hat{a}_2 \ \hat{b}]$: estimated parameters

minimize

$$\|e\|^2 = \{X - \Phi \hat{\theta}\}^T \{X - \Phi \hat{\theta}\}$$

$$= X^T X - 2X^T \Phi \hat{\theta} + X^T \Phi^T \Phi \hat{\theta}$$

$$\frac{d}{d\hat{\theta}} \|e\|^2 = -2X^T \Phi + 2\hat{\theta}^*{}^T \Phi^T \Phi = 0$$

$$\therefore \hat{\theta}^* = (\Phi^T \Phi)^{-1} \Phi^T X$$

Validation

Inputs: f_x , f_y , f_θ

Outputs: x , y , θ

Given parameters: G

$$f_x(n) = 0.1 \text{sgn}(\sin(n\pi\Delta t))$$

$$f_y(n) = -0.1 \text{sgn}(\sin(n\pi\Delta t)) \quad [\text{N}]$$

$$f_\theta(n) = 0.1 \text{sgn}(\sin(n\pi\Delta t))$$

Inputs & Outputs $\xrightarrow{\text{estimation}}$ Parameters

Validation

Inputs: f_x , f_y , f_θ

Outputs: x , y , θ

Given parameters: G

► 5000 data points [1/s]

- Given parameters
- Estimated parameters

	m	d	k		m	d	k
x, y	6.6000	638.80	1313.5	x, y	6.63375	638.76	1313.6
θ	0.13370	25.391	92.847	θ	0.13503	25.389	92.852

Implementation

- Voltage Inputs
- Local forces
- Global forces

Motor law (kth motor)

$$f_k = \begin{bmatrix} a \sin(\omega x_k + \phi) \\ a \sin(\omega x_k + \phi + \pi/3) \\ a \sin(\omega x_k + \phi + 2\pi/3) \end{bmatrix} \begin{bmatrix} v_{1k} \\ v_{2k} \\ v_{3k} \end{bmatrix}$$

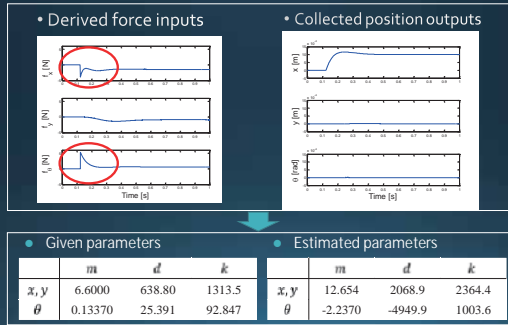
Implementation

- Voltage Inputs
- Local forces
- Global forces

From local forces to global forces

$$\begin{bmatrix} F_x \\ F_y \\ T_\theta \end{bmatrix} = \begin{bmatrix} -1 & 0 & 1 & 0 \\ 0 & -1 & 0 & 1 \\ -R_m & -R_m & -R_m & -R_m \end{bmatrix} \begin{bmatrix} f_1 \\ f_2 \\ f_3 \\ f_4 \end{bmatrix}$$

Implementation



Discussion

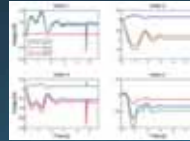
There was some sort of problem in deriving global forces

- The variables were different from those used in the controller

$$f_k = \begin{bmatrix} a \sin(\omega x_k + \phi) \\ a \sin(\omega x_k + \phi + \pi/3) \\ a \sin(\omega x_k + \phi + 2\pi/3) \end{bmatrix} \begin{bmatrix} v_{1k} \\ v_{2k} \\ v_{3k} \end{bmatrix}$$

Variable	Fit
a	2.1467 N-A ⁻¹
ω	70.86 rad-m ⁻¹
ϕ	-3.1087 rad

- Wrong voltage data due to a malfunction of the sensors



Conclusion & Future work

Conclusion

- built a system identification tool using ARX model identification method
- validated the system identification tool
- could not do the proper parameter estimation due to the problem in deriving global forces

Future work

- Validate the parameters in the voltage-force conversion
- Find out the proper sampling rate

Thank you for your attention



What split Bregman can do for image processing

Yoko Okuda

Data mining

Image processing, genome analysis, page rank....

Rank Revealing QR factorization(RRQR)

(1987 Tony F. Chan)

$$A\Pi = QR = Q \begin{pmatrix} \text{large elements} \\ \text{small elements} \end{pmatrix}$$

Another model for data mining

$$\min_S \|S\|_{1,\infty} \text{ such that } X = AS$$



Convex optimization problem

Split Bregman

(Tom Goldstein and Stanley Osher 2007)

Bregman iteration method

Bregman method (L. M. Bregman 1966)

$$\min_x f(x) \text{ s.t. } Ax = b$$

$$\min_x f(x) + \frac{\lambda}{2} \|Ax - b\|_2^2$$

Bregman iteration method is to minimize "Bregman distance" iteratively.

Split Bregman

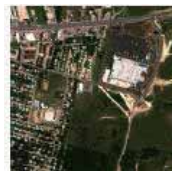
• Image processing problem

Objective function has l1-norm term.

$$\min_{u,d} |d| + H(u) \text{ such that } d = Au$$

$$\min_{u,d} |d| + H(u) + \frac{\lambda}{2} \|d - Au\|_2^2$$

Example for image

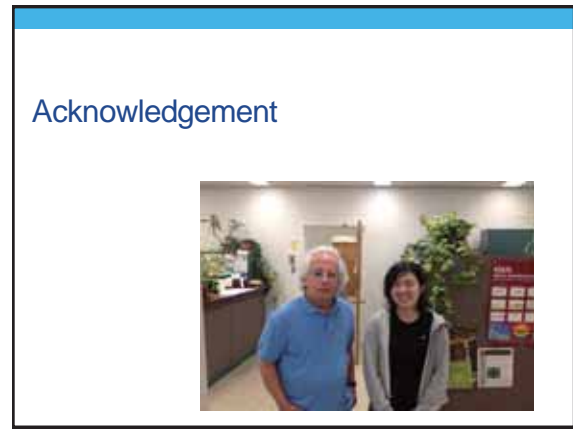
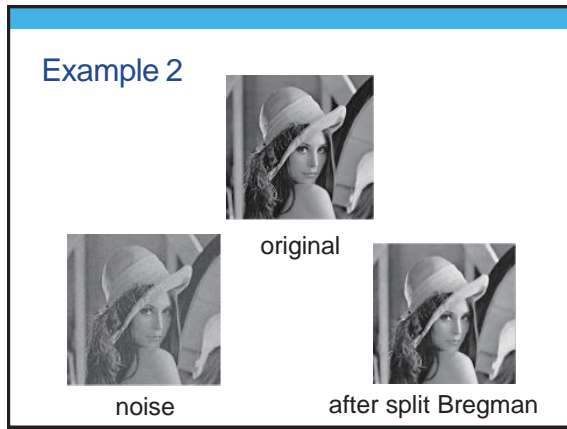


original



road

Yoko Okuda



Kazuki Miyazaki



Impact tolerance of metal, composites, and FMLs

Kazuki Miyazaki
Supervisor: Prof. Jenn-Ming Yang

Department of Materials Science and Engineering , UCLA
From August 4, 2013 to September 14, 2013 (UCLA short)

1



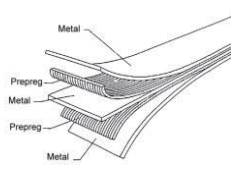
Outline

- ▶ Introduction & Background
 - FML
 - GLARE
- ▶ Purpose
- ▶ Experiment
 - Manufacturing
 - Impact test
- ▶ Result (Impact test)
- ▶ Conclusion

2



Introduction & Background



- ▶ Fiber metal laminates (FMLs) are hybrid composites.

fiber prepregs
+
thin metal layers
- ▶ The fatigue and corrosion characteristics of metal and the bearing strength, impact resistance of composites can be improved by combination of both.

S. Krishnakumar, *Materials and Manufacturing Processes* Vol. 9, No.2, 295-354, 1994

3



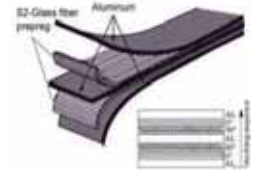
Introduction & Background

- ▶ **What is Glass Fiber Reinforced Aluminum (GLARE)?**
GLARE is a FML with light weight, high strength, excellent corrosion and fire resistance, **good impact properties** and long fatigue life.

Metal: Aluminum alloy 2024-T3
(Pretreatment of aluminum alloy)

+

Prepreg : Glass fiber + Epoxy



- GLARE have been applied to aircraft structure as a replacement of high strength aluminum alloy.

C. A. J. R. VERMEEREN, *Applied Composite Materials* 10 (2003) p189

4



Motivation

▶ To evaluate the impact tolerance of FMLs and compare it with Aluminum alloy 2024-T3 and glass/epoxy composites (GFRP).

5



Sample preparation



Aluminum alloy
GFRP
GLARE

▶ 3X3 inch² panel (1.5 mm thick)
 ▶ Shear cutting machine was used to cut samples.

6

Manufacturing (GFRP)



200g of the epoxy resin and 52g of the curing agent

12 rectangular sheets of glass fiber (30 cm by 20 cm)

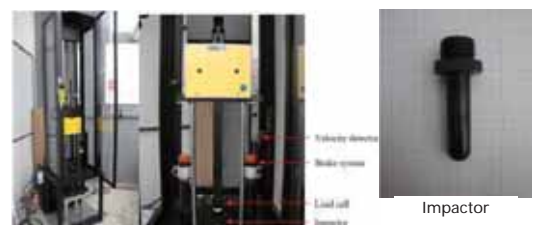
GFRP

UCLA

7

Impact test

Equipment

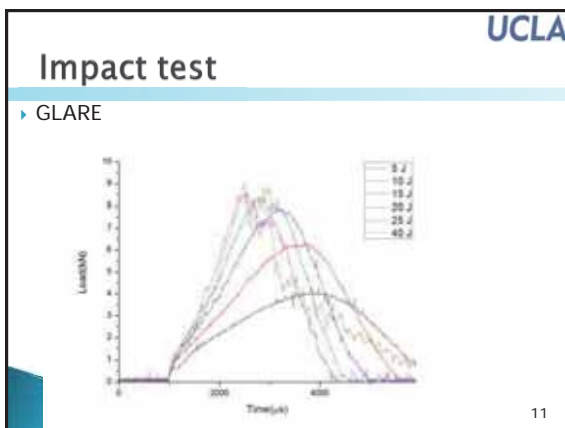
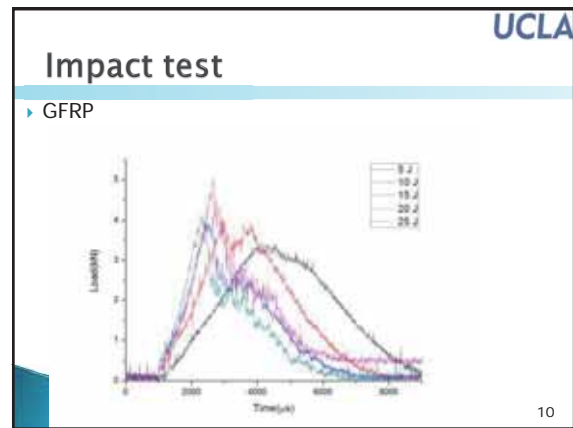
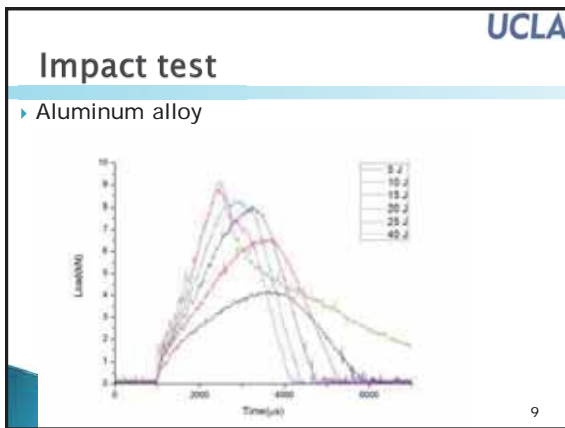


The Dynatup Model 8250 weight drop tower

Impactor

UCLA

8



Comparison



Al (20 J)

Al and GLARE (25 J)

a crack on the GLARE laminate occurred along the fiber directions.

A crack was observed on the aluminum on the nonimpacted side after the impact test (20 J).

Crack damages were observed on the aluminum and the GLARE laminate on the nonimpacted side after the impact test (25 J).

UCLA

12

UCLA

Discussion



The energy absorption of Aluminum
+
The stiffness of the glass fiber composite

Al GLARE GFRP
Impact energy (25 J)

The GLARE exhibited better impact tolerance.

13

UCLA

Conclusion

- ▶ The different levels of damage (dent, crack and penetration) were induced by varying the impact energy.
- ▶ The combined properties of energy absorption of Aluminum and the stiffness of the glass fiber composite, allowed the GLARE to absorb greater impact while exhibiting higher modulus.

1

Thank you for your kind attention

15

Toshihiro Sato

Mechanical stimulation on rat intestinal smooth muscle cells to improve maturity



Toshihiro Sato

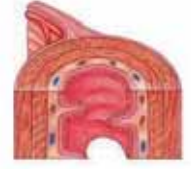
Introduction to the Intestine

Intestine

Unable to regenerate after loss
Ex: SBS, Crohn's Disease

Need for engineered intestine to replace this

- smooth muscle
- propel intestinal contents towards rectum



→ Therapeutic solution to this unmet medical need

Objective

Tissue engineering

→ Fabrication of intestine in vitro

Problem:

- Cells taken from tissue decrease maturity rapidly

•Focus on mechanical stimulation

- Provide mechanical cues to smooth muscle

To provide mechanical stimulation on rat intestinal smooth muscle cells to improve their maturity

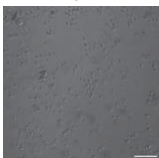
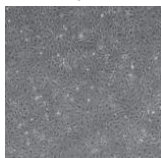
Experimental

width 10mm
length 75mm
height 2mm

- Making PDMS membrane
 - Pour PDMS in to the mold and solidify at 65° Celsius
 - Autoclave to sterilize
 - Coat with Fibronectin(1mg/ml)
- Seed SMCs on the membrane
 - Smooth muscle tissue from rat
 - Seed Smooth muscle cell on the PDMS
 - 1 million cells each membrane



Pictures of cell culture (bright field)

	day0	day4	day7
FBN			
NO FBN			

Bioreactor

- Provide cyclic mechanical stimulation on rat intestinal smooth muscle

condition

- For 7 days
- 10% strain
- 1 Hz



Cutting direction

PDMS membrane

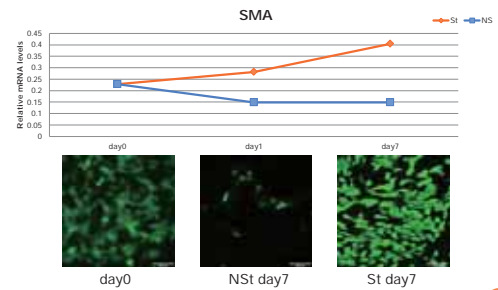


width 10mm
length 75mm
height 2mm

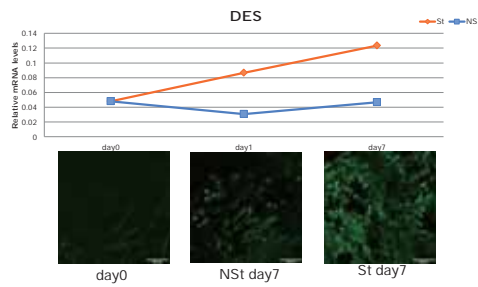
Evaluation factor

- MHC(myosin heavy chain, maturity)
- DES (desmin, intermediate marker)
- SMA(smooth muscle actin, general smooth muscle)

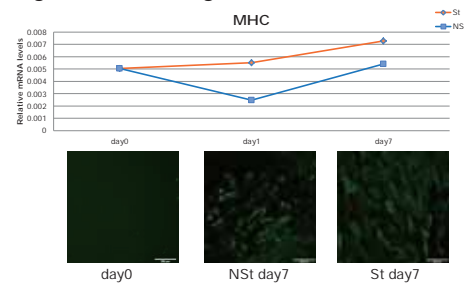
Smooth muscle actin



Desmin



Myosin heavy chain



Discussion and improvement

- Only SMA at day0
 - DES and MHC are markers of maturity
 - Maturity does not exist at day 0
 - Difference in expression time
- Different result of immunostaining and PCR
 - Need to do more PCR to confirm results
 - Peeling of cells while stretching/cutting

Thank you for your kind attention

Shinichi Hayashi

Numerical simulation of wave propagation in composite structures



Shinichi Hayashi
Graduate School of Engineering,
Nagoya University

Ertugrul Taciroglu
Department of Civil & Environmental Engineering,
University of California, Los Angeles

Outline

- Background
- Objective
- Experimental study on composite structures
- Numerical simulation
- Conclusion

Background

Advanced composites are

- used in aircraft and aerospace structures.
- susceptible to hidden defects that may cause sudden catastrophic failure of the entire structures.

Explosion of the Delta II Rocket (1997)



Non-Destructive Evaluation (NDE) method of detect and characterize damages in composite structures

<http://xmb.stuffcanuse.com/xmb/viewthread.php?tid=6869>

Background

- NDE method with systematic modeling
 - An accurately identification of defect's locations and sizes, shapes particular in composite structures.
- A numerical approach for identifying a scatter in elastic heterogeneous media (Jung et al, 2013)[1]
 - The dynamic eXtended Finite Element Method (XFEM)
 - The gradient-based optimization
 - The divide and conquer approach

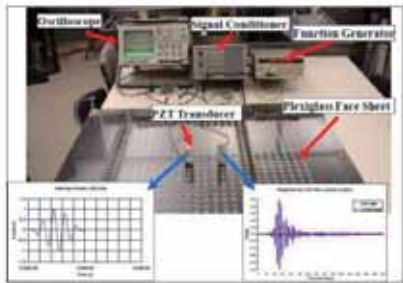
[1] Jung, J., Joong, C., Taciroglu, E. "Identification of a scatter embedded in elastic heterogeneous media using dynamic XFEM". *Comput. Methods Appl. Mech. Engrg.* 259, 50-63 (2013).

Objective

- In Jung's study,
 - The synthetic data are used as measured data.
 - Several numerical simulations clearly show it is effective and accurate.
- Objective
 - Verification of Jung's method against the experimental data.

Based on the actual experimental study, analyze the wave propagation in the composite structures.

Experimental setup[2]



[2] Baid, H., Mal, A., Detection of damage in a composite structure using guided waves. PhD Dissertation, University of California, Los Angeles (2012).

Shinichi Hayashi

Experimental setup

- Two transducers are used as transmitters and receivers of wave.
- The input source has the following form:

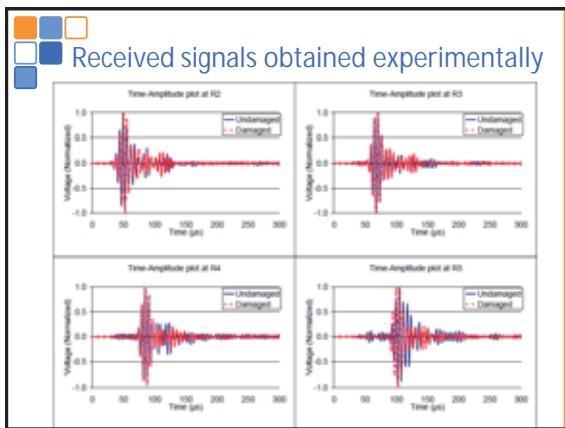
$$P(T) = \frac{1}{2} \left[1 - \cos\left(\frac{2\pi ft}{5}\right) \right] \sin(2\pi ft)$$
 - f : the central frequency; 100[kHz]
- The distribution of transmitter and receiver.

The composite sandwich structure

- The composite sandwich structure are
 - Transversely isotropic.

- The properties of the composite skin and Al honeycomb

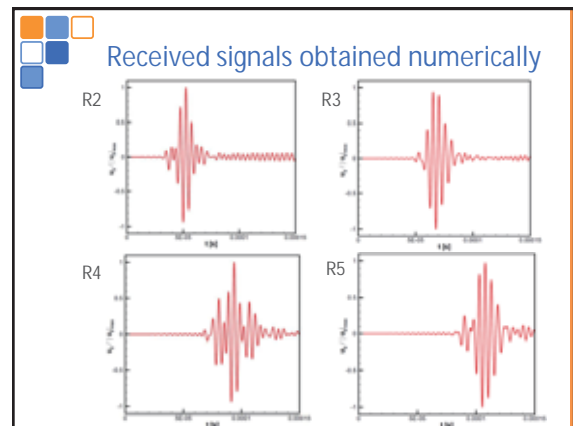
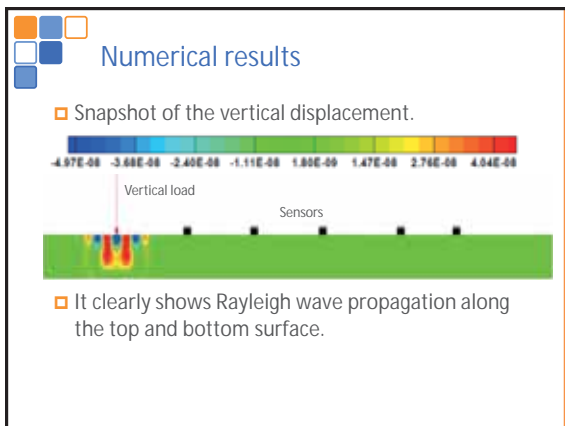
	E_{11}, E_{22} [GPa]	E_{33} [GPa]	G_{12} [GPa]	G_{13}, G_{23} [GPa]	ν_{12}, ν_{13}	ν_{23}, ν_{31}	ν_{32}, ν_{33}	ρ [kg/m ³]
Composite skin	38.8	9.77	14.77	2.94	0.3337	0.0816	0.324	1278
Al honeycomb	3.83×10^{-4}	2.99	8.6×10^{-4}	0.423	1	0.33	3.79×10^{-4}	134.1



Numerical model

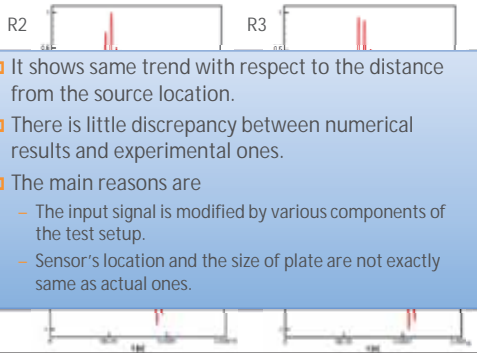
- Conventional finite element method (FEM)
- 2-D plane-strain material domain.

- Quadrilateral element
- Number of elements : 40,500



Shinichi Hayashi

 Received signals obtained numerically



- It shows same trend with respect to the distance from the source location.
- There is little discrepancy between numerical results and experimental ones.
- The main reasons are
 - The input signal is modified by various components of the test setup.
 - Sensor's location and the size of plate are not exactly same as actual ones.

 Conclusions

- The wave response obtained numerically from the composite sandwich structure are analyzed.
- The simulations using FEM for 2-D plane strain model provided a clearly Rayleigh wave propagation.
- There was the little discrepancy between the numerical result and experimental one.
- Nevertheless, it shows same trend with respective sensor's location.

 Thank you.

Study on an Aluminum two-phase heat transfer device using IAS fluid

Aerospace engineering
M2 Shoya Ono

Out lines

- Background
- Aluminum heat transfer device with IAS
- Problem of IAS and our theory
- Experiment
- Result
- Conclusion

Background

Modern electronics produce large amounts of heat. For aerospace, **weight reduction** is required.

Two-Phase heat transfer device

High thermal conductive heat transfer devices using the phase change of the working fluid inside the tube.
Ex) Heat pipe, Thermo-syphon

Material (tube/working fluid)

- High conductive material and high merit number fluid are preferred.
- Water and aluminum react and produce non-condensable gas(NCG).

Tube	Working fluid	Advantage	Disadvantage	
Terrestrial	Copper	Water	High efficiency	Heavy
Space	Aluminum	Ammonia or Methanol	Light	Low efficiency harmful

For aerospace, light and high efficiency heat transfer device is required.

Aluminum / IAS two-phase heat transfer device

This study's final goal is to achieve **Al / IAS** two-phase heat transfer device.

What is IAS (Inorganic Aqueous Solution) ?

- 9 chemical constituents in aqueous solution
- Properties are similar to water

Al - Water reaction

$$2Al(s) + 6H_2O(l) \rightarrow Al_2O_3(s) \downarrow + 3H_2(g) \uparrow$$

NCG is generated and Thermo-syphon will be fail.

Al passivation

$$2Al(s) + 2MnO_4^-(aq) + 2H^+(aq) \rightarrow Al_2O_3(s) \downarrow + MnO_2(s) \downarrow + H_2O(l)$$

$$2Al(s) + 2CrO_4^{2-}(aq) + 4H^+(aq) \rightarrow Al_2O_3(s) \downarrow + Cr_2O_3(s) \downarrow + 2H_2O(l)$$

Aluminum oxide is created and it protect aluminum surface.

Hydrophilic coating

$$Mg^{2+}(aq) + CrO_4^{2-}(aq) \leftrightarrow MgCrO_4(s) \downarrow$$

$$Ca^{2+}(aq) + CrO_4^{2-}(aq) \leftrightarrow CaCrO_4(s) \downarrow$$

$$Sr^{2+}(aq) + CrO_4^{2-}(aq) \leftrightarrow SrCrO_4(s) \downarrow$$

Silver effect

$$Al(s) + 3Ag^+(aq) \rightarrow Al^{3+}(aq) + 3Ag(s) \downarrow$$

$$2Al(s) + 3H_2O(l) - 6e^- \rightarrow Al_2O_3 \downarrow + 6H^+(aq)$$

$$MnO_4^-(aq) + 4H^+(aq) + 3e^- \rightarrow MnO_2(s) \downarrow + 2H_2O(l)$$

$$2CrO_4^{2-}(aq) + 10H^+(aq) + 6e^- \rightarrow Cr_2O_3(s) \downarrow + 5H_2O(l)$$

Solution		Suspension
Positive ions	Negative ions	
Al ³⁺	MnO ₄ ⁻	MgCrO ₄
K ⁺	MnO ₄ ⁻	Small solubility
Mg ²⁺	CrO ₄ ²⁻	MnO ₂
Ca ²⁺	CrO ₄ ²⁻	Only after long time
Sr ²⁺	CrO ₄ ²⁻	
Ag ⁺		

Aluminum / IAS two-phase heat transfer device

This study's final goal is to achieve **Al / IAS** two-phase heat transfer device.

What is IAS (Inorganic Aqueous Solution) ?

- 9 chemical constituents in aqueous solution
- Properties are similar to water

Al - Water reaction

$$2Al(s) + 6H_2O(l) \rightarrow Al_2O_3(s) \downarrow + 3H_2(g) \uparrow$$

NCG is generated and Thermo-syphon will be fail.

Al passivation

$$2Al(s) + 2MnO_4^-(aq) + 2H^+(aq) \rightarrow Al_2O_3(s) \downarrow + MnO_2(s) \downarrow + H_2O(l)$$

$$2Al(s) + 2CrO_4^{2-}(aq) + 4H^+(aq) \rightarrow Al_2O_3(s) \downarrow + Cr_2O_3(s) \downarrow + 2H_2O(l)$$

Aluminum oxide is created and it protect aluminum surface.

Hydrophilic coating

$$Mg^{2+}(aq) + CrO_4^{2-}(aq) \leftrightarrow MgCrO_4(s) \downarrow$$

$$Ca^{2+}(aq) + CrO_4^{2-}(aq) \leftrightarrow CaCrO_4(s) \downarrow$$

$$Sr^{2+}(aq) + CrO_4^{2-}(aq) \leftrightarrow SrCrO_4(s) \downarrow$$

Silver effect

$$Al(s) + 3Ag^+(aq) \rightarrow Al^{3+}(aq) + 3Ag(s) \downarrow$$

$$2Al(s) + 3H_2O(l) - 6e^- \rightarrow Al_2O_3 \downarrow + 6H^+(aq)$$

$$MnO_4^-(aq) + 4H^+(aq) + 3e^- \rightarrow MnO_2(s) \downarrow + 2H_2O(l)$$

$$2CrO_4^{2-}(aq) + 10H^+(aq) + 6e^- \rightarrow Cr_2O_3(s) \downarrow + 5H_2O(l)$$

Problem and Our theory

Past results

Al / IAS thermo-syphon was tested.

Cooling block : similar behavior to Copper / Water thermo-syphon

Natural convection : failed (6 feet long thermo-syphon)

These results are problem when IAS is used for various heat pipes. The purpose of this research is to figure out this reason.

Our theory

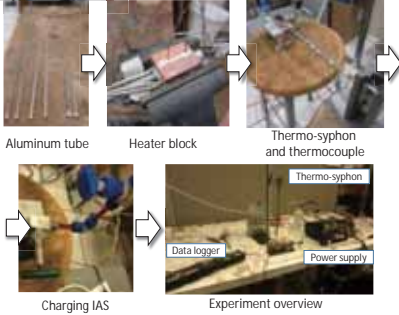
- Cooling method (natural convection) is problem.
- Thickness of backflow is so thin that discontinuity is happened, and NCG is generated

Shoya Ono

Experiment

- Natural convection thermo-syphon was tested to verify our theory.
- Length was changed to verify the length dependence of our theory.

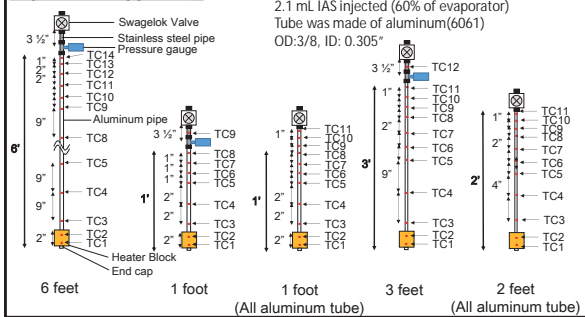
Experiment apparatus



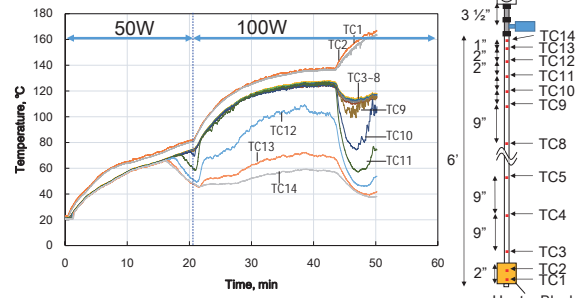
Experiment

- Natural convection thermo-syphon was tested to verify our theory.
- Length was changed to verify the length dependence of our theory.

Experiment apparatus

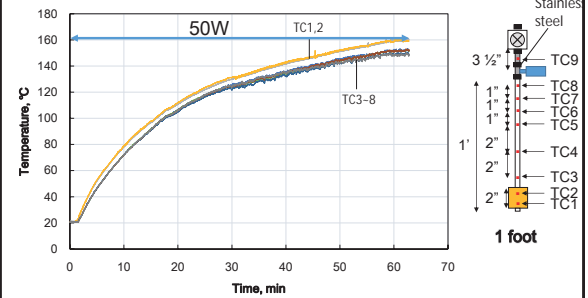


Results - 6 feet -



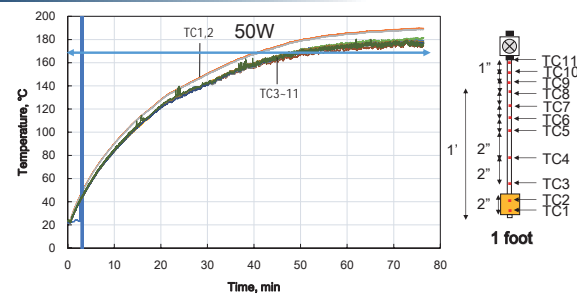
6 feet thermo-syphon failed in 15 min because of NCG
 TC11 returned because the tube pressure increased and NCG was compressed.

Results - 1 foot -



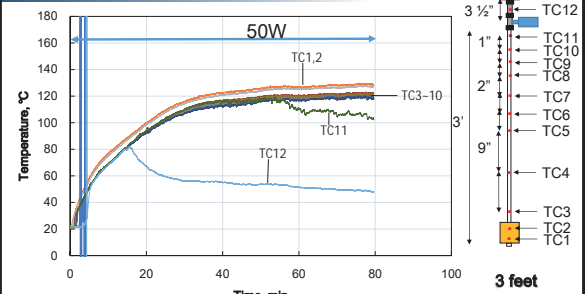
1 foot thermo-syphon doesn't fail.
 The reason of the fail isn't cooling method but discontinuity.
 There is a possibility that discontinuity occurs in the stainless steel region.

Results - 1 foot, all aluminum tube -



1 foot all aluminum tube thermo-syphon doesn't fail.
 Discontinuity didn't occur in 1 foot thermo-syphon.
 Next step, the critical point was verified.

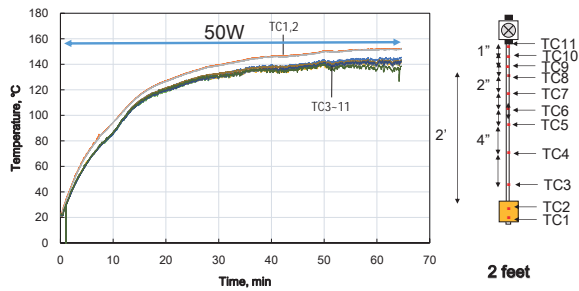
Results - 3 feet -



3 feet thermo-syphon failed in 15 min.
 After 60 min, there is no discontinuity.

Shoya Ono

Results - 2 feet -



2 feet thermo-syphon doesn't fail.

The critical point is between 2 and 3 feet*.

*Test Condition
2.1 mL IAS injected (60% of evaporator)
Tube was made of aluminum(6061)
OD: 3/8, ID: 0.305"

Conclusion

- ✓ The fail theory of natural convection aluminum / IAS thermo-syphon was verified
- ✓ 6, 3, 2, and 1 foot thermo-syphon was fabricated and tested.
- ✓ It was founded that the reason of fail is not cooling method but discontinuity.
- ✓ The critical point was between 2 and 3 feet*.

*Under this condition
2.1 mL IAS injected (60% of evaporator)
Tube was made of aluminum(6061)
OD: 3/8, ID: 0.305"

Oct. 9. 2013

JUACEP Short Term Internship Workshop

Development of a Vibration Excitation system Forced on Piezoelectric Elements

Bogdan Epureanu Research Group
Hiroki Shigematsu

Background and Proposed Method

Background

How to measure the forced response of structures with complex geometry?

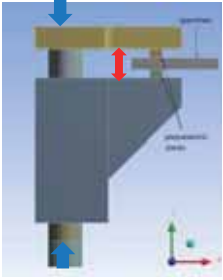
- Speakers to provide pressure waves
 - Merit: No contact to objective structure
 - Demerit: Large amount of power required, Large size
- Use of stingers
 - Merit: Low required power
 - Demerit: strong direct force to structures

Proposed method

- Use piezoelectric elements to excite structures

Introduction of the Model

Use ANSYS to simulate the model



Model in ANSYS

How does this model work?

- Clamp specimen with prestress
- Add voltage to piezoelectric stacks
- Excite specimen at target frequency

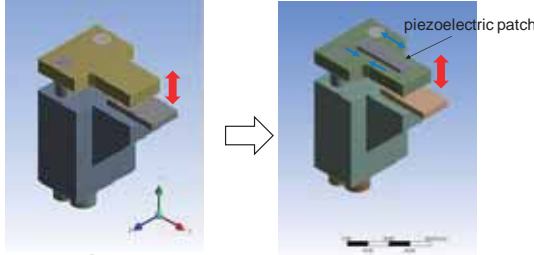
Merit

- Simple structure
- Easy to make
- Low cost

Problem to solve

- Suppression of model itself

Research Objective and Process



piezoelectric patch

- Simulate
 - Modal analysis
 - Harmonic analysis especially upper part's bending shape
- Add piezoelectric material on upper part
- Add voltage to piezoelectric patch

Find worst bending shape and frequency

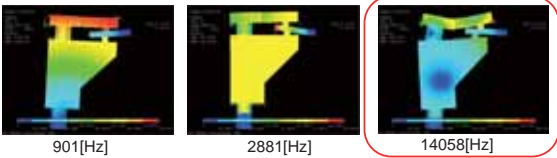
Suppress upper part

Modal Analysis of the Whole Model

Objective

- Find the desired modal shape and its frequency

Picked up modal shapes



901[Hz] 2881[Hz] 14058[Hz]

Problem

- Too high frequency range compared to target frequency range

Close to desired shape

Implement modal analysis divided into specimen and clamp

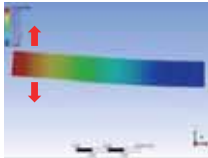
Changing Specimen's Properties

Specimen's properties

Density	E(Young's modulus)	Frequency of first mode[Hz]
1/5	original	8049.6
original	1/100	359.99

Too high

Reasonable

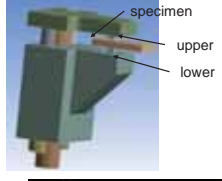


First mode of the specimen

- Change specimen's property as above
- Excite whole model around 359.99[Hz]

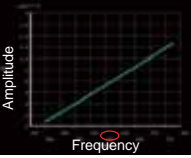
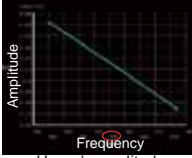
Excite only specimen

Harmonic Analysis around Resonance Frequency of the Specimen



Process

1. Clamp specimen with prestress
2. Add input voltage to piezoelectric stacks
3. Change frequency around 359.99[Hz]
4. Plot frequency and amplitude

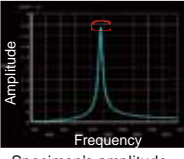
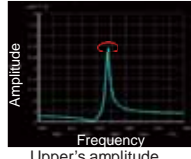
○ :360[Hz]

Specimen's amplitude

Upper's amplitude

➡ No peak can be found

Searching Peak Frequency

○ :Peak

Results

- ◆ No peak around 359.99[Hz]
- +
- ◆ Peak occurred around 838[Hz]



Shape at the peak

➡ Much dependence on clamp body

Modal Analysis without Specimen



650[Hz]



742[Hz]

- ◆ Picked up modal shapes close to desired shape
- ◆ Modal shape at 771[Hz] is close to desired shape



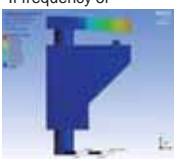
771[Hz]

➡ Try to reproduce shape at 771[Hz] in whole model

Worst Case Analysis

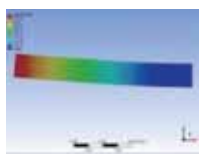
Assumption

If frequency of



Modal shape without specimen (771[Hz])

≈



First Modal shape of the specimen

➡ Worst bending shape occur around the frequency

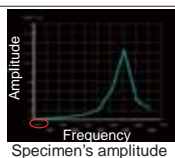
Method

- ◆ Change property of the specimen to reach first modal shape at 771[Hz]

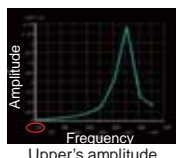
➡ Harmonic analysis around 771[Hz]

Worst Case Analysis

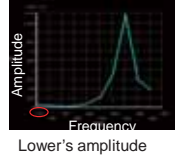
Results of harmonic analysis



Specimen's amplitude



Upper's amplitude



Lower's amplitude

- ◆ No peak around 771[Hz]
- ◆ Peak found around 838[Hz]

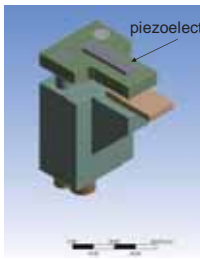
↕

➡ No match with assumption

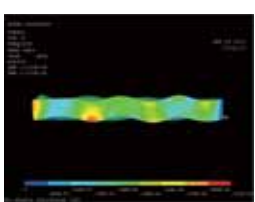
Checking the Movement of the Patch

Objective

- ◆ suppress upper part at worst bending shape(838[Hz])



piezoelectric patch



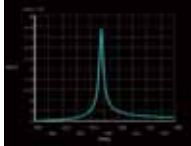
Shape of the patch at 838[Hz] input voltage

➡ Complicated deformation shape

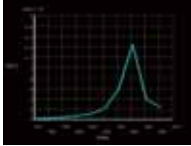
Hiroki Shigematsu

Discussion

Results of harmonic analysis



original Young's modulus (specimen)



1/100 Young's modulus(specimen)

- ◆ Almost **same peak frequency**(about 838[Hz])
- ◆ There was **little dependence on specimen**
- ◆ Frequency of modal shape without specimen is not exactly same as 838[Hz]
- ◆ Some **Errors** in setting of modal analysis without specimen

Piezoelectric patch's weird movement

- ◆ Close to **resonance frequency** of the patch

Conclusion

Conclusion

- Modal analysis of the **whole model**
- Modal analysis **without specimen**
- Change specimen's property to adapt resonance frequency
- Harmonic analysis around modal frequency to get **worst case**
- Checked the movements of piezoelectric patch to **suppress** the whole model

Future Works

- Review of the whole model's property
- Development of suppression system deal with clamp's other vibration shape
- Experiments using prototype model

Akitomo Matsumoto

Effects of the soft tissue stiffness on stress values of femur neck

Akitomo Matsumoto
 Department of Electrical Engineering & Computer Science,
 Graduate School of Engineering

 Supervisor : Professor Gregory M. Hulbert
 Graduate School of Engineering, Nagoya University

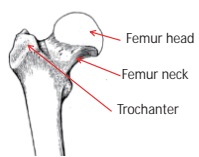
Effects of soft tissue stiffness on stress values of femur neck

OVERVIEW

- ◆ Introduction, Objective
To evaluate effects of soft tissue stiffness as a first step of clarifying effects of body type
- ◆ Analytical model, Method
'Multi-body' model which combined with finite element mesh of hip joint
- ◆ Results
Compare the time history of stress values
 1. Maximum shear and principal stress
 2. Minimum principal stress
 3. Displacement
- ◆ Discussion and Conclusions
Relationship between the history of stress and displacement



Introduction



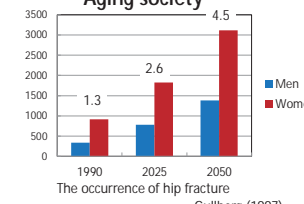
Prevention
↓
Quality Of Life
Cost of the treatment

Objective
Evaluate the effects of soft tissue stiffness on stress values of femur neck

What is femur fracture ?
Femur neck, trochanter, femur head

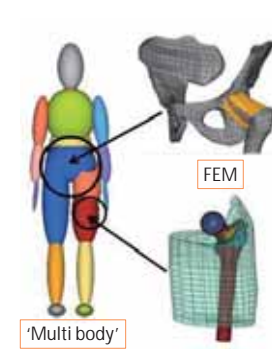
Walking difficulty, Bedridden
 Long-term hospitalization
 Rehabilitation

Aging society



The occurrence of hip fracture
Gullberg (1997)

Multi-body model with FEM



'Multi body'

'Multi body' model
↳ Whole body configuration

+

Finite Element Model (FEM)
Pelvis, Femur, Tendon, Soft tissue

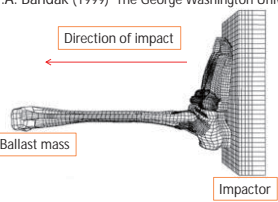
Material properties
Soft tissue : visco-elastic material
Others : linear elastic material

Stature : 149.3 cm
Weight : 55.3 kg

MADYMO

Reference of visco-elastic material

F.A. Bandak (1999) The George Washington University



Simulation set up

- Objective
To understand the mechanical behavior of the ankle joint under injurious situations
- Material property
Soft tissue of plantar Viscoelastic

Three layers of plantar
 First layer : Short and long ligament
 Second layer : Muscles
 Third layer : Fat and skin

Method - Elastic modulus -

	Elastic modulus [MPa]	Poisson ratio	Density [kg/m ³]	Bulk modulus [MPa]	Short term shear modulus [MPa]
Plantar ligament	6.01	0.49	0.75E+03	1.00E+02	2.02
Muscle layer	0.152	0.49	0.75E+03	2.53E+00	0.0509
Fat layer	20.0	0.49	0.75E+03	3.33E+02	6.71

Elastic modulus [MPa]	Bulk modulus [MPa]	Dynamic shear modulus [MPa]
0.15	2.500	0.05034
1.5	25.00	0.5034
5	83.33	1.677
10	166.7	3.355
15	250.0	5.034
20	333.3	6.711
25	416.7	8.389

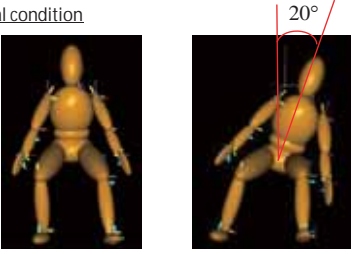
$$K = \frac{E}{3(1-2\nu)}$$

$$G = \frac{E}{2(1+\nu)}$$

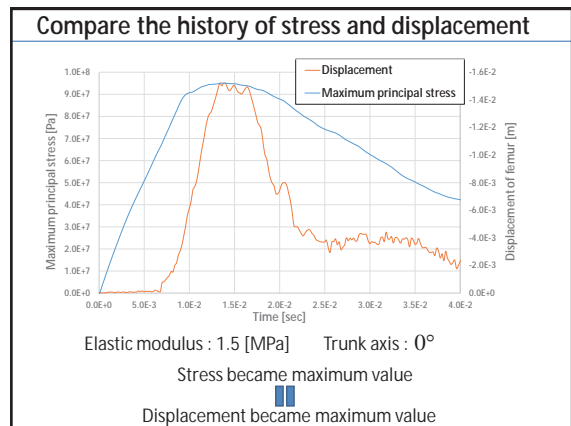
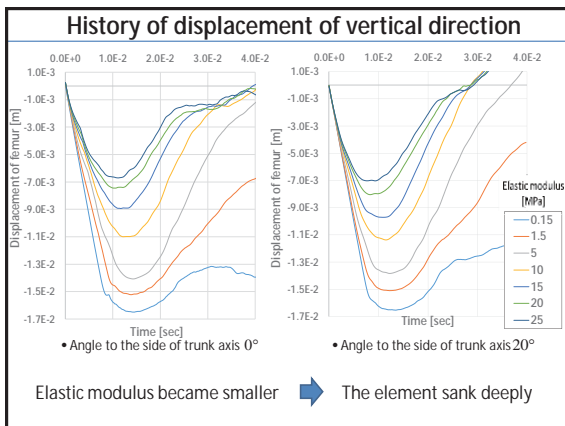
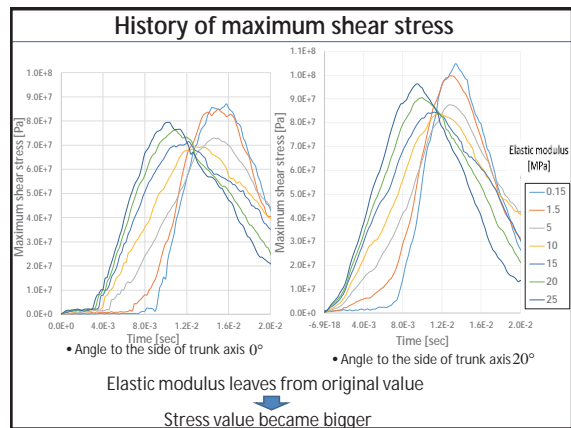
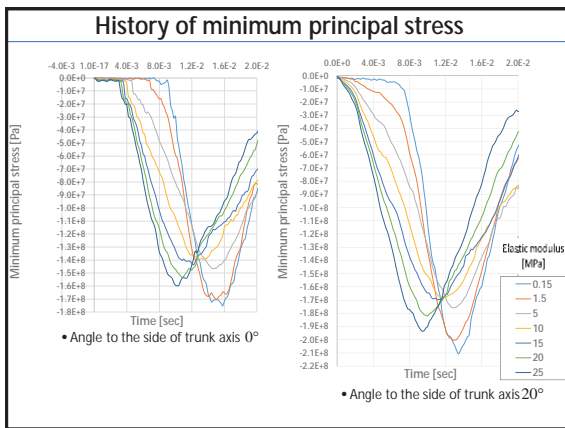
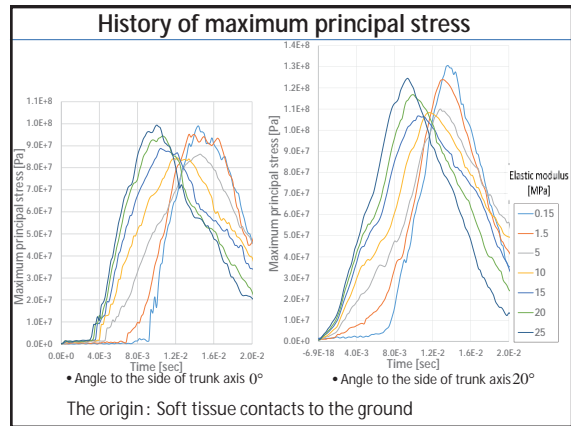
Akitomo Matsumoto

Method - Body configuration -

Initial condition



- Height of buttocks 500 [mm]
- Positions of legs Asymmetrically
- Angle to the side of trunk axis 0°, 20°
- Exposed to gravity



Akitomo Matsumoto

Conclusion

- Elastic modulus : 25 [MPa] \sim 10 [MPa]
Soft tissue could absorb more shock \rightarrow Stress decreased
- Elastic modulus : 10 [MPa] \sim 0.15 [MPa]
Effects of potential energy became bigger \rightarrow Stress increased
- For the further study
Separate muscle part and fat part
Change the shape of model to match body type



1

Analysis of Fluid Flow of Molten Magnesium into Micro-Particles

Tomoko Ozawa
Department of Materials Science and Engineering,
Nagoya University

Supervisor: Katsuyo Thornton, University of Michigan

2

Overview

Introduction
Previous research: Experimental results and analysis of fluid flow into porous medium

Methods
About Darcy's law and assumption of the wettability

Results and Discussion
Definition of wettability, analysis of infiltration distance and comparison of experimental results

Conclusion
Accuracy of results and foresight in the future

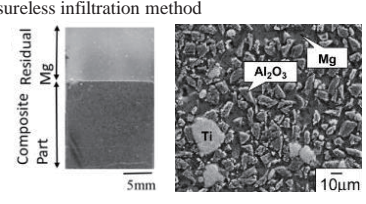
3

1. INTRODUCTION

4

Experimental method

Pressureless infiltration method



Composite Part
Residual Mg

5mm 10µm

Important factor

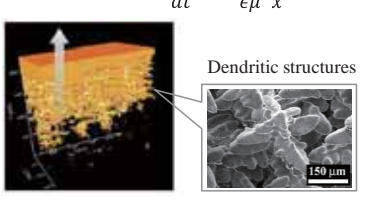
- Wettability between molten alloy and particles
- Penetration with capillary action

Reference
Makoto KOBASHI. Effect of preform processing conditions on microstructure and properties of Al₂O₃/Ti particle dispersed Mg matrix composite fabricated by pressureless infiltration method (2010)

5

Analysis of fluid flow into porous medium

Darcy's Law : $\frac{dx}{dt} = -\frac{K \Delta P}{\epsilon \mu x}$



Dendritic structures

150 µm

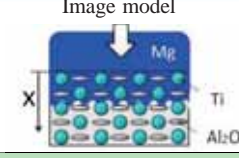
There is no analysis of fluid flow of molten metal through different kinds of solid particles exhibiting different wettability.

Reference
J. Madison, J. Spowart, D. Rowenhorst, L.K. Aagesen, K. Thornton, T.M. Pollock, Modeling fluid flow in three-dimensional single crystal dendritic structures

6

Objective

Image model



X

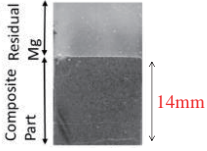
The purpose of this study is to determine how far molten metal penetrates into porous medium compounded **different kinds of solid particles** exhibiting different wettability.

- Definition capillary action as a driving force by myself
- Calculation with the number ratio of titanium to alumina particles from the volume fractions of the samples, which are measured experimentally

7

2. METHOD

◆ **Condition**
 Mg ingot : 8 g (constant)
 Temperature : 927K (600s preservation)
 Composite part : Al₂O₃, Ti



Al ₂ O ₃ size	Ti size	Relative density	Diameter	Height	Weight
10-20 μm	35 μm	0.4	16mm	14mm	4.0g

8

Darcy's law

◆ **Darcy's Law**

$$\frac{dx}{dt} = -\frac{K \Delta P}{\epsilon \mu x}$$


Darcy's law is a phenomenology derived constitutive equation that describes the flow of a fluid through a porous medium.

◆ Kozeny-Carmen
 $k_{KC} = \frac{c \epsilon^3}{55 s_0^2 (1-\epsilon)^2}$

◆ Blake-Kozeny
 $k_{BK} = \frac{c d_p^2 \epsilon^3}{150 (1-\epsilon)^2}$

K : Permeability [m²]
μ : Viscosity [Pa·s]
ε : Porosity (=Vpore/Vtotal)
ΔP : Pressure difference [N/m²]
D_p : Average size of spherical particles

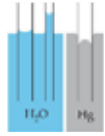
9

Capillary action

◆ **Capillary action**
 Capillary action is the ability of a liquid to flow in narrow spaces without the assistance of, and in opposition to, external forces like gravity.

$$Pc = \frac{2\gamma_{lv} \cos\theta}{r_p}$$

γ_{lv} : Liquid surface tension
 θ : Contact angle
 r_p : Hydraulic radius



◆ **Assumption of pressure**

Type.1: Al₂O₃ (wetting) Type.2: Ti (wetting) Type.3: Al₂O₃ (non-wetting)

Assumption $Pc = \frac{N_{Al_2O_3}}{N_{total}} \times Pc1 + \frac{N_{Ti}}{N_{total}} \times Pc2 + N_{mix} \times Pc3$

10

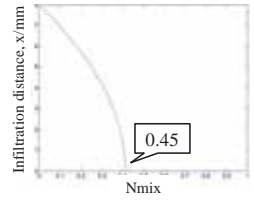
3. RESULTS AND DISCUSSION

- Definition of N_{mix} as wettability,
- Analysis of fluid flow
- Comparison of effect of gravity and permeability

11

Definition of N_{mix}

◆ **Volume fraction**
 Al₂O₃/ Ti = 70/ 30

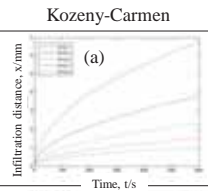
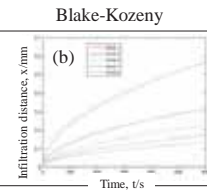
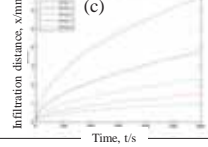
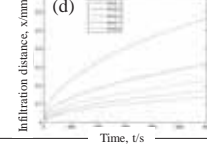


The infiltration distance extremely depends on N_{mix}.
 If N_{mix} > 0.45, penetration does not happen.
 Conversely, if N_{mix} < 0.45, the infiltration distance increases.

Assumption $Pc = \frac{N_{Al_2O_3}}{N_{total}} \times Pc1 + \frac{N_{Ti}}{N_{total}} \times Pc2 + N_{mix} \times Pc3$

12

Infiltration distance

	Kozeny-Carmen	Blake-Kozeny
Capillary		
Capillary + Gravity		

Fluid flow into porous medium 13

- Increasing Penetration like a **logarithmic function** and gradually plateaus with progress of flow.
- The velocity is larger initially, gradually decreasing and converges to zero finally.

(Slope of these plots is the velocity of penetration.)

Infiltration distance 14

	Kozeny-Carmen	Blake-Kozeny
Capillary	(a)	(b)
Capillary + Gravity	(c)	(d)

Volume fraction and effect of gravity 15

- Decreasing infiltration distance with increasing volume fraction of alumina for both results
- Gravity could be negligible.

Permeability, K 16

	Kozeny-Carmen	Blake-Kozeny
Capillary	(a)	(b)
Capillary + Gravity	(c)	(d)

Permeability, K 17

- Not to correspond the plots calculated with the Kozeny-Carmen and Blake-Kozeny permeability
- Be Kozeny-Carmen closer than the experimental result
- In previous research, **Kozeny-Carmen permeability is similar** with current study under $f_s = 0.4$.
- To apply **Kozeny-Carmen** for permeability

Conclusion 18

- Development of a new approach for analysis of fluid flow in different kinds of micro-particles by applying Darcy's law with original assumptions
- Analytical results are much less than experimental results.

To improve the assumption of capillary action as the main driving force by considering another factor

- Particle array
- Change liquid viscosity
- Friction binding force between wall of pipe

Tomoko Ozawa

19

THANK YOU FOR YOUR ATTENTION

Tomoya Nishiyama

Kinematics and Compliance Testing Simulation of an Automobile Using a Rigid Body Suspension Model



Tomoya Nishiyama
Department of Mechanical Science and Engineering,
Graduate School of Nagoya University

10/9/2013

INTRODUCTION

- Essential to measure the vehicle suspension K&C values by K&C tests
 - K&C: Kinematics and Compliance
 - Kinematics: Study of motion without reference to mass or force
 - Compliance: Deflection resulting from the application of force
- K&C test simulations are performed using multibody dynamics software
 - K&C test simulations → Prediction of K&C values
 - Multibody dynamics software → Adams/Car

OBJECTIVE

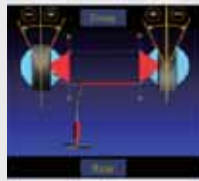
- Perform K&C testing simulations and compare the results changing the hardpoint locations and the spring characteristics
 - Identify the factors affecting K&C values

- Hardpoint locations
 - Distance between the right and left lower ball joints
- Spring characteristics
 - (1) Stiffness
 - (2) Installed length
 - (3) Preload



K&C VALUES

- Toe
 - Angle of the wheel as seen from the **top** of an automobile
 - Angle between the vertical plane through the front and rear centers of an automobile and the vertical plane along with the wheel

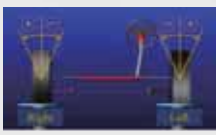


Top view

Related to the **attrition** and the **grip** of tires

K&C VALUES

- Camber
 - Angle of the wheel as seen from the **front** of an automobile
 - Angle between the longitudinal center line and the vertical line of the wheel

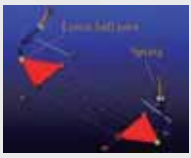


Front view

Related to the **driving stability** and the **grip** of tires

K&C TEST SIMULATIONS

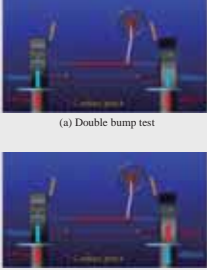
- Suspension Model
 - MacPherson strut**:
 - Most widely used suspension for passenger automobiles in the world
 - Consists of the **rigid** body, damper and spring
 - Suspension parameters
 - Unloaded radius of the tire: 300mm
 - Tire stiffness: 200N/mm
 - Wheel mass: 10kg



MacPherson strut

K&C TEST SIMULATIONS

- Kinematic test simulations
 - Control the displacement of contact patches
 - (a) Double bump test
 - Contact patches move in the **same** direction at the same time
 - (b) Roll test
 - Contact patches simultaneously move in the **opposite** directions



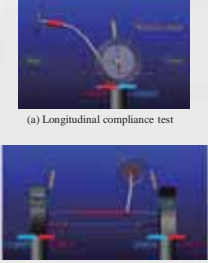
(a) Double bump test

(b) Roll test

6

K&C TEST SIMULATIONS

- Compliance test simulations
 - Control the forces applied at the bottoms of the wheels
 - (a) Longitudinal compliance test
 - The forces are applied in the **longitudinal** direction
 - (b) Lateral compliance test
 - The forces are applied in the **lateral** direction



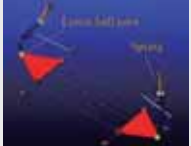
(a) Longitudinal compliance test

(b) Lateral compliance test

7

K&C TEST SIMULATIONS

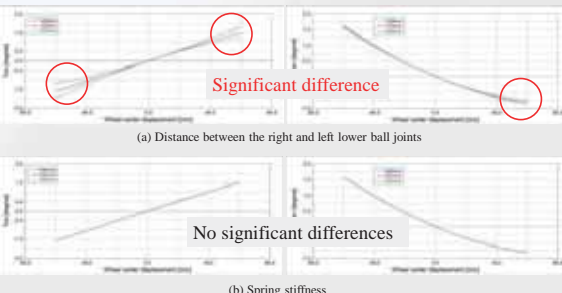
- Simulation conditions
 - (a) Distance between the right and left lower ball joints
 - 1450mm, 1500mm, 1550mm
 - (b) Spring stiffness
 - 40N/mm, 50N/mm, 60N/mm
 - (c) Spring installed length
 - 180mm, 190mm, 200mm
 - (Spring preload is 0N)
 - (d) Spring preload
 - 0N, 500N, 1000N
 - (Spring initial length is 200mm)



8

SIMULASION RESULTS

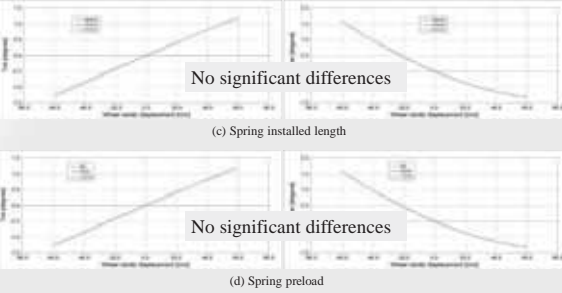
- Double bump test
 - (a) Distance between the right and left lower ball joints
 - Significant difference
 - (b) Spring stiffness
 - No significant differences



9

SIMULASION RESULTS

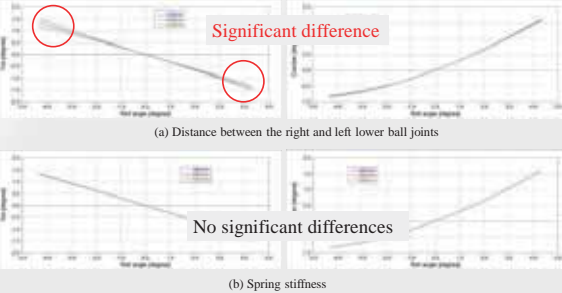
- Double bump test
 - (c) Spring installed length
 - No significant differences
 - (d) Spring preload
 - No significant differences



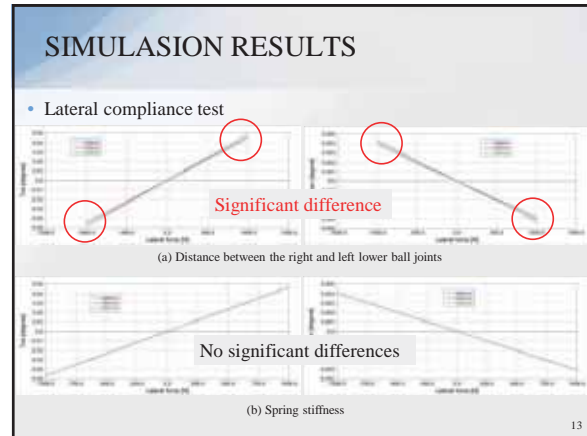
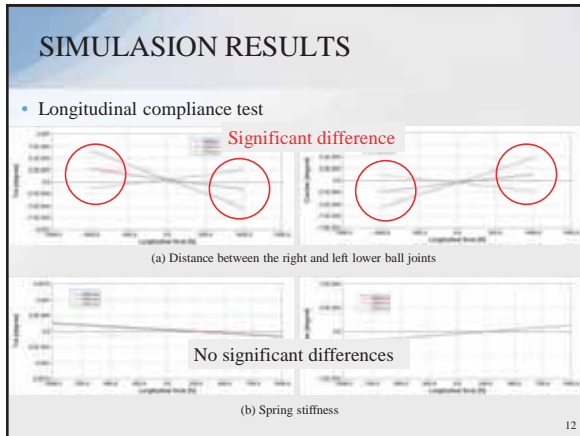
10

SIMULASION RESULTS

- Roll test
 - (a) Distance between the right and left lower ball joints
 - Significant difference
 - (b) Spring stiffness
 - No significant differences



11



CONCLUSIONS

- The positions of the lower ball joints significantly affect K&C values and are so important factors to design suspensions
- The characteristics of the spring such as stiffness, installed length and preload have little influence on K&C values.

14

Thank you for your kind attention.

Research of Organic Functionalized Silsesquioxanes




Yasunori Iijima
 Department of Crystalline Materials Science and Engineering, Nagoya University,
 Researched at University of Michigan, Laboratory of Richard M Laine
 Supervisor: Joseph Furgal

Presentation overview

- Introduction
 - What are silsesquioxanes?
 - Objectives
 - Evaluation methods
- Results and discussion
- Conclusion and future works

What are silsesquioxanes (SQs)?



- Solvent
- H₂O
- Catalyst
- Tri R' silane

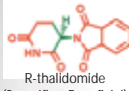
$$\begin{array}{c}
 \text{R}' \\
 | \\
 \text{R}' - \text{Si} - \text{R}' \\
 | \\
 \text{R}'
 \end{array}
 \xrightarrow[\text{condensation}]{\text{hydrolysis}}
 \begin{array}{c}
 \text{R}' \\
 | \\
 -\text{O}-\text{Si}-\text{O}- \\
 | \\
 \text{O}
 \end{array}
 \text{ T unit}$$

Applications

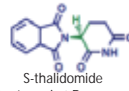
- Coatings or adhesives for electrical, optical equipments
- medical field

Establish novel reaction process of full cage silsesquioxanes

Chiral separating materials

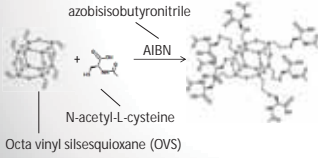


R-thalidomide
(Somnific → Beneficial)



S-thalidomide
(Teratogenic → Dangerous)

Many of drugs contain chiral molecules
 ↓
 Chiral separating materials are important to get drugs safe



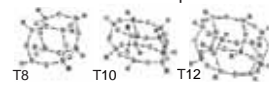
Synthesize novel functionalized silsesquioxane

Evaluation methods

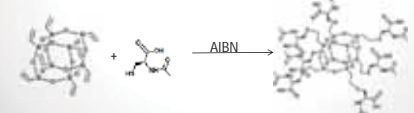
- Fourier Transform Infrared Spectroscopy (FT-IR)
→ look chemical bonds
- Gel Permeation Chromatography (GPC)
→ look molecular weights
- MALDI-ToF mass spectrometry
→ look molecular weights Not shown here
- Chiral Chromatography
→ evaluate chiral separating material
- Circular Dichroism (CD)
→ evaluate chiral molecules Not shown here

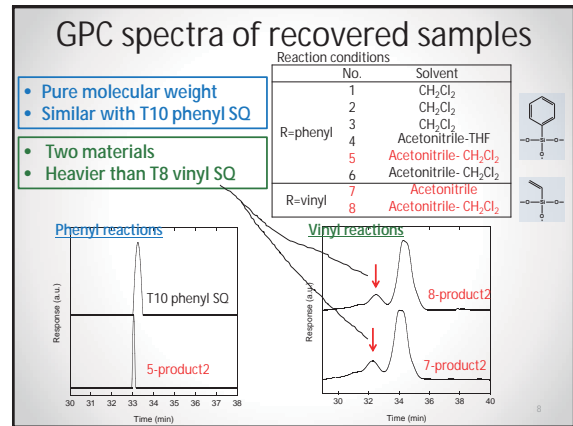
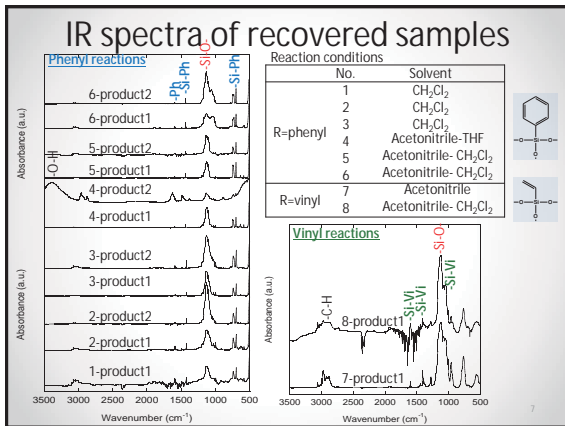
Results and discussion

➤ Establish novel reaction process of full cage silsesquioxanes from the viewpoint of solvents.



➤ Synthesize n-acetyl-L-cysteine functionalized silsesquioxane as a chiral separation material.





Results and discussion

- Establish novel reaction process of full cage silsesquioxanes from the viewpoint of solvents.
- Synthesize n-acetyl-L-cysteine functionalized silsesquioxane as a chiral separation material.

Evaluation of cysteine functionalized SQ

IR spectra and Chiral chromatography results are shown. The IR spectra compare the recovered product, OVS, and cysteine. The chiral chromatography shows the separation of a flowed D,L-limonene mixture (with hexane) through the product separation. The results indicate that CD is inconclusive.

Conclusion and Future Works

novel reaction process

T8, T10, T12

A few interesting results were got from original solvents.

In the future

- Further evaluation (MALDI-ToF)
- Further reaction adjustments

chiral separating material

N-acetyl-L-cysteine functionalized silsesquioxane was successfully synthesized.

In the future

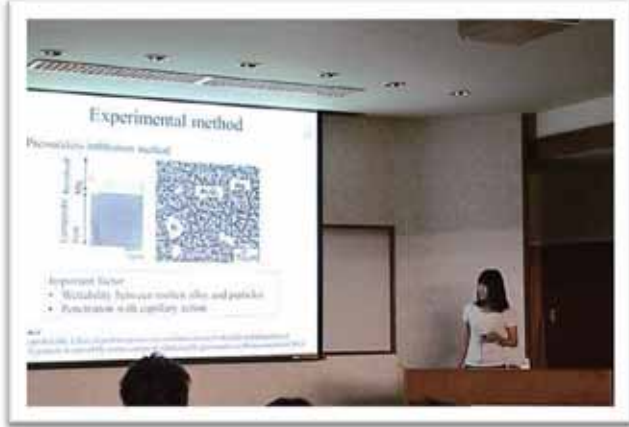
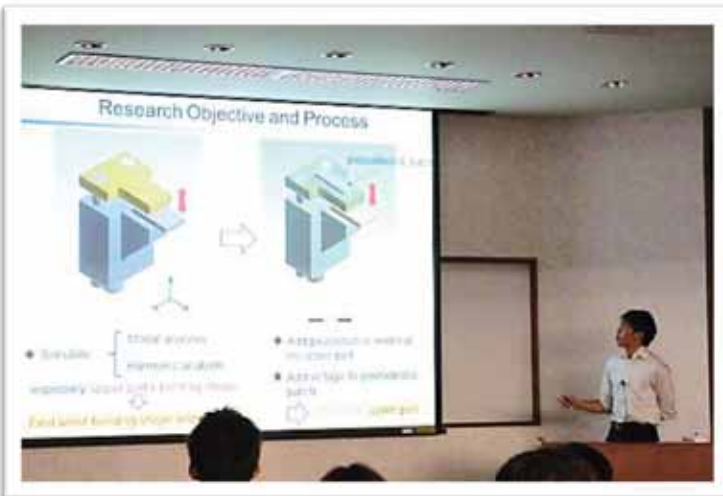
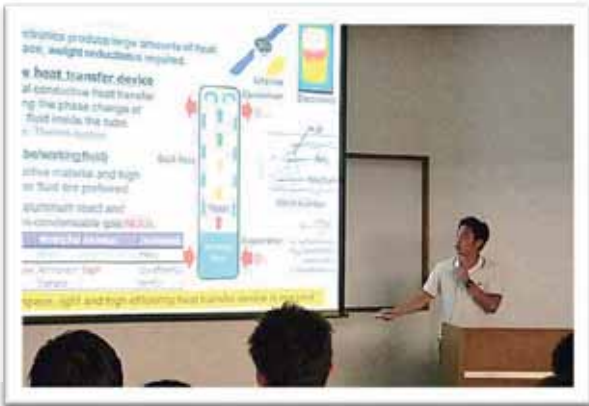
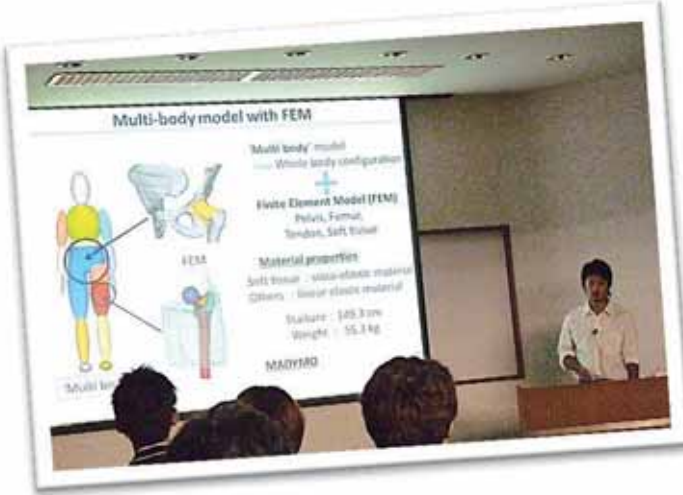
- Further evaluation (CD, MALDI-ToF)
- chloride conversion

Thank you for your kind attention!

References:

- [1] Ronald H. Barney, Masu Itoh, Akihito Sakakibara, Toshio Suzuki, Chemical Review, 1995, 95, 1409-1430
- [2] Maki Itoh, Chemistry of Silsesquioxane Materials and Their Applications, csmbooks, 2013
- [3] <http://www.ijehing.jp/ehing/07/0916A06.pdf>
- [4] H. Jiang, J. C. Fargal, T. Goodson, III, T. Mizuno, M. Schwartz, K. Zhou, J.F. Veroet, R. M. Laine, *J. Polym. Sci. Part A: Polym. Chem.* 2012, 50, 1883-1895. DOI: 10.1021/jo300587a
- [5] Fargal, J. C.; Jiang, J.H.; Goodson, T.; Laine, R.M. "Analyzing Structure-Photophysical Property Relationships of Isolated T₈, T₁₀, and T₁₂ Silbenzyl Silsesquioxanes." 2013. 1225-1226. DOI: 10.1021/jo404300z
- [6] Fargal, J. C.; Goodson, III, T.; Laine, R. M. "Synthesis of Decaphenyl Silsesquioxane (DS-T₁₀) and Larger cages by Fluoride Catalyzed Rearrangement of (PhSiO₂)₄ and Phenyltrichlorosilane with Steady State Spectroscopy Compared to Simple SQs (D and T type) and Proposed Mechanism." (Manuscript in Preparation)

-Presentations-



-Award Ceremony-



<4> Reports on JUACEP Program

My precious experience in Los Angeles

Name: Takafumi Hattori

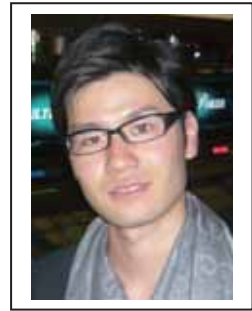
Affiliation (Dept & Univ): Department of Mechanical Science and Engineering, Graduate School of Engineering, Nagoya University

Participated program: Middle term (Spring to Summer), 2013

Research theme: CHARACTERIZATION OF MOLDED SUPERHYDROPHOBIC SURFACES

Advisor at UCLA: Prof. Chang-Jin "CJ" Kim

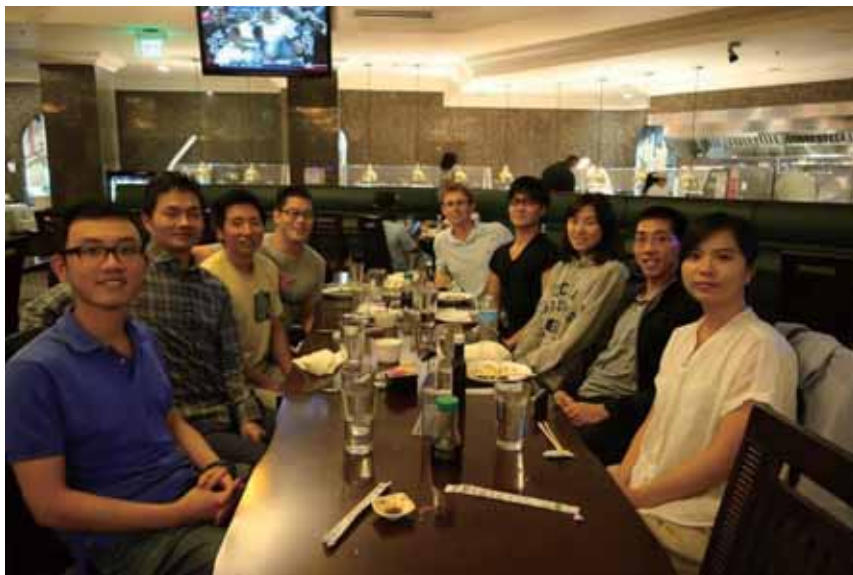
Affiliation (Dept.): Mechanical and Aerospace Engineering Department, Henry Samueli School of Engineering and Applied Science, University of California, Los Angeles (UCLA)



My research project at UCLA was to characterize molding of superhydrophobic surfaces with microstructures. I learned the US research process through this practical research project. Also, since I had the opportunity to have discussions with the other laboratory members in the group meetings which were held every Friday, I gradually became able to speak English fluently. I am sure that I can make use of this precious experience in my future research endeavors and career. I appreciate my Supervisor CJ Kim for the opportunity to work under his patient guidance.

Los Angeles is a great, comfortable city. One amazing fact about this city is that there was no rain during my entire 6 months stay. When you walk in the Westwood village, which is very close to UCLA campus, you can see lots of people having pizza and drinking coffee in the sunshine thanks to its comfortable, low humidity climate. Furthermore, Los Angeles has lots of places to go, such as Santa Monica beach, Hollywood, Beverly Hills and so on. In addition there are many beautiful national parks near Los Angeles that I was able to visit on the weekends.

Throughout the UCLA campus, beautiful historical architecture attracts visitors, as well as UCLA students. UCLA boasts a high reputation as one of the most prestigious universities in the world. At the same time, UCLA has reputation as a powerhouse in sports, especially football and basketball. Therefore, there are students from a variety of nationalities, such as African, Asian, European, and so on. These students have many opportunities to interact with each other. Fortunately, now JUACEP can provide you with such an opportunity to be one of them. I made a lot of international friends during my stay and I am very proud of many unforgettable UCLA experiences with them. There is no choice but to study at UCLA! I am sure that you will have a great experience.



JUACEP Report

Name: Yoko Okuda

Affiliation: Computational Science and Engineering, Department of Engineering,
Nagoya University

Participated program: Medium term 2013

Research theme: How split Bregman can apply for non-negative matrix factorization

Advisor at UCLA: Prof. Stanley Osher

Affiliation: Department of Mathematics



I was working on applied mathematics in the department of mathematics at UCLA for six months. Especially, I studied “split Bregman” algorithm, which solves convex optimization problem. This algorithm is now one of popular methods and I could learn what is going on at UCLA math department. One of its applications is image processing so I could also expand my knowledge to applications. I am going to start my master thesis based on this theme and it would be an interesting topic later.

During my stay at UCLA, I attended the conference SIAM (Society for Industry and Applied Mathematics) annual meeting 2013 in San Diego. I saw international faculties and PhD students from all over the world and the talking with them also inspired me. I could feel how super famous and great my supervisor is and it was a great honor to visit UCLA applied math field. This meeting is one of my best experiences in my research life.



At SIAM Meeting

It is the best thing for me to make friends from other countries. I appreciate all of their kindness and I enjoyed my life to spend with them. I hope to visit my friends in U.S. or their countries and show them around Japan.

With Prof. Osher



Awesome experience in the Michigan

Name: Fumitake Nonoyama

Affiliation: Mechanical Science Engineering, Nagoya University

Participated program: Medium term 2013

Research theme: 3D-printed bone-mimicking material for orthopedic surgical simulation

Advisor at Univ. Michigan : Prof. Albert Shih

Affiliation: Mechanical Engineering,



Albert Shih Lab focuses on mechanical and biomedical engineering. My research topic is 3D-printed material for orthopedic surgical training. I had never known about 3D-printing and medical terms until I started my research at the University of Michigan, so it is a very good experience for me to learn them.



During this stay, I watched sports matches including football, baseball and tennis. The University of Michigan is famous for football and has the biggest stadium in the US called "The Big House". I went there to see the first football match in 2013. Although the capacity of the stadium was less than 110 thousand seats, more than 110 thousand people gathered there on that day. Almost of them wore maize or blue clothes to cheer the Michigan football team. They became so excited every time play stopped and screamed "Go Blue!".

The stadium is also used for the commencement. I was lucky to join the commencement as an audience because my roommate graduated after this spring semester and he had some free tickets. All graduate students wore the black robe and hat. After the commencement, our lab held a farewell party at my professor's house. Prof. Shih's wife served many Chinese meals and most of the students brought their traditional foods. That's why I can eat various cuisines at once there.

I traveled at least once a month. The most amazing place is Yellowstone National Park, which is the first national park in the world. The nature in the US is pretty different from that in Japan. The area of Yellowstone National Park is as large as that of Shikoku island. Then, I felt as if I lived on different place.

In a word, I really enjoyed the stay in the University of Michigan and I had an impressive experience there!!



JUACEP Report

Name: Iijima Yasunori

Affiliation: Crystalline Materials Science, Graduate School of Nagoya University

Participated program: Short (Summer) 2013

Research theme: Research of Organic Functionalized Silsesquoxanes

Advisor at Univ. Michigan : Prof. Richard M Laine

Affiliation: Materials Science and Engineering, University of Michigan



➤ Research

I have been trying to synthesize novel materials in Japan. This time I challenged mastering different materials and method. I had a lot of troubles to remember experimental tools and listen to technical terms. I bought textbook in Japanese. It greatly helped me learn because I could not ask questions well about various phenomena. I felt Japanese textbooks are very important to study abroad.

➤ College life

Main campuses were Central and North. We could move everywhere in campus of University of Michigan by school bus freely. I usually went lunch to cafeteria at North campus with lab members. The new school term started from September. There were many events such as briefing sessions, welcome parties, free market at the campus. We could go there and get complimentary food.

➤ Food

Hamburger and pizza are popular food in America. Most of the Candies, juice and cookies are extra sweet for me. When I was bored by them, I could eat Japanese, Korean, Indian, Mexican, Chinese foods.

➤ City

Ann Arbor was a safe city, but prices were a little bit expensive. The climate was cool in spite of it was August and September. There were no natural disasters. There were many M logo goods all over the city. The logo means University of Michigan. The car was important to move anywhere. I thought it was easy place to live.

➤ Culture

Most of the people were kind. They usually open the door for other person. Though many people were loose for time, they worked more effectively than Japanese people. We had to pay tip to waitress. Many units were used in America, for example km and mile, kg and pond, l and gallon and so on. It was difficult for me to use such many units, but American seemed not to be confused.

➤ Travel

If we want to travel near the Ann Arbor, we must use car. I went to Chicago, Niagara, Sleeping Bare National Park, New York and so on. I don't recommend a day trip.

➤ Differences from Japan

We can use wi-fi at much more places than Japan. Because various nationalities were in America, we can be aware of the world. We can find something Japanese such as car, food and so on at many places.



JUACEP Report

Name: Akitomo Matsumoto

Affiliation: Graduate School of Engineering, Nagoya University

Participated program: Short (Summer) 2013

Research theme: Effects of soft tissue stiffness on the stress values of femur neck

Advisor at Univ. Michigan: Professor Gregory M. Hulbert

Affiliation: Department of Electrical Engineering & Computer Science, Graduate School of Engineering



The subject of my research in University of Michigan was to evaluate the effects of soft tissue stiffness on stress values of femur neck. At the beginning, I presented about my research in Nagoya University to professor Hulbert. We have discussed about what is the best subject for me at this program. We had a discussion every week to analyze the result of research and talk about policy for the future study. It was worthwhile to discuss about research in English. There was a lot of computers I can use and many kinds of soft ware were installed in those computers. For example, I used HyperMesh (Altair HyperWorks) to analyze the results of simulation.

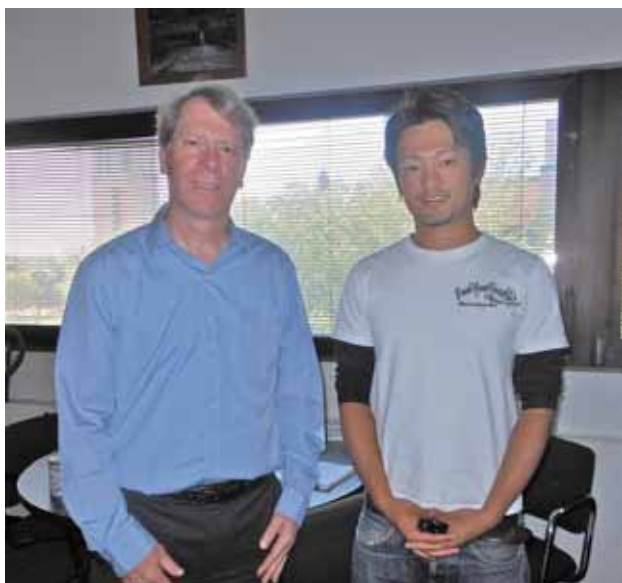
University of Michigan is much wider than Nagoya University. It is surrounded by nature and sometimes we can see the deer and squirrels. Tall tower is built in the central of North Campus and it rings the bell. There is a big fountain and some people was reading a book around it. We can eat Chinese dishes at Panda express and if you want to have a break, it is a good idea to go to the Cafe near the library. Furthermore, various events have been held for international students. You can get free food at there.

Students of University of Michigan can catch the blue bus it is the bus you can ride for free. You can go to the Central Campus in Ann Arbor city taking the blue bus. People living in Ann Arbor love American football. When a team of University of Michigan have the game, the whole city becomes like a festival. Everyone celebrate the victory of the team.

It takes 5 or 6 hours to Chicago and Niagara falls from Ann Arbor if you will go there by car. These are good place to go.

There are many students who came from foreign countries. They have a big dream and do their research to achieve a big goal of each. Talking with them inspired me. I'm interested in working abroad in the future now.

I had a very good experience through this program.



With Prof. Hulbert



Life in the USA

Name: Tomoya Nishiyama

Affiliation: Department of Mechanical Science and Engineering,
Graduate School of Nagoya University

Participated program: Short (Summer) 2013

Research theme: Kinematics and Compliance Testing Simulation of an Automobile
Using a Rigid Body Suspension Model

Advisor at Univ. Michigan: Prof. Gregory Hulbert

Affiliation: Department of Mechanical Engineering,



My study was on the suspension of an automobile. I simulated kinematics and compliance tests using a rigid body suspension model. I investigated K&C values such as toe and camber with change of the configuration of the suspension body and the characteristics of the springs.

In my daily life, I had had non-nutritious foods such as burgers and French fries. There were too many fast food restaurants in the USA such as Burger King, Big Boy and McDonald's. I was getting tired of burgers.

I went on a trip many times with my friends. We visited Niagara Falls, Chicago and so on. Niagara Falls were so magnificent and the view of Chicago was so beautiful.



Niagara Falls



Chicago

We made friends with a lot of students at University of Michigan. We enjoyed a BBQ in the park close to the north campus. They held a farewell party for us and we enjoyed drinking and talking.



BBQ



Farewell Party

Memorial summer in University of Michigan

Name: Tomoko Ozawa

Affiliation: Materials, Physics and Energy Engineering, Nagoya University

Participated program: Short (Summer) 2013

Research theme: Analysis of fluid flow of molten Magnesium into micro-particles

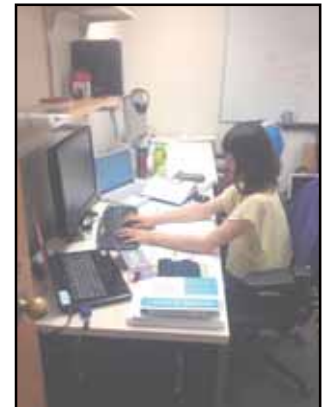
Advisor at Univ. Michigan: Prof. Katsuyo Thornton

Affiliation: Materials Science and Engineering



I had spent in University of Michigan for two months with two objectives. The one is the challenge to study something new, then, the second is to know American cultures through communication with brilliant students and researchers in University of Michigan.

In this program, I had worked the field of not experiment but analysis firstly. While I had a lot of trouble and unknown things, PhD students in same laboratory prepared the perfect environment like a picture and advised a lot of things. I especially appreciate that Chinese PhD researcher considered my analysis kindly and sometimes invited me to a dinner. I also presented my progress in the group meeting which took place once a week and attended the class of my supervisor. It was so exciting to spend in the laboratory and discuss with American researchers and students as a student in University of Michigan.



Besides, I had spent interesting weekend traveling Chicago and Canada, watching football, attending home party with members of laboratory and the farewell party with members of JUACEP.

I hope to continue the relation with member of laboratory and students in University of Michigan and contribute to expanding my view by such a valuable experience. Finally, I would like to show my greatest appreciation to Prof. Katsuyo Thornton who provided carefully considered feedback and valuable comments. I would also like to express my gratitude to my family for their moral support and warm encouragements. Finally, I would like to express my gratitude to JUACEP for their financial support.



Appearance of life in the lab



Farewell party with JUACEP members



Watching football in Detroit

JUACEP Report

Name:Hiroki Shigematsu

Affiliation:Mechanical Science and Engineering, Nagoya Univ.

Participated program: Short (Summer) 2013

Research theme: Development of a Vibration Excitation System Forced on Piezoelectric Elements

Advisor at Univ. Michigan: Prof. Bogdan Epureanu

Affiliation: Department of Mechanical Engineering, University of Michigan



I visited University of Michigan for two months and researched in Prof. Bogdan Epureanu's research group. I introduce what the life in University of Michigan was like.

First, I introduce about the research I did in Bogdan research group. Bogdan research group's main research theme is vibration and acoustic. My research theme was "Development of a Vibration Excitation System Forced on Piezoelectric Elements". The excitation system using piezoelectric material is defined by Prof. Bogdan Epureanu and our research group tried to generate the simulation model and analyze the model's harmonic response. Our research group also tried to generate prototype model and experiment by using the model. My specific task was modal and harmonic analysis of the simulation model and generation of suppression system of the model. I used ANSYS, a engineering FEM software to simulate the model. But I had never used ANSYS before, so first thing I did was to learn how to use ANSYS. After I learned how to use ANSYS basically, I edited the model and analyzed. I wish I could success in simulation and apply the results to prototype model but unfortunately there were some errors in the model and results were not reasonable. I couldn't fix the error within two months.

Second, I introduce college life. Most of our lab members were consisted of Asian people such as Chinese, Korean, Taiwanese, and Japanese. There were a lot of Asian students not only our lab but also other labs and everywhere in campus. I think this is more obvious in engineering department. Because of such a situation, it was not so difficult to communicate each other. Asian student's English was easier to understand compared to native students. I didn't take any classes but classes in University of Michigan seemed to be very busy. There were lots of homework and group projects. I thought it was much harder than classes in Japan. Many of undergraduate or master students wanted to get Ph.D degree. I think this is a big difference between Japanese students and American university's students. In Japan, there are limited opportunities for Ph.D students to get good jobs but in US, there are many opportunities. I think lots of Japanese students hesitate to get Ph.D degree because of such reason, but situation in US is opposite. By the way, lots of college events were held. Especially, I was surprised by events held by Crist church. It was casual but there was really strong religious belief.

About general life, I missed food in Japan almost all of the term. The foods I could get in the campus were pizza, sub(hard sandwich), Chinese first food, and so on. These foods were not so cheap and the taste was so-so. So I bought some Japanese foods, fruits, and salads to enjoy meals. But some restaurants were really good. Especially I liked a Indian restaurant. University of Michigan is placed in Ann Arbor. Ann Arbor is very clean, safe city. There are no subways in Ann Arbor but instead of subway, a lot of buses run. But in weekends, numbers of buses decreases. So it is a little inconvenient to go around. I hoped that I'd have a car many times.

Finally, I introduce my travel and holiday experiences. I traveled a lot of places in the two months. For example Chicago, a national park, Boston, NY, Toronto, etc. I also watched lots of sports such as American football, baseball, tennis, and MMA. I was so excited to watch college football game. University of Michigan has one of the biggest football stadium and the capacity of the stadium is over 110,000. On match day, lots of people who supports UM wear yellow (team color) T-shirt and walk to the stadium. The atmosphere was amazing.



JUACEP Report

Name:Shunji Shibata

Affiliation: Micro-Nano Systems Engineering, Nagoya University

Participated program: Short (Summer) 2013

Research theme: Tapered Etch Profile of Silicon

Advisor at Univ. Michigan: Prof. Euisik Yoon

Affiliation: Electrical Engineering and Computer Science



Research

Our laboratory member has a passion toward their research. So many students spent a lot of time in research activities. Especially they have a spirit of inquiry hence they get ideas through discussion with not only the laboratory members but also the people in other department. At first it is difficult to get used to this research activity. However, thanks to our group member's help I could do my research.

Life

Campus life

North Campus of University of Michigan is surrounded by beautiful nature. The Michigan students grab lunch, talk or play outside on North campus. At the beginning of school term many events are held on North campus like a welcome party. In addition to this relaxed atmosphere the up-to-date research environment help us to do our research comfortably.

Daily life

We went to Campus by bus on weekdays. The ride which is a city bus and M-bus which is a school bus are the main transportation-system. Once you issue your M-card which is student identification cards, we can ride both buses for free. However, the number of shuttles decreases on holidays. Hence we rent a car and went sightseeing and shopping on holidays.



Welcome Party



Lurie Nanofabrication Facility

My impression of two months life in USA

Name: Shun Tamamura

Affiliation (Dept & Univ): Biomechanics Engineering, Nagoya University

Participated program: Short (Summer) 2013

Research theme: Evaluation of auricular biomechanical property by FEM

Advisor at Univ. Michigan: Prof.Scott Hollister

Affiliation (Dept.): Biomedical Engineering



Firstly, I write about my research in University of Michigan. Fortunately, I could do research which has similar contents to my research in Japan. Therefore, it is not difficult for me to understand about background, objective and so on of my research in UofM. People in laboratory and university, including Professor, were all kind, and they taught me kindly when I asked things I do not know. In addition, most people in hotel, shop and so on were very kind for us. On the date of arrival at Ann Arbor, we lost our way to the hotel. At that time, an old woman calls out us and helps us. She carried us and our all baggages by her car to the hotel. In addition to this, we got helped many times by various people.

We could used our day off to go to various places to play and sightseeing by rented car, for example Chicago, Niagara Falls, Michigan Lake and so on. It was very excited and great opportunity for us to visit these places because it is difficult to go on a travel to these various places.

I felt that this program has many chance and possibility for all students in Nagoya University. I hope many student to participate it and enjoy their life in United States of America.



JUACEP Report

Name: Takayuki Yamada

Affiliation (Dept & Univ): Micro-Nano Engineering, Nagoya University

Participated program: Short (Summer) 2013 Michigan

Research theme: Calibration of a Strain Gauge for
Force Measurement in a Palatal Expander

Advisor at Univ. Michigan: Prof. Yogesh B. Gianchandani

Affiliation (Dept.): Electrical Engineering and Computer Science

The most impressive thing I thought in US is I had many chance to communicate with kind people. The professor and students in my visiting laboratory treated me nicely. Other laboratory members in University of Michigan also dealt with me nicely. Not only in University but also in my private life, many people helped me. For example, in the first day in US, we could not reach a hotel and we were in trouble. A woman asked us "Are you OK?" and she took us to the hotel by her car. The front desk of a hotel were also kind for us. He always spoke to us in the morning "Ohayougozaimasu" and he told us good place to see or to buy something. These information really helped us. I attached a picture of him with us.

I studied in the university but I learned a same thing both inside and outside of the university. It is that to express my intentions is very important. When I talked with the professor about my research topics, I talked with my laboratory members about what I did on holidays and also I ordered some foods in a burger shop, I should always speak something even if I didn't have confidence with my English. Holding my tongue is worse than speaking bad English. Most people in US listened to my speaking. I can speak English with confidence because of this experience.

These people and the confidence are my treasures.



JUACEP Report

Name: Hiroshi Fuji

Affiliation: Department of Mechanical science and Engineering,
Graduate School of Engineering, Nagoya University

Participated program: Short (Summer) 2013

Research theme: Modeling for a Nano-precision System

Advisor at UCLA: Prof. Tsu-Chin Tsao

Affiliation: Mechanical an Aerospace Engineering

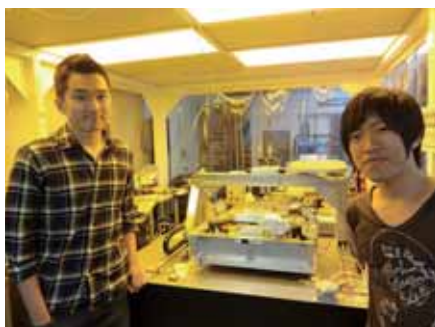


It was a great honor to be able to take part in this program. It gave me great opportunities to experience a lot of things and it helped me broaden my minds. I joined a mechanical and control laboratory, and I was researching about modeling for a nano-precision system. Before I joined this program, I felt a little nervous because I knew few technical English words related to the research. When I just started the research, I was actually having some trouble communicating with the laboratory members due to lack of vocabulary. But they kindly taught me a lot of things, so I did not feel uncomfortable at all, and I gradually learned to discuss technical matters. Staying there for 40 days was too short to learn English enough, but this experience definitely motivated me to improve my English more. I will continue to study English from now on. Researching at the laboratory, I was really impressed with the laboratory members' passion towards their research. I felt people there conduct their research more independently than we do in Japan. I was also impressed with their ability to solve problems by their own. They are highly motivated. One of the great things about the laboratory which I joined was that it had various kinds of equipment, so I could learn not only about theory and software but also about hardware although it was a short time.

I could enjoy not only the research but also interacting with people there. One day the laboratory members invited me to BBQ where there were people from other laboratories. Then I met a lot of people and we enjoyed cultural exchange. I was surprised to know that some of them were really interested in Japanese cultures. They knew a lot about Japan, and we talked about Japanese anime, music, sight-seeing areas and so on. We also talked about cultural differences between countries. I found sharing those differences really interesting.



I really liked the UCLA campus. Every building was really beautiful. I sometimes took a walk around the campus. The weather was nice and I could see beautiful buildings and diverse of people. It was so much fun. I could also enjoy food there. Inside and outside the campus, there are many kinds of restaurants and I could enjoy food from all over the world.



To sum it up, through this program I had a lot of experiences which I had never had in Japan. I am grateful to every encounter. Everyone I met was so nice to me and every conversation we had was precious. Those experiences would help me see things from a different perspective. I am sure this experience influences my future life.

JUACEP Report

Name: Shinichi HAYASHI

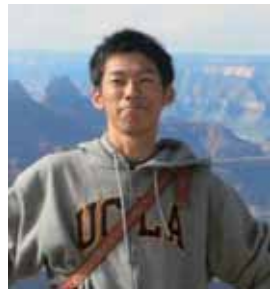
Affiliation (Dept & Univ): Mechanical engineering, Nagoya University

Participated program: Short (Summer) 2013

Research theme: Numerical simulation of wave propagation
in composite structures

Advisor at UCLA: Prof. Ertugrul Taciroglu

Affiliation (Dept.): Civil & Environmental Engineering



I stayed in Los Angeles for a month and a half. The climate of L.A. was very comfortable and we had rain only one time during our stay. The life in USA is exciting for me. I had some trouble, for example, I couldn't get student card of UCLA and my hotel doesn't have laundry and so on, but the overcoming these problem was good experience for me and made me tough.

I also spent the satisfying weekends. I went to Disney land and Universal studio and watched show in Hollywood and played in the beach. I could be more active than in Japan. The most impressive one is Grand Canyon and Las Vegas. We rent a car and drove 1200 mile in 3 days. The vast nature and luxury hotel surprised me.

The experience in laboratory of UCLA was also nice. We decided the theme of study after the presentation of my study in Japan. I worked on developing the non-destructive evaluation method using XFEM. I studied with PhD student and did meeting with supervisor on every Friday. The stay is short, but the knowledge and experience got in UCLA will make my research better.

Finally, I would like to appreciate to JUACEP officer for getting VISA and tickets for the hotel and flight. Thanks to their support, I could spend good time in L.A.



JUACEP Report

Name: Sakina Kondo

Affiliation (Dept & Univ): Engineering, Nagoya University

Participated program: Short (Summer) 2013

Research theme: Effect of protein charge on adsorption to apatite and cell viability

Advisor at UCLA: Prof. Benjamin M. Wu

Affiliation (Dept.): Bioengineering



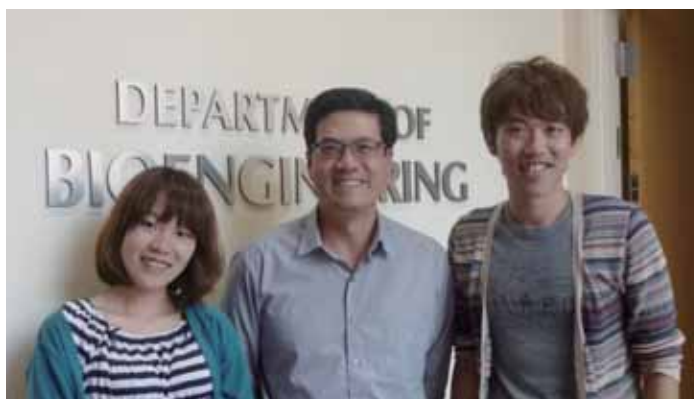
Spending in USA during this summer was a very good experience for me.

First, I have done experiment using cells. In Japan, I use hydroxyapatite, a component of natural bone, which is bioactive material that has the ability to bind to living bone directly. I could do experiment investigating hydroxyapatite and cells because they use both of hydroxyapatite and cells at the laboratory in UCLA. I had never done experiment using cells in Japan. So I didn't have any knowledge about biochemical and cells. I studied biochemical and cells with the papers and books. When I had some questions, I always ask Ph.D. student who took care of me in the laboratory. He also taught me how to grow cells and experimental precaution. So I could learn both knowledge about biochemical and technique for experiment with cells.

Second, I could realize the difference of weather, culture, life style and so on. In Los Angeles, it is always sunny, warm and dry. It is cooler in Los Angeles than in Japan despite of about the same latitude. It was very comfortable for me. I realized treasure in the water. Foods (such as hamburger, french fried potato, pizza, ice cream, juice and so on) in America were much bigger than that in Japan. I was surprised at the size of foods. I also surprised that cars were driven on keeping to right side. I felt strange when I rode car or bus. "Chip system" was very difficult for me because this system was not popular at all in Japan.

Finally, American people always helped me. When I faced problems and asked them favors, they always told me answers. Bus driver and passengers told me the way which I wanted to go. Ph. D. student who took care of me told me how to experience, knowledge about bioengineering and biotechnology. He also taught me English words and conversational expression. My friends who met in Los Angeles told me many restaurants, hamburger shops, ice cream shops, and bars which they recommended. They also took me to many famous places. I feared to ask American people at first because I thought they couldn't understand my poor English. However, they always listened to my English and told me answer in clearly understandable terms. So I became able to ask people in a positive manner.

I am grateful to have precious experiences. Thank you very much.



JUACEP Report

Name: Kazuki Miyazaki

Affiliation (Dept & Univ): Department of Micro-Nano Systems Engineering
Nagoya University

Participated program: Short (Summer) 2013

Research theme: Impact tolerance of metal, composites, and FMLs

Advisor at UCLA: Prof. Jenn-Ming Yang

Affiliation (Dept.): Materials Science and Engineering Department



The engineering research experience and cultural experience I gained in the U.S were very wonderful. In this program, I studied at the University of California, Los Angeles for 40 days.

I had worked on a research on Fiber Metal Laminates that are used in air craft structures. This research was not related with my research in Nagoya University, so I had the chance to gain new knowledge in this field. I studied in Prof. Jenn-Ming Yang laboratory, and the lab members were so kind to support my research. Without their guidance and persistent help, my research would not have been possible.

Los Angeles is one of the largest cities in the U.S., so I had the opportunity to have a relationship with many people from all over the world. Especially in this program, it was precious to me to belong to the laboratory and under supervision of the Post-Doctoral Research Scientist. Not only he but also the other members talked with me very friendly. I was glad to know about food, climates, tourist spots, and so on with talking with them. It was one of the best memories that they took me and my friends to the sushi restaurant for lunch and the B.B.Q. on the beach. In daily life, I had many challenges because when I did not know how to do anything, I had to manage to do without speaking in Japanese. For example, going laundry, getting dinner ready, getting on a bus and so on. These challenges were exciting for me.

Finally, I would like to express my gratitude to Prof. Jenn-Ming Yang for his generous support for my fulfilling work at UCLA.



JUACEP Report

Name: Shoya Ono

Affiliation (Dept & Univ): Aerospace engineering, Nagoya University

Participated program: Short (Summer) 2013

Research theme: Study on an aluminum two phase device using IAS fluid

Advisor at UCLA: Prof. Ivan Catton

Affiliation (Dept.): Material and Aerospace engineering



I was worried very much until this program began whether this program was good for me because I was denied by three professors who I ask to accept me and I couldn't get touch at all with the professor who accepted me. My research theme hadn't been decided and I couldn't prepare about my research before I left Japan, so, I was worried whether I can be satisfied with my research in very short term such as 40 days. However, I finished this program now and think such worry was not necessary at all.

It was the first time that I talk with my professor when I arrived at Los Angeles. The next day, I had a meeting with the member of the laboratory in the room of professor. It was so active and effective that I have never seen in Japan. The professor asked to his students "Do you have any research theme which we can finish within 40 days and makes this Japanese guy happy?". After that, my research theme was decided within 30 minutes. I researched about thermo-syphon under Qi who is PhD student. He is so caring that he answered all I couldn't understand about my research and he is also effective. Result, I can be satisfied with my research. I think it was very good experience for me that I was able to interact with excellent student in the world in this program.

Furthermore, Los Angeles was a very attractive town. Because Los Angeles has many beautiful places such as Santa Monica beach, Science museum, and Hollywood, I went there after school and weekend, and I could have very good time there. This program was the first time that I met other Japanese students who went with me, but, we could get along with them through this program and I was able to extend friends and acquaintances. I also think that is the charm of this program.

My experience in LA

Name: Toshihiro Sato

Affiliation (Dept & Univ): Engineering& Nagoya University

Participated program: Short (Summer) 2013

Research theme: Mechanical stimulation on rat intestinal smooth muscle cells to improve maturity

Advisor at UCLA: Prof. Benjamin M.Wu

Affiliation (Dept.): Bioengineering



I had a great time in Los Angeles. Many people in Los Angeles are very kind and they helped me when I had no idea about my research in UCLA. At first, I could not communicate with students in UCLA because I am not good at English. I felt deeply regretted. So I decided what I studied English hard. I listened to English when I went to school and looked up the phrase in my hotel. Finally I can communicate with them and my project in UCLA made it in time. I worked under Prof. Wu. He advised me so that my experimental results got better. They told me that the results were great. I was happy to hear it. I made the greatest memories in LA. The NU students who intend to go to America might want to study English hard before they go there.

And the students having studied abroad before in Nagoya University drove me to *Santa Monica beach* to do BBQ. We surrounded fire and baked the bread and sausage and I was taught American culture and customs by them. I was very fun and had good taste.

UCLA has a good gym, training rooms and so on. I played basketball twice a week. Many American people are good players. I was very fun to play with them.

